Distribution Locational Marginal Price in the Distribution Level Electricity Market

A Dissertation Presented for the
Doctor of Philosophy
Degree
The University of Tennessee, Knoxville

Xiaofei Wang
August 2023

Acknowledgment

I would like to express my deepest gratitude to all those who have supported and contributed to my research and the completion of this thesis.

First and foremost, I extend my sincere appreciation to my supervisor, Dr. Fangxing (Fran) Li. His continuous encouragement, insightful feedback, and expertise in the field have been instrumental in shaping this thesis and all my other research. During my years of Ph.D. studies, he has guided me on how to be a good researcher and how to be a well-rounded person. I am truly grateful for his guidance and mentorship.

I would also like to thank my committee members, Dr. Kevin Tomsovic, Dr. Hector Pulgar, and Dr. Jianming (Jamie) Lian, for their valuable input and constructive comments. Their expertise and suggestions have greatly improved the quality of this work.

In addition, I would like to thank all the members of our Enliten group for their kind help in both research and life. The free and creative environment makes the study more enjoyable. I am also grateful for the support from the faculty, staff, and friends at the Center for Ultra-Wide-Area Resilient Electric Energy Transmission (CURENT).

My special thanks go to the support and assistance provided by researchers at Oak Ridge National Laboratory (ORNL). Their stimulating discussions, willingness to share experiences, and collaborative spirit have been truly inspiring.

Finally, I would like to express my deepest thanks to my parents, whose unwavering belief in me and continuous support have been the driving force behind the completion of my Ph.D. study. Their love, understanding, and encouragement have been immeasurable.

Abstract

The proliferation of DERs in the distribution system is driving the transition from a passive distribution system to an active and flexible one. In this context, both industrial and academic fields have proposed to extend the transmission level market to the distribution level, and various local electricity market concepts appear. At the same time, the pricing mechanism is critical for the distribution-level electricity market. Therefore, many studies have extended the locational marginal price (LMP) to the distribution locational marginal price (DLMP) to capture the characteristics of the distribution system. This dissertation presents an in-depth study of the DLMP in the distribution-level market.

First, the DLMP is proposed to guide the daily consumption of residential loads, such as HVACs and EVs. A tri-level distribution market framework is established to model the relationship between the distribution system operator (DSO), load aggregators (LAs) and individual residents. Incentivized by the DLMP, residents are likely to adjust their consumption behaviors to save electricity bills and satisfy their comfortable requirements.

Second, uncertainties from all three levels and multiple sources are integrated into the above work. Interval optimization and stochastic optimization are utilized to model different uncertainties. Utilizing the latest released operating information, a rolling horizon optimization (RHO) scheme is employed to continuously obtain the consumption schedule and mitigate the day-ahead schedule's radicalness and conservativeness.

Third, the DLMP is utilized as price signals for future unit investment. Battery energy storage systems (BESSs) are selected as the research target. Then a profit-oriented BESSs siting and sizing problem is formulated to maximize investors' arbitrage revenue under a limited investment budget.

Finally, a peer-to-peer (P2P) market is studied. A hybrid two-layer distribution electricity market framework is established with a pool-based distribution market at the upper level and a decentralized P2P market at the lower level. Physical constraints are considered in the pool-based market, and the privacy of the grid and peers is preserved because only DLMP and energy quantity are exchanged between the two layers.

Keywords: demand response, distributed and decentralized solution methods, distribution-level electricity market, distribution locational marginal price (DLMP), peer-to-peer (P2P) energy trading.

Table of Contents

Chapter 1 Introduction 1
1.1 Transition of Distribution Systems 1
1.2 Distribution-Level Market: Participants, Architecture, and Pilot Projects 1
1.2.1 Market Participants 3
1.2.2 Pool-based Market 5
1.2.3 Peer-to-Peer Market 5
1.2.4 Comparison Between Pool-based Market and P2P Market 8
1.2.5 Distribution Market Pilot Projects 8
1.3 DLMP: Properties and Comparison with Other Electricity Tariffs 11
1.3.1 Market Properties of DLMP 12
1.3.2 Comparison Between LMP and DLMP 12
1.3.3 Comparison Between Other Electricity Tariffs and DLMP 13
1.4 Dissertation Outline 16
Chapter 2 Literature Review 17
2.1 Market Clearing Model 17
2.1.1 Mathematical formulation 17
2.1.2 Model relaxation 18
2.1.3 DLMP formulation 21
2.2 Market Clearing Solution Methods 23
2.2.1 Centralized methods 23
2.2.2 Distributed methods 25
2.2.3 Decentralized methods 27
2.3 Applications of DLMP 28
2.3.1 Boost flexibility 28
2.3.2 Incentivize DER operations 29
2.3.3 Guide DER planning 30
2.3.4 Improve system reliability 31
2.4 Conclusions 32

Chapter 3 Tri-level Scheduling Model Considering Residential Demand Flexibility of Aggregated HVACs and EVs under Distribution LMP 33
3.1 Introduction 33
3.2 Structure And Participants of Distribution-Level Electricity Market 37
3.2.1 Market Structure 37
3.2.2 EV Aggregator 37
3.2.3 HVAC Aggregator 39
3.2.4 DG Models 40
3.3 Tri-level Model 42
3.3.1 First Level 42
3.3.2 Second Level 42
3.3.3 Third Level 44
3.3.4 Solution Method of the Coupled First Two Levels 46
3.4 Case Studies 48
3.4.1 IEEE 33-Bus Distribution System 48
3.4.2 Analysis of Case 1 50
3.4.3 Operation and Economic Analysis under Different Flexible Load Ratios . 53
3.4.4 Economic Analysis under Different System Load Levels 56
3.5 Conclusions 60
Chapter 4 Tri-level Hybrid Interval-Stochastic Optimal Scheduling for Flexible Residential Loads under Multiple Uncertainties 61
4.1 Introduction 61
4.2 Modeling Residential Loads with Uncertainties 64
4.2.1 HVAC Model 64
4.2.2 EWH Model 65
4.2.3 EV Model 65
4.3 Day-Ahead: Tri-Level Market Framework 65
4.3.1 First Level: LAs 66
4.3.2 Second Level: DSO 68
4.3.3 Third Level: Individual End Users 70

4.4 Uncertainty Modeling and Solution Methods 70
4.4.1 Uncertainty Handling 70
4.4.2 Solution Method 74
4.5 Real-Time: Rolling Horizon Optimization 74
4.6 Case Studies 75
4.6.1 Modified IEEE 69-bus Distribution System 77
4.6.2 PV Scenarios 77
4.6.3 Day-ahead Scheduling 77
4.6.4 Real-time Scheduling 84
4.7 Conclusions 88
Chapter 5 Profit-Oriented BESS Siting and Sizing in Deregulated Distribution Systems 89
5.1 Introduction 89
5.2 Problem Formulation 93
5.2.1 The First Stage Problem: Optimal Siting & Sizing 93
5.2.2 The Second Stage Problem: BESS Operation in a Deregulated Distribution Market 95
5.2.3 Compact Notation 98
5.3 Scenario Extraction and Variable Nodal Loads 98
5.3.1 Scenario Extraction 99
5.3.2 Variability in Nodal Loads 99
5.4 Solution Methods 101
5.4.1 Solving the Bilevel Problem 101
5.4.2 Solving the Two-stage Problem 103
5.5 Case Studies 105
5.5.1 IEEE 33-Bus Distribution System 105
5.5.2 IEEE 123-Bus Distribution System 114
5.6 Conclusions 117
Chapter 6 A Hybrid Two-layer Pool-based and P2P Distribution Market Integrating Network Constraints and Transaction Autonomy 121
6.1 Introduction 121

6.2 Network Topology Determinization 125
6.2.1 Radial Network Constraints 125
6.2.2 Capacity Bank Operating Constraints 126
6.2.3 Switch Operating Constraints 126
6.2.4 DG Operating Constraints 126
6.2.5 Network Configuration Formulation 127
6.3 Two-Layer Distribution Market Formulation 128
6.3.1 Distribution Level Market 128
6.3.2 Community-based P2P Market 129
6.4 Peer Matching Via ADMM 130
6.4.1 Buyer Update 131
6.4.2 Seller Update 131
6.4.3 Community Manager Update 132
6.4.4 Scaled Dual Variable Update 132
6.4.5 Preferences of Buyers and Sellers 133
6.5 Solution Framework 133
6.5.1 Overall Solution Procedure 133
6.5.2 Quantity Adjustment Strategy 134
6.6 Case Studies 137
6.6.1 Simulation Setup 137
6.6.2 Network Topology 137
6.6.3 Consensus of P2P Market Participants 139
6.6.4 Convergence Between the Two-layer Markets 139
6.6.5 Net Load of P2P Markets in One Day 141
6.7 Conclusions 143
Chapter 7 Conclusions and Future Works 145
7.1 Summary of Current Progress 145
7.2 Future Directions 146
7.2.1 Coordination Between Transmission-level Market and Distribution-level Market 146

7.2.2 Integration with P2P Energy Trading 147
7.2.3 Profit-oriented Investment 147
7.2.4 Pricing Uncertainty 148
7.3 Possible Barriers and Challenges of Implementing DLMP 148
7.3.1 Aggregation Technology 148
7.3.2 Variability and Acceptance of DLMP 149
7.3.3 Investigation of Policy to Ensure Fairness and Efficiency of Distribution Markets 149
7.3.4 Market Power in Distribution Markets 149
References 151
Appendices 175
Appendix A Supplemental Materials of Chapter 3 175
Appendix B Supplemental Materials of Chapter 4 180
Appendix C Supplemental Materials of Chapter 5 182
Appendix D Supplemental Materials of Chapter 6 186
Appendix E Publications 191
Vita 193

List of Tables

Table 1.1. Comparison between pool-based market and P2P market..... 9
Table 1.2. Distribution level market pilot projects 10
Table 2.1. Modeling details and comparisons 19
Table 2.2. Different relaxation methods 19
Table 2.3. Summary and comparison of solution methods..... 24
Table 3.1. Proposed DG-LSPE algorithm..... 41
Table 3.2. HVAC aggregator load dispatching algorithm 45
Table 3.3. Parameters of single EV and HVAC..... 49
Table 3.4. Parameters of Aggregators..... 49
Table 3.5. Different Cases 51
Table 3.6. Absolute maximum dispatch error under different gaussian parameters 54
Table 3.7. Benefits of DLMP to the system..... 54
Table 3.8. Payment increase and its decomposition between 4.3 and 7.3 MW system load level..... 57
Table 4.1. Scenario reduction algorithm..... 73
Table 4.2. Procedure of RHO algorithm..... 76
Table 4.3. Parameters of the modified IEEE 69-bus system..... 79
Table 4.4. Aggregator payments and system generation cost under different uncertainty levels 82
Table 4.5. DLMP and its components of one branch at t = 19:00. 83
Table 5.1. Detailed procedure of scenario extraction and reduction algorithm..... 100
Table 5.2. Overall solution procedure..... 104
Table 5.3. Parameters of the modified IEEE 33-bus system 106
Table 5.4. Different cases 109
Table 5.5. Results of different cases 109
Table 5.6. Comparison of intermediate results 109
Table 5.7. Different DER penetration levels 112
Table 5.8. Simulation results 113
Table 5.9. Comparison with other models..... 115
Table 5.10. Parameters of the modified IEEE 123-bus system 116
Table 5.11. Results of different cases 118
Table 5.12. Comparison of Intermediate Results..... 118
Table 5.13. Comparison with other models..... 119
Table 6.1. Overall solution procedure..... 135
Table 6.2. P2P markets..... 138
Table 6.3. Network topology 138
Table 6.4. Capacitor bank operating status..... 138
Table 6.5. Net loads of P2P markets..... 142

List of Figures

Figure 1.1. Diagram of power system transition 2
Figure 1.2. Pool-based market architecture 6
Figure 1.3. P2P market architecture 6
Figure 3.1. Three-layer day-ahead distribution-level electricity market 38
Figure 3.2. Modified IEEE 33-Bus system 49
Figure 3.3. LMP, fixed load, PV, and outdoor temperature on a summer day 51
Figure 3.4. Spatial and temporal distribution of DLMPs and voltages 51
Figure 3.5. H2's load demand and indoor temperatures 52
Figure 3.6. Load profile of E1 and load dispatching error of H2 and E1 52
Figure 3.7. System load profiles under different flexible ratios 54
Figure 3.8. Voltage profiles of at t = 19:00 under different flexible ratios 55
Figure 3.9. HVAC and EV payment versus different load levels with various flexible loads 57
Figure 3.10. DLMP at node 18 with step changes under different system load levels 59
Figure 4.1. Illustration of the rolling horizon optimization scheme. 76
Figure 4.2. The modified IEEE 69-bus system. 78
Figure 4.3. PV power scenario sets. 80
Figure 4.4. Expected DLMP. 82
Figure 4.5. System load profiles under different uncertainty levels for the pessimistic model. 85
Figure 4.6. System load profiles under different uncertainty levels for the optimistic model. 85
Figure 4.7. Load profiles of total flexible load in day-ahead and real-time schedules. 86
Figure 4.8. Indoor temperature profiles of HVACs and water temperatures of EWHs for 150 intervals of 10 minutes/interval. 87
Figure 5.1. The framework of the TS-SBP model 94
Figure 5.2. Modified IEEE 33-bus system. 106
Figure 5.3. LMP patterns, load patterns, and their discrete joint probabilities 107
Figure 5.4. Average annual net profit of all scenarios and that of extracted scenarios 107
Figure 5.5. Expected DLMP of Case 5 111
Figure 5.6. System load profiles with and without BESSs 111
Figure 5.7. Nodal voltage profiles with BESSs 112
Figure 5.8. Modified IEEE 123-bus system. 115
Figure 5.9. System load profiles with and without BESSs 118
Figure 5.10. Nodal voltage profiles with BESSs 119
Figure 6.1. Framework of the two-layer market. 124
Figure 6.2. Network topology of the modified IEEE 33-bus system. 138
Figure 6.3. Consensus of a P2P market. 140
Figure 6.4. Convergence of the quantity adjustment. 142
Figure 6.5. Net load of P2P markets throughout one day. 144
Figure 6.6. DLMP at five buses. 144

List of Abbreviations

ADN	Active distribution network
ACOPF	Alternating current optimal power flow
ADMM	Alternating direction method of multipliers
ATC	Analytical target cascading
APP	Auxiliary problem principle
BESS	Battery energy storage system
BMP	Buyer's marginal profit
BS	Bill sharing
CAISO	California independent system operator
CB	Capacity bank
CHP	Combined heat and power
CPP	Critical peak pricing
DG-LSPE	Data generation and least squares parameter estimation
DA	Day-ahead
DR	Demand response
DCOPF	Direct current optimal power flow
DER	Distributed energy resource
DG	Distributed generator
DLMP	Distribution locational marginal price
DMO	Distribution market operator
DNO	Distribution network operator
DSO	Distribution system operator
GEB	Efficient buildings
EV	Electric vehicle
EWH	Electric water heater
ESS	Energy storage system
FC	Fuel cell

FIT	Feed-in tariff
GAN	Generative adversarial network
GA	Genetic algorithm
HVAC	Heating, ventilation, and air conditioning
ICT	Information and communication technology
KKT	Karush-Kuhn-Tucker
LC	Large consumer
LP	Linear programming
LPF-D	Linearized power flow for distribution
LA	Load aggregator
LEM	Local energy markets
LFM	Local flexibility markets
LMP	Locational marginal price
LF-D	Loss factors for the distribution
MPEC	Mathematical programming with equilibrium constraints
MG	Microgrid
MT	Microturbine
MMR	Mid-market rate
MILP	Mixed-integer linear programming
NB	Nash bargaining
NLP	Nonlinear programming
OPF	Optimal power flow
PSO	Particle swarm optimization
PTR	Peak time rebate
P2P	Peer-to-peer
PV	Photovoltaic
PMP	Proximal message passing
QP	Quadratic programming
RCI	Relaxed Consensus + Innovation
RT	Real-time

RTP	Real-time pricing
RHO	Rolling horizon optimization
SCF	Single Commodity Flow
SDP	Semidefinite programming
SOCP	Second-order cone programming
SMP	Seller's marginal price
SOC	State of charge
SVC	Static Var compensator
TLBO	Teaching-learning-based optimization
TCL	Thermostatically controlled load
TOU	Time of use
TSO	Transmission system operator
TS-SBP	Two-stage stochastic bilevel programming
TS-SMILP	Two-stage stochastic mixed-integer linear programming
WT	Wind turbine

Chapter 1 Introduction

This chapter discusses two types of distribution level markets and properties of the DLMP, and compares the DLMP with other electricity tariffs.

1.1 Transition of Distribution Systems

Traditionally, power systems are unidirectionally structured, that is, electricity is generated by generators and then transported via transmission and distribution lines to customers, who are at the end of the electricity delivery chain. However, in recent decades, the electricity industry has witnessed the emergence of various distributed energy resources (DERs) in the distribution system. At the generation side, the deployment of distributed generators (DGs), such as photovoltaics (PVs), microturbines (MTs), wind turbines (WTs), and energy storage systems (ESSs), etc., in modern distribution systems continues to grow [1][2]. At the demand side, industrial and commercial customers are incentivized and encouraged to participate in demand response (DR) programs. The desire to further expand DR potential, combined with advances in information and communication technology (ICT), has led to residential loads, such as smart home appliances, being widely studied in recent years [3]-[6].

The proliferation of a variety of DERs has transformed the once unidirectional power system into a bidirectional system, making the distribution system more flexible and active, but also more complex. This transition is illustrated in Figure 1.1.

1.2 Distribution-Level Market: Participants, Architecture, and Pilot Projects

Optimizing both the generation and the consumption of electricity locally can provide many advantages for a power system, such as reducing operating stress in peak load hours, reducing the risk of system failure, and deferring future grid investment. To take advantage of these new opportunities and to keep pace with the deregulation process, the distribution system needs to change the traditional business model, market design, and system operation [7].

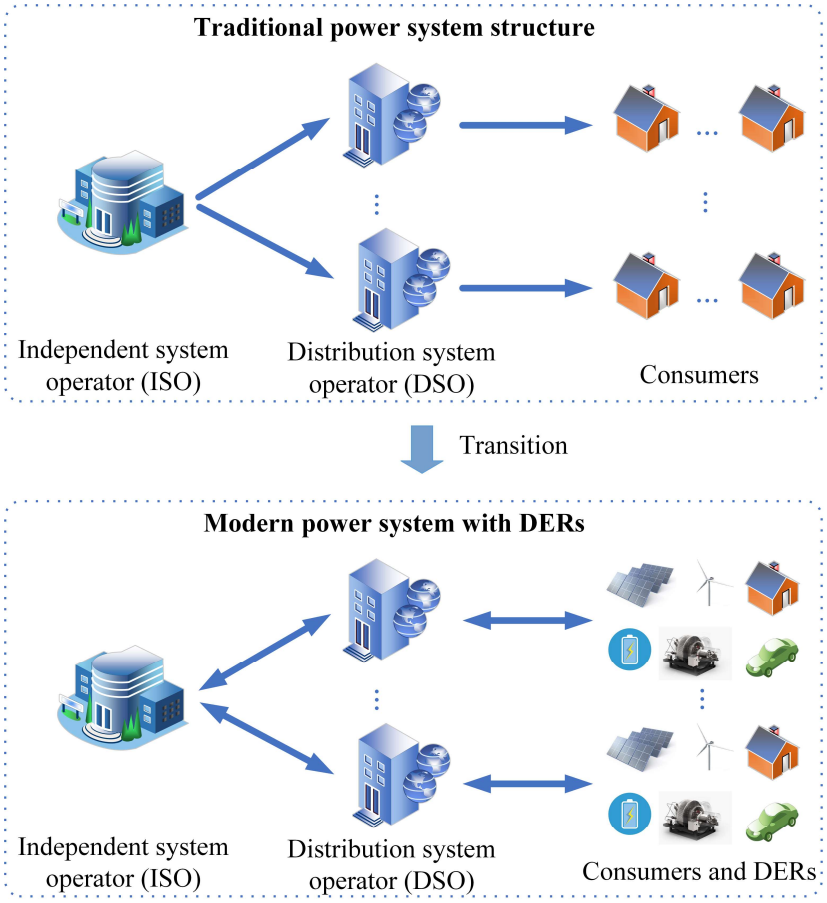


Figure 1.1. Diagram of power system transition.

In the research community, it is believed that a market-based distribution system is a promising means of achieving the optimal allocation of all DERs and improving the system operating efficiency [8]. Various electricity market concepts at the distribution level have been proposed, such as retail markets [9], local flexibility markets (LFM) [10]-[12], local energy markets (LEM) [13]-[15], and transactive energy schemes [16]. In the power industry, there are several ongoing local market pilot projects [17]-[25]. Based on different transaction forms, these distribution-level markets can be classified into two categories: the pool-based market and the peer-to-peer (P2P) market.

1.2.1 Market Participants

An electricity market is a place where transactions can happen between power suppliers and consumers. The power suppliers are diversified in an active distribution system, including PVs, WTs, MTs, ESs, combined heat and power (CHP), etc. Consumers, the individuals or communities of multiple end-users, are becoming proactive.

Participants in the distribution-level market can generally be classified into the following categories: distribution market operators (DMOs) [26], distribution network operators (DNOs), electricity retailers [27], DGs, ESSs, microgrids (MGs), large consumers (LCs), and load aggregators (LAs).

It should be noted that the first three entities, DMOs, DNOs, and electricity retailers, typically stem from conventional DSOs which are the companies in the regulated distribution industry. Therefore, the DMOs, DNOs, and electricity retailers may reside in the same holding company even in a deregulated environment. As such, many papers in the literature use the term DSO even though it may refer to one or more entities among DMOs, DNOs, and electricity retailers. In this chapter, the generic term DSO will also be used for simplicity, although the discussion below distinguishes between DMOs, DNOs, and electricity retailers based on their different functions in the distribution market.

1) DMO: As a profit-neutral entity, a DMO provides a trading platform that enables transparent energy transactions between electricity producers and consumers, clears the market, broadcasts price signals, determines market settlement, and so on, at the distribution level.

2) DNO: As the network operator, a DNO is responsible for system planning and operation, power outage restoration, network security management, and so on. It may be the owner of distribution networks as well. Since both DMO and DNO are regulated, they may both reside within the same holding company as different departments. In some literature such as [28], the DNO charges a tariff to the energy sellers and buyers for network usage.

3) Electricity retailer: As a retail service provider, an electricity retailer interacts with the external grid to maintain the power balance of the distribution-level market (e.g., purchasing electricity from the wholesale market when there is an electricity deficit and selling electricity to the wholesale market when there is extra generation in the local market). The electricity retailer can also provide ancillary services to the transmission system operator (TSO).

4) DGs: DGs are generators that have a relatively large power capacity that satisfies market access conditions in a distribution system. The typical DGs include MTs, PVs, WTs, CHP, etc. These types of DGs can participate in the market directly by offering a certain amount of electricity at a certain price [29].

5) ESSs: As the penetration level of ESSs increases, they become an important and integral part of a distribution system. An ESS can be regarded as a prosumer due to its dual roles of producer and consumer. ESSs are assumed to have enough rated power and rated energy to participate in the distribution market. They can operate in an arbitrage manner or provide ancillary services to receive revenue [30].

6) MGs: MGs are viewed as a localized group of small DGs, small ESSs, and loads. An MG is also a prosumer in that it exports or imports electricity through the tie-line that connects to the distribution network. Therefore, an MG can both provide offers when it has extra power generation and bid when its self-production is insufficient.

7) LCs: LCs, such as manufacturing factories and commercial centers, usually have a large load demand and can participate in the market directly [31].

8) LAs: Individual consumers are usually not eligible to participate in the market directly due to the complex market rules, strict participation requirements [32], small adjustable capacities, and heavy calculation burden [33]. Typically, an LA is proposed to manage the

flexibilities offered by multiple consumers and act as the intermediary between individual consumers and the DSO. By collecting the consumption preferences and operation status of consumers, LA bids in the distribution market on behalf of consumers and dispatches the purchased power to contracted consumers. By doing so, the LA not only provides flexibility to the distribution system but also explores new business models for individual consumers to increase energy efficiency.

1.2.2 Pool-based Market

The mission of the pool-based electricity market is to provide reliable electricity at the lowest cost to consumers [34]. Similar to the wholesale market, the transactions in a pool-based distribution market are centralized, hierarchical, and top-down. The DSO, a profit-neutral organization, is responsible for the efficient market operation and coordination of various DERs. The DSO collects the bids and offers from all market participants, then clears the market in a centralized way, and provides incentives to the owners of DERs to further deploy these resources [35]. The architecture of the pool-based market is illustrated in Figure 1.2.

In References [8][36], the DSO cleared the market by solving the optimal power flow (OPF) problem with the objective of minimizing the system generation cost or maximizing social welfare. The optimal power quantity was broadcast to the participants, together with the distribution locational marginal price (DLMP) that was derived from the dual variables. The influence of the uncertain DERs on the market and the DLMP was studied in [37][38]. In [39][40], the single-phase OPF formulation was extended to three phases, and the schedule of DERs in each phase was calculated.

1.2.3 Peer-to-Peer Market

The P2P market architecture is a less centralized, freer, and bottom-up electricity market where suppliers and consumers can transact electricity and other services autonomously. In this peer-centric architecture, each participant is capable of negotiating, accepting, or rejecting a trade according to their preferences, rationalities, and privacy considerations [41]. Demand and supply are finally matched by the specific distributed algorithms. A general P2P market architecture is illustrated in Figure 1.3.

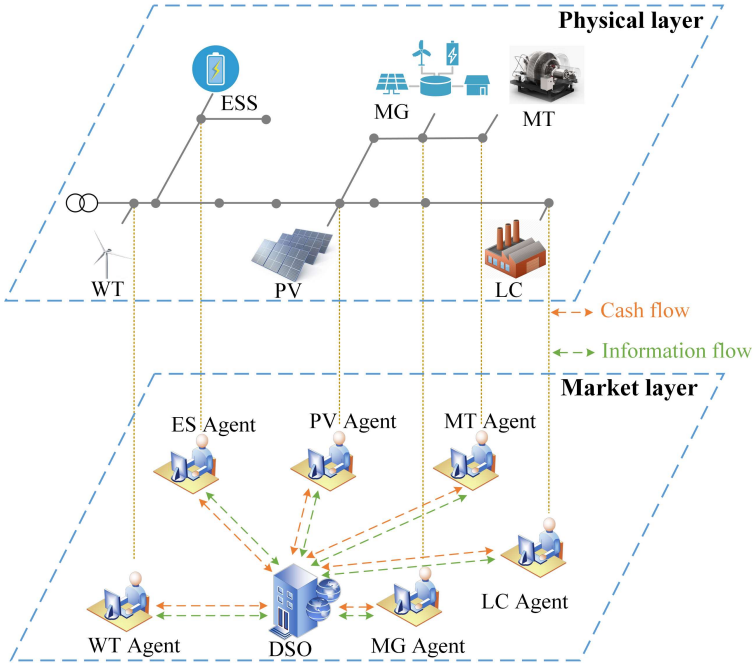


Figure 1.2. Pool-based market architecture.

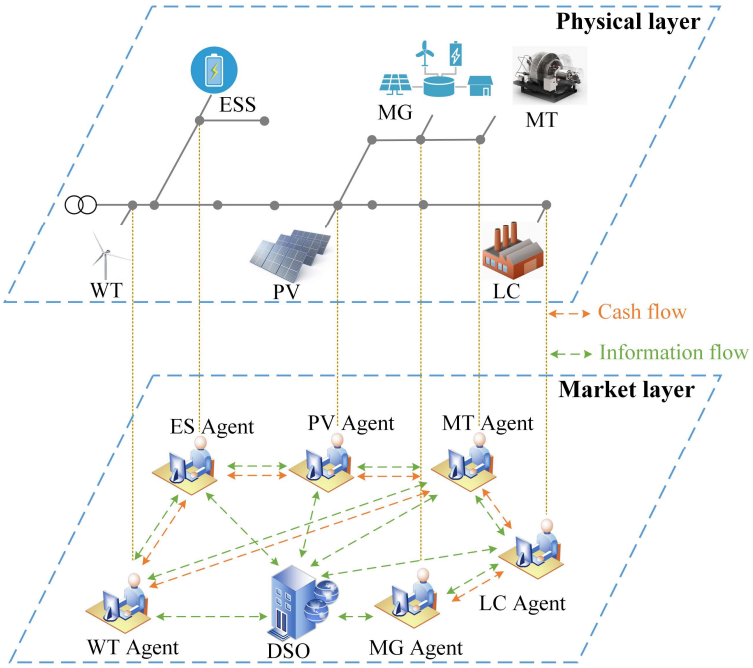


Figure 1.3. P2P market architecture.

Unlike the pool-based market, the design of a P2P market remains an open area and lacks consensus. Thus, this subsection intends to shed some useful light on market structure classification, physical network consideration, and DLMP deployment based on the existing literature. The market structure has been summarized and discussed in [42][43][44], and includes four types: 1) fully decentralized P2P markets where participants can directly negotiate with each other to complete trading; 2) coordinated P2P markets where trading is performed centralized in a community with a community manager; 3) community-based P2P markets where peers exchange limited information with the coordinator to preserve their privacy and autonomy; 4) hybrid (or composite) P2P markets where the fully decentralized and the community-based P2P markets are combined. In some other studies, network constraints have been considered, and the DSO is placed in the negotiation loop. In [41], a new P2P platform was conceptualized with the DSO as a delivery service provider. Peers first set up their trades by a peer matching algorithm, then the DSO checked the feasibility of the alternating current optimal power flow (ACOPF). If constraints were violated, the DSO updated the network usage price DLMP, and peers updated the cost function and redid the trade matching. This process continued until the ACOPF was feasible and all trades were unchanged. In this work, the DLMP promoted the P2P transactions that facilitated system operations and penalized those that were unfavorable from the perspective of the DSO. In [45], a two-stage P2P energy trading model was proposed. Trades were settled among peers in the first stage, then submitted to the utility for approval in the second stage. Certain trades were disapproved to ensure secure system operations. In [46], a coordinated P2P and ancillary service market was proposed, where the components of the DLMP were utilized as price signals for procuring ancillary services to ensure secure operation. In the auction-based P2P market proposed in [47], the DLMP was integrated into the payments of both prosumers and consumers to cover the power loss and voltage regulation costs.

Efficient algorithms are the key to enabling P2P transactions. Accordingly, various distributed algorithms and blockchain technologies have been proposed and developed to this end [48][49].

1.2.4 Comparison Between Pool-based Market and P2P Market

Though the pool-based market and P2P market have different market architectures and market rules, they do share many similarities, including but not limited to: 1) boosting DER utilization; 2) increasing system resilience and reliability; 3) lowering consumer's payments; and 4) improving system operation efficiency. Their strengths and weaknesses are compared and summarized in Table 1.1.

We are not going to claim that one market architecture is always more attractive than the other. Rather, we have provided a concise comparison study to give readers a basic understanding of these two markets.

1.2.5 Distribution Market Pilot Projects

To take advantage of DER flexibility and receive economic benefits, governments, institutions, and investors have conducted multiple distribution-level market pilot projects. Based on the business model and research focus, three types of projects are reviewed here: the TSO-DSO coordination trial, the pool-based market, and the P2P market. Several representative projects are summarized in Table 1.2.

The Transmission and Distribution Interface 2.0 [17] and SmartNet [18] mainly focus on TSO-DSO coordination schemes. In these schemes, the DSO manages flexible DERs in distribution to provide ancillary services to the TSO. Several key points regarding TSO-DSO coordination have been studied.

The Cornwall Local Energy Market [19], Piclo Flex [20], NODES [21], and EcoGrid 2.0 [22] are pool-based markets. The commonalities of these projects are that a local market has been created and flexibility is the main products traded in the market. Different price mechanisms, such as pay-as-bid and pay-as-clear, have been utilized in different projects.

EMPOWER [23] is a less centralized market, and it has studied approaches to exploring and developing ICT solutions to support local business models. The Brooklyn Microgrid [24] and P2P-SmarTest [25] are P2P markets. The Brooklyn Microgrid has created a platform where consumers and prosumers can trade self-produced energy locally in a P2P manner. P2P-SmarTest has simulated energy trading among interconnected MGs, as well as entities outside MGs.

Table 1.1. Comparison between pool-based market and P2P market.

Categories	Strengths	Weaknesses	Refs.
Pool-based market	1) Market is straightforward and easy to implement. 2) System operating conditions (e.g., congestion, voltage) are easier to manage. 3) DERs investment is clear due to explicit market price signals.	1) Aggregation technology is indispensable to aggregate multiple individual small-scale consumers. 2) Market power and strategic bidding of some participants exist. 3) The DSO should be accessible to all DERs, bidding price, quantity, and constraints.	[8][36] [37][38] [39][40]
P2P market	1) Greater number of free choices among energy consumers and producers. 2) Information privacy of market participants can be preserved. 3) Preferences of consumers (e.g., cost, renewable, location) can be satisfied.	1) Trading negotiation between peers is of high computational burden, the scalability and convergence are challenges. 2) Behaviors of participants are less predictable to the DSO. 3) DERs investment becomes obscure due to the free and autonomous negotiations. 4) Network constraints should be addressed carefully.	[41][42] [46][47] [48][49]

Table 1.2. Distribution level market pilot projects.

Project name	Country/ Region	Starting year	Business model	Price mechanism	Products
Transmission & Distribution Interface 2.0 [17]	United Kingdom	2017	TSO-DSO	NA	Flexibility services
SmartNet [18]	European Union	2016	TSO-DSO	Pay-as-clear	Ancillary services
Cornwall Local Energy Market [19]	European Union	2017	Pool-based	Pay-as-bid and pay-as-clear	Flexibility services
Piclo Flex [19]	United Kingdom	2019	Pool-based	Pay-as-bid	Flexibility services
NODES [21]	Norway	2018	Pool-based	Pay-as-bid	Flexibility services
EcoGrid 2.0 [22]	Denmark	2016	Pool-based	Pay-as-bid	Flexibility of aggregators
EMPOWER [23]	European Union	2015	Less centralized	NA	Local energies
Brooklyn Microgrid [23]	United States	2016	P2P	Pay-as-clear, pay-as-bid, and fixed price	Local energies
P2P-SmarTest [25]	European Union	2015	P2P	Pay-as-clear	Energies among microgrids

1.3 DLMP: Properties and Comparison with Other Electricity Tariffs

Tied to the emerging research on distribution-level markets is a need to improve the pricing mechanism for distribution market operation [50]. The pricing mechanism should have the following attributes: 1) coordinate with the existing wholesale market, 2) incentivize DERs to be properly operated and developed, 3) reflect the cost and physical operating conditions of the distribution system, and 4) reward DERs for flexibility and grid service provided. These attributes will facilitate the integration of DERs into distribution networks.

The dominant pricing method at the transmission level is the locational marginal price (LMP) which has been widely implemented across the U.S. and some other electricity markets worldwide. In essence, the LMP reflects the marginal cost of energy supply, active transmission security constraints, and transmission losses at each bus in the system [51]. This is a good reference for the distribution network. Many studies have been done to extend the LMP to the distribution locational marginal price (DLMP) to capture the temporal and spatial value of electricity.

The DLMP or distribution-level nodal pricing was first proposed in [52], in which the DLMP was distinguished from the direct current optimal power flow (DCOPF) based pricing by considering network losses. The value of DGs was quantified by reducing line losses and loading. The DLMP developed in [53] included energy, congestion, and power loss components to drive controls in a distribution system that employed electronic devices. In [36][54], the distribution system operator (DSO) determined the DLMP based on generation offers and load bids by clearing the distribution market, in which the DLMP was discovered in a market environment. In [8], the DLMP was extended to include voltage components by considering the voltage constraints. The contribution of DERs in distribution system operation via voltage support and loss reduction was rewarded by the DLMP. Reference [55] estimated the intervals of the DLMP and the confidence levels with the consideration of renewable generation. Reference [56] presented a detailed analysis of three approaches toward understanding the DLMP because the interpretation of the DLMP is critical for policymaking in the growth of future distribution markets. These works show

that DLMP has received broad attention and that it can maintain price attributes and reflect the operational conditions and DER values in a distribution system.

1.3.1 Market Properties of DLMP

DLMP, extended from LMP, shares many common market properties including Pareto efficiency, generation cost recovery, and incentive compatibility [57][58]. When the market objective is to maximize social welfare, the market equilibrium is achieved with Pareto efficiency because no Pareto improvement can be made [32]. Revenue adequacy indicates that the revenue of the market operator can cover the expenses of market operation. Generation cost recovery means that the electricity producer's profit is non-negative when DLMP is used for settlement. Incentive compatibility implies that when each participant pursues its best profit by following the market rules, all their behaviors promote the achievement of group goals.

It should also be noted that the above analysis assumes a perfectly competitive market. The actual market environment could be imperfect, and participants with market power can cause an inefficient market. However, despite the possibility of inefficiency, this assumption still works well in many markets due to the "invisible hand". Additionally, the above analysis also sheds light on the policies that aim to improve the market environment.

1.3.2 Comparison Between LMP and DLMP

The LMP and DLMP share a lot of similarities, from their derivation and their physical meaning. For instance, they both have the combination of shadow prices of binding constraints, and both reflect the marginal cost at a node. However, they do have several differences which stem from the physical differences between the transmission and distribution networks. This can be summarized in the following four aspects.

1) Congestion: Line congestions occur more frequently in the transmission network due to the meshed structure and bulk electricity transactions. A feeder or lateral in a radial distribution network is usually designed to undertake the peak power flow, which makes it very rare for congestion to occur. However, in the future, if there is a higher penetration of DERs and MGs with possible network reconfigurations, power flow patterns may change and have congestion issues similar to transmission systems.

2) Power losses: A distribution line usually has a higher R/X ratio and thus a higher power loss factor than a transmission line. Thus, the amount of power losses is not negligible at the distribution level while it is not unusual to omit losses at the transmission level when DCOPF is employed.

3) Voltage: The voltage drop is a more severe issue in the distribution system due to its radial topology. Additional measures are necessary to maintain the system voltage in the acceptable range, and the corresponding cost should be reflected in the DLMP. In contrast, the wholesale LMP model may simply assume a flat voltage magnitude in the DCOPF model.

4) Imbalance: Imbalance is a unique feature of distribution systems, while transmission systems are generally considered balanced. Thus, a proper DLMP model should be extendable to incorporate multiple phases and include the cost of special strategies to alleviate the imbalance level.

In addition to marginal energy price, the above discussion reveals the distinctions and the possible price components in LMP and DLMP. However, the number of price components in LMP or DLMP is not fixed. Depending on the application and the studied distribution network, one or more specific pricing components may be ignored.

1.3.3 Comparison Between Other Electricity Tariffs and DLMP

Suitable pricing schemes are essential in distribution markets, and many other tariffs have also been studied in the literature. Based on the usage and design purposes, they can be classified into three categories: 1) DR-based prices, 2) P2P incentivizing prices, 3) Nash bargaining (NB) -based prices.

1) DR-based prices: This category includes price-based or incentive-based DR programs. The former mainly consists of time of use (TOU), critical peak pricing (CPP), and real-time pricing (RTP), while the latter includes direct control, interruptible loads, and peak time rebate (PTR) [59]-[64]. These economic signals via either financial incentives (i.e., coupons or rebates) or dynamic prices are proposed mainly to incentivize consumers to change their power consumption to relieve the operating stress of the power system.

The main difference between these electricity tariffs and the DLMP lies in how the electricity rate is generated. Fundamentally, DR-based prices or tariffs are exogenously generated by an electricity retailer or a DSO, possibly via a LA, conventionally in the regulated industry as a means to increase demand flexibility. In contrast, the DLMP is endogenously generated in distribution markets' bidding and offering process. It is a market-determined price reflecting the marginal or incremental cost of electricity services provided (e.g., power injection or withdrawal at a specific moment and location). In this sense, they arguably may not be very comparable to each other.

Technically, since power losses and voltage constraints are considered in the market clearing, the DLMP varies in both time and location. Also, the DLMP is composed of the shadow prices of the operating constraints, thus it exactly reflects the physical operating conditions of the system. In contrast, the operational constraints and load quantity variations barely affect the DR-based prices which are pre-determined. These DR programs are simple and straightforward to implement, and they do offer some flexibility to end consumers. However, their temporal granularity is usually coarse (e.g., peak and off-peak price for TOU, peak prices for CPP), and their spatial granularity is not reflective of network topologies [41], while the DLMP can increase the spatiotemporal granularity of electricity tariffs.

Nevertheless, they are not necessarily mutually exclusive, and can be coupled or co-exist in the same distribution market. For instance, an LA and its DR participants can adopt a DR-based price scheme. In this way, the DLMP can work as an indicator for the LA to set up proper DR prices to recover the operation cost and the payment of purchasing electricity from the distribution market. Meanwhile, the revenue obtained from DR prices can also provide information for the LA bidding prices when the LA participates in the market. For example, in [65], TOU is used to charge power consumers, and the DLMP is generated as the power trading price between DGs and electricity retailers.

2) P2P incentivizing prices: These pricing schemes aim at incentivizing trading energy internally among peers in a P2P market. Three examples are: 1) the mid-market rate (MMR) scheme [66][67], the bill sharing (BS) scheme [68][69], and the single linear programming (LP) pricing scheme [70].

The MMR and single-LP scheme can decrease the local electricity buying price and increase the local electricity selling price for DERs in a P2P community such that the P2P trading is more economical than DERs trade directly with the external grid. Thus, prosumers will pay less and receive more revenue when trading in the community market. These price mechanisms attract prosumers to trade internally within the community rather than directly interacting with the external grid. The BS scheme reduces both the local buying price and selling price. Thus, consumers' payments are reduced but producers will experience a revenue deficit. As a result, DGs may not be motivated to participate in P2P energy sharing, especially those who own a significant local generation. In addition, the BS pricing scheme offers a flat rate, and its load shifting effect is limited.

Compared to the DLMP, these three pricing mechanisms currently only reflect the power balance constraint in a P2P market. Further study is needed to integrate other physical operating constraints (e.g., power losses, voltages, congestions) in the model.

3) NB-based prices: Game theory has been used to model energy trading in some studies. For example, NB was proposed as an incentive mechanism to encourage interactions and benefit-sharing among MGs [71]. In [28], the network usage price was derived in an NB-based market to cover the cost of the network operator. It is an alternative to the DLMP working as the network usage price, as was proposed in [41].

Based on the above descriptions and comparisons, price schemes in different market structures and designs may vary. For example, the DLMP can work as a general pricing method and be used in the settlement of power producers and consumers, as well as the network usage charge, while P2P incentivizing prices, such as MMR and single-LP, can be employed for internal trading within a community or MG. NB-based prices can be used to achieve fair benefit allocations.

In summary, while the DLMP is the dominant pricing approach in the literature for modern distribution markets, other pricing schemes can be utilized on their own for different market designs or co-exist with the DLMP.

1.4 Dissertation Outline

This chapter provides a comprehensive and in-depth overview of the state-of-the-art works regarding the concepts and properties of distribution level electricity market and DLMP. Characteristics of pool-based market and decentralized P2P market are summarized and compared. Additionally, the properties of the DLMP and the comparison with other electricity tariffs are presented.

Chapter 2 presents a comprehensive survey of the mathematical formulation of the market clearing model as well as the model relaxation methods. Three types of solution methods, namely centralized, decentralized and distributed algorithms, are summarized and compared. Four most promising DLMP applications in the distribution system are also discussed.

In Chapter 3, DLMP is utilized to guide the consumption of flexible residential loads in a tri-level distribution market framework. The first two levels form a bilevel model to optimize the aggregators' payment and to represent the interdependency between LAs and the DSO using DLMP, and the third level is to dispatch the purchased load of LAs to individual residents.

Following that, in Chapter 4, the uncertainties from all the three levels are modeled, including the random consumption behavior of individual consumers, forecasted climate temperature, and forecasted PV power output. A hybrid interval-stochastic optimal scheduling is proposed to deal with these uncertainties.

In Chapter 5, profit-oriented BESSs planning in the distribution level market is studied. Incentivized by the DLMP, private investors have the motivation to install BESS at the optimal sites and sizes to maximize their profits. The problem is formulated as a two-stage stochastic bilevel level model and is solved by a series of equivalent reformulations and relaxation methods.

In Chapter 6, a hybrid two-layer distribution electricity market is established with a pool-based distribution market at the upper level and a decentralized P2P market at the lower level.

Finally, Chapter 7 concludes the dissertation, provides directions for future studies and points out the possible challenges and limitations.

Chapter 2 Literature Review

This chapter first provides a general distribution-level market clearing model and reviews the model relaxation methods. Then, the state-of-the-art solution methods for market-clearing are reviewed and divided into centralized, distributed, and decentralized methods. Finally, applications of the DLMP from both the DER side and grid side are discussed.

2.1 Market Clearing Model

Detailed reviews on the P2P market have been performed in [42][43][44]. To avoid repetition and to clearly present the DLMP derivation and explanation, here a centralized pool-based market model is built.

Note that although this market model mainly refers to the energy market, which is an essential part of electricity market operation in general, the ancillary market can also be integrated into the current model as a co-optimization formulation.

2.1.1 Mathematical formulation

A typical market-clearing model is shown below.

$$\min \sum_{i \in G} f\left(P_i^G, \widehat{Q}_i^G\right) \tag{2.1}$$

$$s.t.$$

$$\sum_{i \in G} P_i^G - \sum_{i \in N} P_i^D - P^{loss} = 0 : \lambda^p \tag{2.2}$$

$$\sum_{i \in G} Q_i^G - \sum_{i \in N} Q_i^D - Q^{loss} = 0 : \lambda^q \tag{2.3}$$

$$S_l^{\min} \le S_l \le S_l^{\max} : \omega_l^{s,\min}, \omega_l^{s,\max}, \forall l \in \Omega_L \tag{2.4}$$

$$V^{\min} \le V_j \le V^{\max} : \omega_j^{v,\min}, \omega_j^{v,\max}, \forall j \in \Omega_N \tag{2.5}$$

$$P_i^{G,\min} \le P_i^G \le P_i^{G,\max} : \omega_i^{p,\min}, \omega_i^{p,\max}, \forall i \in \Omega_G \tag{2.6}$$

$$Q_i^{G,\min} \le Q_i^G \le Q_i^{G,\max} : \omega_i^{q,\min}, \omega_i^{q,\max}, \forall i \in \Omega_G \tag{2.7}$$

$$-Q_i^G \le \widehat{Q}_i^G, Q_i^G \le \widehat{Q}_i^G : \kappa_i^-, \kappa_i^+, \forall i \in \Omega_G \tag{2.8}$$

where the objective function (2.1) is to minimize the total electricity generation cost including the electricity purchasing cost from the wholesale market and the generation cost of DGs. Constraints (2.2) and (2.3) represent the active and reactive power balance constraints; (2.4) is the congestion constraint; (2.5) is the voltage constraint; (2.6) - (2.7) are the generators' active and reactive power output limits; and in (2.8), $\widehat{Q}_{i,t}^{G} = \left|Q_{i,t}^{G}\right|$ since both absorbing and generating reactive power will induce cost [8].

The market-clearing model (2.1) - (2.8) provides a general and concise formulation. It can easily be extended to multiple time slots by adding time coupling constraints, and to more complicated formulations by considering different constraints and specific operating conditions. A detailed comparison of constraint considerations is summarized in Table 2.1. It can be observed that in addition to constraints (2.2) - (2.8), other constraints are also considered. In [74], the uncertainties of renewable energies and load demand were modeled, and the uncertainty price was included in the LMP. In [35], the stochasticity of renewable DERs was internalized in the DLMP by applying conic duality to a chance-constrained ACOPF. In [38], the concept of an uncertainty DLMP was proposed to charge the uncertain resources and was seen as the marginal cost of dealing with the next unit increment of uncertainty in the distribution system. An imbalanced distribution system has been studied in [39][40][73], in which the single-phase DLMP was extended to three phases, and each phase had its own DLMP. The authors in [75] integrated the transformer loss of life in the relaxed branch flow model and added transformer degradation cost in the DLMP.

2.1.2 Model relaxation

Due to the high nonlinearity and nonconvexity of the ACOPF in distribution systems with high R/X ratios and power losses, it is generally hard to solve the clearing model, especially for a large system. To improve calculation efficiency as well as maintain accuracy, various methods have been proposed to approximate and relax the ACOPF model. The basic idea is to transform the nonlinear problem into a linear or convex problem. According to their mathematical properties, these approximation and relaxation methods can be categorized into linearization and convexification [76] in Table 2.2.

Table 2.1. Modeling details and comparisons.

Refs.	Loss	Congestion	Voltage	Uncertainty	Imbalance	Reactive power	Reserve
[8]	✓	✓	✓	--	--	✓	--
[36]	✓	--	✓	--	--	✓	--
[97]	--	✓	--	--	--	--	--
[98]	--	✓	--	--	--	--	--
[99]	✓	✓	--	--	--	--	--
[55]	✓	✓	✓	--	--	✓	--
[50]	--	✓	--	✓	--	--	✓
[35]	✓	✓	✓	✓	--	✓	✓
[38]	--	--	✓	✓	--	✓	✓
[39]	✓	--	✓	--	✓	✓	--
[40]	✓	--	✓	--	✓	✓	--
[73]	✓	--	--	--	✓	✓	--
[75]	✓	✓	✓	--	--	✓	--
[100]	✓	--	✓	--	--	✓	--
[101]	✓	--	✓	--	--	✓	✓

Table 2.2. Different relaxation methods.

Categories	Specific methods	Refs.
Linearization	DCOPF	[97][98]
	Linearized *Distflow*	[8][77][79][86]
	Polygonal approximation	[8][35]
	Modified *DistFlow*	[76]
	LPF-D, LF-D	[36][40][80]
	Taylor approximation	[81][82][83]
	Data-driven linearization	[84][85]
Convexification	SDP	[87][88][89][94][95]
	Moment relaxation-based SDP	[90]
	SOCP	[91][94][95][96][102]
	Sequential SOCP	[93]

In the linearization category, the nonlinear ACOPF model is approximated to a linear model via certain assumptions. A widely used model is the linearized *DistFlow* model [77], in which power loss and voltage angle are neglected. In [78], the quadratic calculation of branch power loss was linearized through the piecewise linear formulation. In [8][35], a polygonal approximation was used to linearize the quadratic congestion and power output constraints. Reference [76] proposed a modified *DistFlow* by using the ratios of active and reactive power to voltage magnitude as state variables. By introducing the path-branch incidence matrix, power flows and voltage magnitudes were written in a matrix form. In [36][80], a new model of linearized power flow for distribution (LPF-D) and loss factors for the distribution (LF-D) were proposed to linearize the ACOPF, in which the active and reactive power were expressed as linear functions of voltage magnitudes and phase angles. In [81]-[83], based on a pre-determined initial operating point, the Taylor approximation was utilized to linearize the *DistFlow* model. In addition to these model-based linearization approaches, data-driven power flow linearization approaches have been proposed by utilizing the power system measurement data [84][85]. In these approaches, with the determination of the constant terms and the regression parameter matrices, the active and reactive power injection were expressed as affine functions of voltage magnitudes and angles, or vice versa. Some studies have also focused on the linearization in the imbalanced system. In [79][86], the single-phase linearized *DistFlow* has been extended to an imbalanced three-phase model with the assumptions that voltages of three phases are similar and line losses are small. In [86], the three-phase power flow in the bus injection model was linearized for an active distribution network (ADN). In [40], LPF-D and LF-D were extended to three-phase systems.

In the convexification category, the ACOPF is usually convexified via two relaxation methods: semidefinite programming (SDP) [87]-[89] and second-order cone programming (SOCP) [91][92]. In [87], SDP was first proposed to relax the ACOPF. The authors in [88] proposed using SDP to solve the dual of an equivalent form of the ACOPF problem instead of the ACOPF problem itself, and a necessary and sufficient condition was provided to ensure the zero-duality gap. In [89], SDP relaxation of the ACOPF was proposed for multiphase distribution networks with wye and delta connections. In [90], the imbalanced

ACOPF problem was formulated as a moment relaxation-based SDP model, with system sparsity used to boost computing efficiency. In the SOCP category, the main idea was to relax the quadratic equality constraints into inequality constraints. The ACOPF was relaxed into a SOCP model for a radial network in the bus injection model in [91] and in the branch flow model in [92]. The accuracy and exactness of the SOCP method have been proven in [92]. In case the SOCP relaxation is not exact, reference [93] has proposed a sequential SOCP approach to recover the actual optimal solution. References [94][95] have provided a detailed tutorial for the SDP and SOCP relaxation of the generic ACOPF problem. One can refer to [94][95] for more details regarding the formulation, derivation, and sufficient conditions to ensure the exactness of relaxations.

Additionally, some of the previously mentioned papers also present a numerical comparison in terms of the accuracy of these approximation and relaxation methods. These papers are summarized here for readers convenience: [36][76][79][84] [85][86][87][89][93].

2.1.3 DLMP formulation

Based on (2.1) - (2.8), the Lagrangian function of the clearing model can be written as follows.

$$\begin{aligned} L = & \sum_{i\in G} f\left(P_i^G, \widehat{Q}_i^G\right) \\ & - \lambda^p \left(\sum_{i\in G} P_i^G - \sum_{i\in N} P_i^D - P^{loss} \right) \quad - \lambda^q \left(\sum_{i\in G} Q_i^G - \sum_{i\in N} Q_i^D - Q^{loss} \right) \\ & - \sum_{l\in L} \omega_l^{s,\min} \left(S_l - S_l^{\min}\right) - \sum_{l\in L} \omega_l^{s,\max} \left(S_l^{\max} - S_l\right) \\ & - \sum_{j\in N} \omega_j^{v,\min} \left(V_j - V^{\min}\right) - \sum_{j\in N} \omega_j^{v,\max} \left(V^{\max} - V_j\right) \\ & - \sum_{i\in G} \omega_i \cdot g_i\left(x\right) \end{aligned} \tag{2.9}$$

where $g_i(x)$ represents the power output limits in (2.6)-(2.8).

The active power DLMP and reactive power DLMP are the first-order partial derivatives of the Lagrangian function with respect to the active and reactive load demands, respectively.

$$\pi_i^p = \frac{\partial L}{\partial P_i^D} = \lambda^p + \lambda^p \cdot \frac{\partial P^{loss}}{\partial P_i^D} + \lambda^q \cdot \frac{\partial Q^{loss}}{\partial P_i^D} + \sum_{l \in L} \left(\omega_l^{s,\max} - \omega_l^{s,\min} \right) \cdot \frac{\partial S_l}{\partial P_i^D} + \sum_{j \in N} \left(\omega_j^{v,\max} - \omega_j^{v,\min} \right) \cdot \frac{\partial V_j}{\partial P_i^D} \tag{2.10}$$

$$\pi_i^q = \frac{\partial L}{\partial Q_i^D} = \lambda^q + \lambda^q \cdot \frac{\partial Q^{loss}}{\partial Q_i^D} + \lambda^p \cdot \frac{\partial P^{loss}}{\partial Q_i^D} + \sum_{l \in L} \left(\omega_l^{s,\max} - \omega_l^{s,\min} \right) \cdot \frac{\partial S_l}{\partial Q_i^D} + \sum_{j \in N} \left(\omega_j^{v,\max} - \omega_j^{v,\min} \right) \cdot \frac{\partial V_j}{\partial Q_i^D} \tag{2.11}$$

where π_i^p and π_i^q refer to the active DLMP and reactive DLMP at node *i*, respectively.

In (2.10), the active DLMP consists of four components: the marginal energy price, the marginal power loss price, the marginal congestion price, and the marginal voltage support price. The marginal price represents the additional cost of supplying the next MWh of electricity. Note that this additional cost can be decomposed into the subset of shadow costs associated with the binding constraints for that node. The marginal energy price is set by the marginal unit in the distribution system. The marginal congestion price reflects the marginal cost of congestion at a given node. Although congestion rarely happens in traditional radial distribution networks, it is possible in ADNs due to the high penetration of DERs or MGs. The marginal power loss price is set to reflect the power losses associated with power delivery which is not negligible because the power loss amount in a distribution system is usually higher than that in a transmission system. The voltage support price represents the cost of maintaining voltage at an acceptable level, and it will be zero if the voltage constraints at a node are not binding. An in-depth understanding of the DLMP components can help stakeholders make better decisions and is discussed in Subsection 2.3.

There have been discussions about whether and how reactive power should be priced. In [8][36], the concept of a reactive DLMP which could act as a candidate choice to price the reactive power was proposed. In [103], the author stated that a reactive DLMP could be used as a tool to improve system stability and power quality. Thus, the reactive DLMP was kept for flexibility. If the reactive LMP is not considered in the transmission network, it is simply set to zero at the power supply point; if considered, such as the Q-LMP proposed in [104], (2.11) can be adopted directly to calculate the reactive DLMP.

It should be noted that the above formulation (2.10) - (2.11) is based on the typical market model (2.1) - (2.8). When other constraints are considered, additional price components such as marginal imbalance price [40] and transformer degradation price [75] can be included.

2.2 Market Clearing Solution Methods

The DLMP is usually recovered from the dual variables when the market-clearing model is solved. Thus, solving the OPF problem of the distribution system is the prerequisite of the DLMP. This section reviews the solution methods of the market clearing model. In the literature, these methods can be categorized into three groups: centralized methods, distributed methods, and decentralized methods. Their features are summarized and compared in Table 2.3.

2.2.1 Centralized methods

Centralized optimization is defined as a coordinated policy for solving a problem that considers the system under study as a whole. In power systems operation, it means the control center collects all required information and performs centralized decisions [105]. From Section III, the clearing model can be classified into different optimization fields based on mathematical properties, such as LP, quadratic programming (QP), mixed-integer linear programming (MILP), SOCP, nonlinear programming (NLP), etc. Various centralized solution methods have been proposed and can be generally classified into either mathematical programming-based algorithms or metaheuristic algorithms.

1) Mathematical Programming-based Algorithms

Programming-based algorithms, like the simplex method, interior point method, and branch and bound method, can find the optimal solution for typical OPF problems. Various commercial solvers that have integrated these algorithms can also solve the clearing model effectively and efficiently, such as CPLEX, GUROBI, MINOS, and IPOPT. The main advantage of a programming-based algorithm is that the global optimum can be guaranteed if the problem is convex. The main drawback is that the computation time increases significantly with the scale of the problem. In [36][97], the market model was linearized to form an LP problem that is solved effectively.

Table 2.3. Summary and comparison of solution methods.

Categories	Algorithms	Pros	Cons	Refs.
Centralized methods	Programming-based	Can find the global optimum if the problem is convex.	High computation burden in a large-scale problem.	[36][81] [97][98] [106]
	Metaheuristic	Can find a sub-optimal solution even if the problem is nonconvex and nonlinear.	High computation burden due to a large group of populations and a large number of iterations.	[96][107]
Distributed methods	ADMM	Can decompose a problem into sub-problems to improve the computational efficiency. Data privacy is well protected.	Convergence rate of ADMM is not always satisfactory, and variants of ADMM are often needed for specific problems.	[109][110] [111][112] [113][114] [115][116]
	ATC	Suitable for hierarchical design optimization problems.	Implementation is complex, may not be able to efficiently handle a meshed network.	[117][118] [119][120] [121][122]
Decentralized methods	PMP	High computational efficiency due to in-parallel solution of sub-problems.	Information exchange among sub-problems is complex.	[123][124] [125][126]
	APP	An early algorithm that makes decomposition possible in non-separable situations.	Information exchange among sub-problems is complex, similar to PMP.	[127][128] [129][130]

In [98], the system operation cost and electric vehicle (EV) aggregator operation cost were modeled as quadratic functions, thus the market model belongs to QP. The ACOPF was convexified as a SOCP relaxation method in [81] and solved by GAMS. Some NLP methods have also been proposed. In [106], the trust-region method was utilized to solve the ACOPF based market.

2) Metaheuristic Algorithms

Metaheuristic algorithms, such as the genetic algorithm (GA), particle swarm optimization (PSO), and teaching-learning-based optimization (TLBO), are powerful in the sense that they can be applied to most optimization problems. However, it should be noted that these algorithms do not guarantee that the final solution is the optimal one. The pros are that they can find a sub-optimal solution for a nonlinear and nonconvex problem that mathematical programming-based algorithms cannot solve directly. The cons are that these algorithms are time-consuming because a large group of populations and many iterations are needed. Reference [96] proposed a methodology to achieve the optimal network reconfiguration with the application of the DLMP in distribution networks by utilizing GA. In [107], a modified PSO approach was proposed to obtain the optimal locations for the EV charging stations in a two-area distribution system.

2.2.2 Distributed methods

As the number of participants in the distribution market increases, it is challenging for centralized optimization methods to solve large-scale problems due to the computational burden. Also, data privacy is another concern for participants. Therefore, various distributed optimization methods have been proposed [108]. The basic idea of distributed optimization is to decompose the original model into a set of smaller sub-problems and solve each sub-problem independently till convergence, usually facilitated by a coordinator to exchange the information of coupling variables among sub-problems. As such, the computational burden is alleviated. Two commonly used distributed algorithms are reviewed: the alternating direction method of multipliers (ADMM) and the analytical target cascading (ATC).

1) Alternating direction method of multipliers

The ADMM is an augmented Lagrangian relaxation-based algorithm that can solve arbitrary-scale optimization problems and support distributed computation [109]. It utilizes the dual decomposition method to break a large-scale problem into smaller ones and the augmented multipliers method to deal with the convergence issue. The ADMM algorithm needs a central coordinator to update the dual variables. Overall, the ADMM is a robust algorithm that does not require strong assumptions and has good data privacy protection.

The ADMM has been applied frequently to power systems problems. Reference [110] utilized the ADMM algorithm to clear a market with high penetration of residential loads, in which residential LAs communicated with the DSO with limited information and thus protected residents' privacy. In [111], a consensus-based ADMM approach was proposed to solve the DCOPF problem with DR. Three types of ADMM-based distributed algorithms were performed, and different convergence performance and communication requirements were discussed. In [112], the ADMM algorithm was utilized to clear the market to protect the privacy of EVs and renewable DGs. Reference [113] proposed a consensus-based Jacobian ADMM algorithm to maximize grid welfare in a distributed and parallel manner, in which an RTP price scheme was derived to facilitate automated DR. In [114], the ADMM was utilized to clear a distribution-level flexibility market in which aggregator payback condition is considered. In [115], a multi-block ADMM algorithm was proposed to solve the market-based multi-period ACOPF, and a distributed Douglas-Rarchford Splitting method was utilized to ensure the convergence. In [116], a consensus-ADMM structured trust region algorithm was proposed to solve the nonlinear and nonconvex ACOPF for multiple regions.

2) Analytical target cascading

The ATC algorithm is a system design approach enabling top-level design targets to be cascaded down to the lowest level of the modeling hierarchy [117]. In the ATC method, the entire system is partitioned into a set of subsystems that are hierarchically connected [118]. No coupling variables exist among subsystems in the same level; instead, coupling variables only exist between systems in adjacent levels.

In [119], the ATC theory was introduced in the economic dispatch of an ADN. The ATC algorithm decoupled the dispatching of distribution networks and multi-MGs by considering them as different stakeholders that can independently optimize their operation and economic benefits. In [120], the ATC method was adopted to achieve win-win cooperation between the ADN and virtual MGs in a coupling bi-level dispatching model. In [121], an accelerated robust ATC method was proposed to solve the OPF problem. A function was designed to determine a balancing coefficient to avoid premature convergence or divergence and reduce the number of iterations. In [122], EV charging stations and the DSO were formulated as a bi-level model. Then the ATC algorithm was proposed to decouple the bi-level model with the tie-line power as the only exchanged information.

2.2.3 Decentralized methods

Similar to distributed methods, decentralized methods also decompose a large-scale problem into smaller ones. The main difference is that the distributed method still requires a coordinator which exchanges limited information of coupling variables among sub-problems, while the latter one does not involve a central coordinator at all and sub-problems only exchange information with their neighbors [118]. Here, two decentralized algorithms are reviewed: the proximal message passing (PMP) and the auxiliary problem principle (APP).

1) Proximal message passing

As stated in [118], the PMP algorithm is a special application of the ADMM. However, unlike the sequential multiplier update of the ADMM, the PMP algorithm is fully decentralized and the sub-problems are solved in parallel. Since the PMP algorithm inherits from the ADMM, all convergence properties that hold for the ADMM also hold for the PMP algorithm [123]. In [124], PMP algorithms with different penalty factors were tested on a distribution market clearing problem. Each device optimized its sub-problem and exchanged information with neighbors at the end of each iteration. Reference [125] addressed the convergence issue of the PMP algorithm caused by the binding voltage constraints and discovered the DLMP. In [126], the APP algorithm and PMP algorithm were combined to solve a multiple-period OPF problem. The APP algorithm first

distributed the computation to several dispatch periods, then the PMP algorithm solved each period across different power devices.

2) Auxiliary problem principle

In [127], the APP algorithm was proposed to decompose a problem into auxiliary problems with shared variables. Each auxiliary problem interchanged information with its neighbors via shared variables and no central coordinator was required. The APP algorithm has been applied in power system optimization problems. In [128], the whole power system was decomposed into multiple areas, and fictitious nodes were added to decouple the neighboring areas. Each area was an independent OPF problem, so it interchanged with neighbors at the end of each iteration until the convergence criteria were satisfied. In [129], the APP algorithm was utilized to solve a DCOPF problem of multiple interconnected systems. Each subsystem was solved independently with limited information exchange, avoiding sharing the local generation cost information. Reference [130] first partitioned the ADN into different voltage control zones, then proposed an APP-based algorithm to solve each zone with limited data exchange.

2.3 Applications of DLMP

In a market environment, the DLMP is an effective economic signal that can both reflect the marginal operating cost of the distribution system and provide continuous incentive market signals for the operation and future investment of DERs. It has the possibility to change the conventional operation and planning pattern of the distribution system. In this section, the impacts of the DLMP on system flexibility, operation, planning, and reliability are reviewed from different perspectives.

2.3.1 Boost flexibility

Electric flexibility refers to adjusting electricity production or consumption in response to system variability or activation signals. In general, it has five attributes: (a) direction (up or down), (b) power capacity, (c) starting service time, (d) service duration, and (e) location [131]. These attributes can be utilized properly to provide specific services to the system.

In a distribution system, DERs are the primary sources of flexibility, and they can be divided into the generation and demand sides. Power suppliers, such as WTs, fuel cells

(FCs), and ESS units, are dispatchable and they can work in coordination with each other to foster system flexibility [132]. On the other hand, consumers provide flexibility from the load side. This load-side flexibility is released by adjusting consumers' consumption behaviors via incentives or price signals [133].

In a regulated system with a flat tariff, DERs usually behave as price takers. They passively receive the electricity price and do not have much motivation to improve their consumption or generation schedules. DERs flexibility has been obstructed due to the absence of a proper price policy. Other tariffs, such as TOU, PTR, CPP, and RTP, have been utilized to incentivize DERs to release some flexibility. However, the potential of DER flexibility has not been fully explored and can be further released by suitable market mechanisms.

With the continuous improvement study of the DLMP and its spatial-temporal and operating condition reflective characteristics, the deployment of the DLMP can incentivize DERs to unlock their flexibility for better benefits. How the boosted flexibility will influence DERs operation, planning, and system reliability are analyzed as follows.

2.3.2 Incentivize DER operations

With the DLMP in place, energy consumers and producers can make decisions based on incentives that reflect the economic values related to DER operations.

On the demand side, consumers wish to reduce their electricity procurement costs. This can be done by optimizing the time-shiftable loads under the condition of dynamic electricity pricing [134]. Consumers can shift electricity consumption from peak price hours to low price hours. Time-shiftable loads include charging of EVs, washing machines, dryers, etc. Among all residential loads, thermostatically controlled loads (TCLs) (e.g., heating, ventilation, and air conditioning (HVAC) systems and electric water heater) and EVs account for a large share of the electricity consumption and have similar energy storage characteristics [4][135]. These characteristics render them the ideal residential DR candidates that can respond to varying price signals. In [63][133][136], precooling or preheating for TCLs have been proposed to reduce electricity bills by avoiding consuming electricity in peak hours. A bi-level model was proposed in [81] to optimize EV charging schedules.

On the generation side, DGs can provide offers at a marginal cost to maximize their profits [52]. PVs and WTs usually have low marginal costs, so they can easily win the bid, which will promote renewable penetration. Other DGs, such as MTs, FCs, CHP, and geothermal generators, are usually dispatchable but have a high marginal cost. Therefore, they can bid in the energy market to provide energy at peak hours to earn profits since the DLMP in these hours is usually high, or they can participate in the ancillary service market to maintain the stable operation of the distribution system [138].

For prosumers in the system, such as ES units and MGs, consumption/generation schedules can also be affected by the DLMP. Beyond their ability to restrain the uncertainties of renewables, prosumers can also operate in an arbitrage manner by utilizing the temporal difference of the DLMP. That is, prosumers buy electricity at low DLMP hours and sell electricity at high DLMP hours. In [38][139], bi-level models were proposed for MGs and the DSO. As the price taker, the optimal response of MGs under the DLMP has been studied. In [26], regarding the DLMP as the bidding price of MGs and clearing price of the DSO, a bi-level model was built and a bidding strategy was proposed for MGs to minimize their operation cost and maintain the secure operation of the distribution system.

2.3.3 Guide DER planning

In general, DER planning focuses on minimizing both investment and long-term operating costs as well as satisfying system operational requirements, such as meeting the demand growth, providing sufficient reserve, and reducing power losses, typically from the perspective of a DSO or a utility [140]-[144]. However, with the liberalization of distribution systems, the new pricing mechanism can provide stakeholders with incentive market signals. Given the DLMP's spatial and temporal properties, private investors will be motivated to build DERs (e.g., renewable DGs, ESSs) at ideal sites with optimal sizes to maximize their profits. They become the primary decision-makers during the planning phase.

Some studies have investigated this new planning scenario. In [145], a game-based model for the multiperiod planning of MGs in a competitive market was presented. The best locations were first determined based on the weighted sum of the loss sensitivity factor

and voltage sensitivity factor, and then a bi-level model was used to find the best installation time and DER types. In a competitive market with specified candidate sites, Reference [146] selected the best sizes for renewable DGs and ESSs. In [147], an adaptive robust model for DER planning was proposed in which the 8760-hour operational conditions in each planning year were reduced to a solvable number. In [148], an exhaustive search approach was proposed to identify the most suitable WTs allocation and installation priority with fixed sizes. In [149], the DLMP was utilized to guide new line constructions and DER planning to maximize asset owners' profit. Reference [150] proposed that the DLMP can provide effective market signals for future unit investment in a deregulated distribution system. A two-stage stochastic bi-level programming model was formulated for investors to best site and size battery energy storage systems.

It should be noted that some of these studies [145]-[148] employed price signals to direct the DER planning, though none used a full-fledged DLMP algorithm. Nevertheless, they do supply some insights for this transition.

2.3.4 Improve system reliability

From the viewpoint of the DSO, the introduction of the DLMP is a promising method to improve the system operating condition. With proper incentive regulations, DERs have changed their consumption/generation behaviors as discussed in previous subsections. These changes in turn greatly benefit the distribution system, with the benefits including but not all limited to load shifting, peak shaving, reactive power support, renewable energy integration, carbon emission reduction, investment deferral, congestion, and voltage management [75][103][115]. The system stability and resilience are improved, which is aligned with the incentive compatibility.

In [151], the DLMP was used to reduce a network's power losses and emissions. In [81][97][98], the temporal characteristic of the DLMP was utilized to optimize the charging schedule of EVs to alleviate the congestion issue. In [99][133][152], the DLMP was proposed to guide household DR to prevent congestion. EVs and PVs were studied to prevent congestion in [153]. The DLMP was raised to a high value in these studies when congestion occurred, incentivizing EV and DR owners to lower their demands. A similar principle has been applied to improve the voltage profile. In [100], it was demonstrated

that the DLMP could also be very high when voltage constraints are binding. Thus, flexible HVAC and EV demands were shifted to low DLMP periods to alleviate the voltage violation. At the same time, DGs could increase their power production at these hours to improve their revenue. In the summers of 2020 and 2021, the California Independent System Operator (CAISO) advised consumers to turn off unnecessary appliances and defer the use of major appliances to alleviate the shortage of power supply, such as pre-cooling buildings before afternoon [154]. In a deregulated system, consumers will likely take the initiative to perform these price-responsive activities according to the time-varying DLMP.

2.4 Conclusions

DLMP-based distribution-level electricity markets provide an effective solution to managing large amounts of DERs and MGs. Many pioneering works have been done on this topic in recent years. Hence, a summary of the state-of-the-art research on this topic is necessary to promote future studies in this area. In this chapter, a general market-clearing model was first established, and various distribution-related operation constraints and model relaxation methods are summarized. Then, the state-of-the-art solution methods to solve the market clearing model is summarized. Further, various DLMP-related applications in distribution system operation and planning were discussed.

Chapter 3 Tri-level Scheduling Model Considering Residential Demand Flexibility of Aggregated HVACs and EVs under Distribution LMP

Residential loads, especially heating, ventilation and air conditioners (HVACs) and electric vehicles (EVs), have great potentials to provide demand flexibility which is an attribute of grid-interactive efficient buildings (GEB). Under this new paradigm, first, EV and HVAC aggregator models are developed in this chapter to represent the fleet of GEBs, in which the aggregated parameters are obtained based on a new approach of data generation and least squares parameter estimation (DG-LSPE), which can deal with heterogeneous HVACs. Then, a tri-level bidding and dispatching framework is established based on competitive distribution operation with distribution locational marginal price (DLMP). The first two levels form a bilevel model to optimize the aggregators' payment and to represent the interdependency between load aggregators and the distribution system operator (DSO) using DLMP, and the third level is to dispatch the optimal load aggregation to all residents by the proposed priority list-based demand dispatching algorithm. Finally, case studies on a modified IEEE 33-Bus system illustrate three main technical reasons of payment reduction due to demand flexibility: load shift, DLMP step changes, and power losses. They can be used as general guidelines for better decision-making for future planning and operation of demand response programs.

3.1 Introduction

Inspired by the smart grid concept, at the generation side, the deployment of distributed generators (DGs), such as photovoltaic (PV), microturbine (MT) and wind turbine (WT), has been increasing in the past decades in distribution systems [1]. Meanwhile, at the load side, industrial and commercial customers are encouraged to participate in demand response (DR) programs. The proliferation of all these types of distributed energy resources (DERs) makes the distribution system more flexible and active [8]. Also, the advanced metering infrastructure like bilateral smart meter facilitates the information exchange between DERs and the distribution system operator (DSO) [3]. With this background, it is

believed that DERs are driving the transition from a passive distribution system to a market-based one that aims to achieve the optimal allocation of all DERs in the distribution system [10].

In the transmission level market, locational marginal price (LMP) has been widely implemented by ISOs, such as PJM, New York ISO, ISO-New England, etc. [51]. In general, the LMP obtained by the DCOPF consists of energy and congestion components. However, congestion rarely occurs in the distribution network due to its radial topology. Furthermore, the high R/X ratio and voltage drop are typical characteristics of the distribution network, but the transmission-level LMP model does not include these components. All these show that LMP is not appropriate in the distribution network. In the research community, some previous works are extending LMP to distribution locational marginal price (DLMP). In [52], DLMP is developed in a distribution system. In [36] [54], DSO determines DLMP based on generation offers and load bids by clearing the market. Refs. [8] and [26] integrate the voltage component for DLMP and LMP, respectively. Ref. [55] provides an interval prediction for the DLMP considering the uncertainty of renewables. All these works show that DLMP can reflect characteristics of operation and electricity pricing information in the distribution system. Thus, DLMP can be naturally considered as a price signal to incentivize consumers to adjust their loads to save electricity bills.

According to [159], heating, ventilation and air conditioners (HVACs) account for 45% of average summer peak-day loads. Also, the building's characteristic of thermal storage provides great demand flexibility by shedding and shifting HVAC load because the indoor temperature does not change fast due to thermal inertia [4][160]. Together with electric vehicles (EVs) that have electricity storages, they are the ideal residential DR candidates to provide demand flexibility which is an attribute of grid-interactive efficient buildings (GEB).

Appropriate price signals can efficiently guide consumers to change their consumption patterns. This is beneficial to both consumers and the distribution system. Previous studies of the residential DR in response to price signals can be categorized into two groups based on the existence of the completely competitive distribution level market.

1) No such a market: time of use (TOU), critical peak pricing (CPP), peak time rebate (PTR), and real-time pricing (RTP) are the commonly used electricity rates. They are usually pre-determined and fixed, and in a mandatory manner [59]. In [60], the authors design a Smart Home Controller strategy to maximize customer economic saving with the adoption of TOU. The survey of a CPP experiment in California [61] shows a statistical response of residential loads to the CPP. Rational consumer behavior in a PTR mechanism is investigated in [62]. [63] studies the optimal precooling of HVACs under time-varying electricity prices. [64] proposes a dynamic DR control strategy to adjust the set-point temperature of HVACs according to RTP. [33] presents an alternating direction method of multipliers (ADMM)-based residential DR management strategy.

2) With a completely competitive market: the works in [161] proposes an optimal bidding strategy for the load serving entity to profitably bid aggregated DR in the day ahead wholesale market. In [97][98], DLMP is utilized to optimize the EV charging schedule to alleviate the congestion issue. In [99][133], DLMP considering distribution congestion price is proposed to guide the DR to prevent congestion. These studies show the effectiveness of DLMP in congestion management. However, the power losses are usually too high to be neglected due to the high R/X ratio, and the voltage is critical for the reliable operation of a distribution system, DLMP should be able to reflect these costs. In addition, compared with the broad DR concept, proper integration with the actual HVAC/EV models is highly necessary for industrial deployment. Also, as a participant in a competitive market, residential loads integrated at a large scale can affect DLMP. Thus, residents have the motivation to consume electricity strategically to minimize their electricity bills, possibly via an aggregator.

Based on these considerations, this chapter focuses on reducing residents' electricity bills by proposing a novel tri-level model based on DLMP. The first level is to minimize residents' electricity payment by optimizing aggregated residential HVAC/EV schedules according to DLMP in the second level. The second level is to clear the day-ahead distribution market and integrate power losses and voltage constraints in DLMP. Since the first two levels are coupled, they are solved by reformulating it as a single level mathematical programming with equilibrium constraints (MPEC) by Karush-Kuhn-Tucker

(KKT) optimality conditions and then mixed-integer linear programming (MILP) by the big-M method [162]. Once the optimal aggregated HVAC/EV schedule is obtained, the third level is solved to dispatch all participating residents based on the aggregated schedule. The main contributions are as follows:

- The HVAC aggregator and EV aggregator models are developed on behalf of end users. In particular, a data generation and least-square parameter estimation (DG-LSPE) algorithm is applied to obtain the aggregated parameters of heterogeneous HVACs, which differs from the literature which assumes homogeneous HVACs.
- A tri-level model is proposed for aggregators to manage the individual residents and to minimize the electricity payment as well as maintain the secure and economic operation of the distribution system. This is achieved in a competitive distribution market with DLMP as the electricity rate, which is different from many other works assuming fixed rates or time-differentiated but pre-defined rates.
- The analysis and results demonstrate and validate three main reasons, DLMP step changes, load shifts, and power loss reductions, which contribute to the payment saving for residential demands in a competitive DLMP market. Also, it is discovered that the step change pattern in DLMP can be caused by binding voltage constraints which have not been previously observed in the transmission-level LMP markets.

The rest of this chapter is organized as follows. Section 3.2 describes the three-layer day-ahead distribution market structure and market participants including EV aggregator, HVAC aggregator, and DGs. Section 3.3 proposes the tri-level optimization model and presents the solution methods. Case studies in Section 3.4 demonstrate the effectiveness of the proposed model and analyze both economic and operational benefits of flexible demand. Section 3.5 concludes the chapter.

3.2 Structure And Participants of Distribution-Level Electricity Market

This section describes the structure of the distribution-level electricity market and models of different participants.

3.2.1 Market Structure

In general, an individual resident is not eligible to participate in the market directly due to the complex market rules, strict participation requirements [32], and heavy calculation burden [33]. To address these challenges, aggregators have emerged to serve as intermediaries between these residents and DSO to provide demand flexibility. The structure of the three-layer distribution-level electricity market is illustrated in Figure 3.1.

3.2.2 EV Aggregator

For the sake of simplicity, EV aggregators are assumed to locate at the same nodes with charging stations, and there are limited charging piles in each charging station. Thus, aggregated EV charging and discharging power are limited by this constraint. Here, the EV aggregator is modeled as the summation of all EVs.

$$E_{i,t+1} = E_{i,t} + \eta^{C} P_{i,t}^{C} - 1/\eta^{D} \, P_{i,t}^{Dri} \tag{3.1}$$

$$SOC_i^{E,\min} \cdot E_i^{R} \le E_{i,t+1} \le SOC_i^{E,\max} \cdot E_i^{R} \tag{3.2}$$

$$0 \le P_{i,t}^{C} \le P_i^{C,\max} \tag{3.3}$$

$$E_{i,t=0} \le E_{i,t=T} \tag{3.4}$$

$$\sum_{t=1}^{T} P_{i,t}^{Dri} = \sum_{j=1}^{N_i^e} e_j^d \cdot d_j \tag{3.5}$$

where (3.1) represents the energy of EV aggregator *i*, assuming all EVs have the same charging and discharging efficiency, (3.2) represents the state of charge (SOC) limits, (3.3) is the charging power limits, (3.4) ensures the total charging energy is no less than the total discharging energy over one day, (3.5) describes the driving consumption constraints, the sum of the energy consumption of individual EVs should be equal to that of aggregator model. $P_i^{C,max}$, E_i^{R} and $E_{i,t=0}$ are obtained as follows.

$$P_i^{C,\max} = \sum_{j=1}^{N_i^{piles}} p_j^{C} \tag{3.6}$$

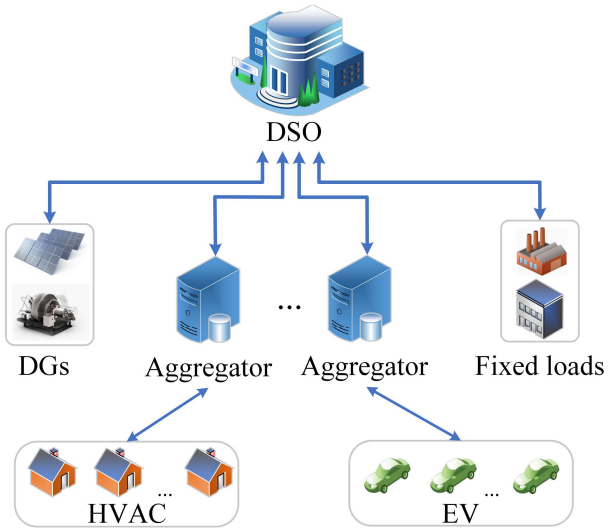


Figure 3.1. Three-layer day-ahead distribution-level electricity market.

$$E_i^R = \sum_j^{N_i^e} E_j^{rated} \tag{3.7}$$

$$E_{i,t=0} = \sum_j^{N_i^e} E_{j,t=0} \tag{3.8}$$

3.2.3 HVAC Aggregator

1) Single HVAC: For simplicity, the first-order thermal transfer function is utilized to model a building's dynamic indoor temperature [4]. Thus, each HVAC in cooling mode can be modeled with the following equations:

$$\theta_{j,t+1} = a_j \theta_{j,t} + b_j \theta_{out,t} + g_j u_{j,t} \tag{3.9}$$

$$\theta^{\min} \le \theta_{j,t+1} \le \theta^{\max} \tag{3.10}$$

where $a_j = 1 - 1/C_j R_j$, $b_j = 1/C_j R_j$, $g_j = -\eta^H P^{rated} 1/C_j$.

2) HVAC aggregator: Different from the analytical HVAC aggregation which assumes a homogeneous collection of HVACs [163], this chapter supposes that HVACs are heterogeneous to ensure the diversity of individual buildings. Here, based on a typical house with parameters R_A and C_A, Gaussian distribution is applied to generate R_j and C_j to simulate physical differences among buildings. Then, a least squares-based approach, Algorithm 1, is proposed to estimate aggregated parameters. After that, the HVAC aggregator's thermal equation is modeled and the corresponding operation constraints are presented below.

$$\tilde{\theta}_{i,t+1} = \tilde{a}_i \tilde{\theta}_{i,t} + \tilde{b}_i \theta_{out,t} + \tilde{g}_i \tilde{u}_{i,t} \tag{3.11}$$

$$P_{i,t}^H = \tilde{u}_{i,t} \cdot N_i^h \cdot P^{rated} \tag{3.12}$$

$$\theta^{\min} \le \tilde{\theta}_{i,t+1} \le \theta^{\max} \tag{3.13}$$

$$syn_i^{\min} \le \tilde{u}_{i,t} \le syn_i^{\max} \tag{3.14}$$

$$-\Delta u_i^{dr} \le \tilde{u}_{i,t+1} - \tilde{u}_{i,t} \le \Delta u_i^{ur} \tag{3.15}$$

$$SOC_i^{H,\min} \le SOC_{i,t} \le SOC_i^{H,\max} \tag{3.16}$$

where (3.11) represents the dynamic temperature of the HVAC aggregator, $\tilde{\theta}_{i,t} = \sum_{j=1}^{N_i^h} \theta_{j,t} \Big/ N_i^h$, $\tilde{u}_{i,t} = \sum_{j=1}^{N_i^h} u_{j,t} \Big/ N_i^h$, $\tilde{u}_{i,t}$ is approximated as a continuous variable in [0,

1], (3.12) is to obtain the active power of HVAC aggregator, (3.13) is comfortable temperature constraint, (3.14) is synchronicity constraint which limits the number of HVACs to be turned ON at the same period, (3.15) is ramp up/down constraint to limit the state transfer speed of HVACs, (3.16) is energy constraint to reduce the probability of all HVACs centering at the temperature boundaries [164] to improve the load dispatching performance. The $SOC_{i,t}$ is formulated as:

$$SOC_{i,t} = \frac{\sum_{j=1}^{N_i^h}\left(\theta_{\max} - \theta_{j,t}\right)}{N_i^h\left(\theta_{\max} - \theta_{\min}\right)} = \frac{\theta_{\max} - \tilde{\theta}_{i,t}}{\theta_{\max} - \theta_{\min}} \tag{3.17}$$

3) DG-LSPE: The HVAC control strategy plays an important role in the simulation of HVACs. Priority list control [165], a direct and effective control strategy, is utilized to control the state transformation of HVACs. Based on this, a DG-LSPE algorithm is designed to determine $\tilde{a}_i$, $\tilde{b}_i$ and $\tilde{g}_i$. Because every HVAC aggregator uses the same estimation algorithm, subscript i is neglected and procedures are described in Table 3.1. In this algorithm, we define $\boldsymbol{A}\boldsymbol{x} = \boldsymbol{c}$, $\boldsymbol{A} = \left[\boldsymbol{A}_{\tilde{u}=0.1},...,\boldsymbol{A}_{\tilde{u}=1}\right]^T$, $\boldsymbol{c} = \left[\boldsymbol{c}_{\tilde{u}=0.1},...,\boldsymbol{c}_{\tilde{u}=1}\right]^T$, $\boldsymbol{A}_{\tilde{u}=k} = \left[\left[\tilde{\theta}_1, \theta_{out,1}, \tilde{u}=k\right];...;\left[\tilde{\theta}_T, \theta_{out,T}, \tilde{u}=k\right]\right]$, $\boldsymbol{x} = \left[\tilde{a}, \tilde{b}, \tilde{g}\right]^T$, $\boldsymbol{c}_{\tilde{u}=k} = \left[\tilde{\theta}_2,...,\tilde{\theta}_{T+1}\right]^T$.

3.2.4 DG Models

According to the active or reactive power output and control strategy, most DGs fall into synchronous machines, inverter-based machines, and var compensation devices. For simplicity, three typical representatives are included.

MT is a synchronous machine-based DG. Its output power should satisfy the physical constraints and the power factor requirement [8]. In this chapter, α_i is set to 0.95.

$$P_{i,t}^{MT,\min} \le P_{i,t}^{MT} \le P_{i,t}^{MT,\max} \tag{3.18}$$

$$0 \le Q_{i,t}^{MT} \le P_{i,t}^{MT} \tan(\arccos\alpha_i) \tag{3.19}$$

PV is an inverter-based generator that can both absorb or generate reactive power. The power factor range is [α_i lagging, α_i leading].

Table 3.1. Proposed DG-LSPE algorithm.

Algorithm 1:	DG-LSPE
Input	HVACs' initial indoor temperatures $\theta_{j,t=0}$
Output	Aggregated parameters $\tilde{a}$, $\tilde{b}$, $\tilde{g}$
1	**Generate a data set:** Simulate the dynamic indoor temperatures of N^h buildings in a whole day;
2	Generate R_j and C_j for N^h buildings according to Gaussian distribution;
3	**for** $\tilde{u}$ =0.1: 0.1: 1 **do**
4	**for** t = 1: 1: T **do**
5	Get the number of devices to be turned on: $N_{on} = N^h \cdot \tilde{u}$;
6	Choose the top N_{on} HVACs to form the ON list ($u_{j,t}$ = 1) according to the descending order of $\theta_{j,t\text{-}1,}$ and the rest form the OFF list ($u_{j,t}$ = 0);
7	**for** j = 1, … N^h **do**
8	Update $\theta_{j,t}$ by (3.9);
9	**end for**
10	Calculate average temperature $\tilde{\theta}_t$, and store [$\tilde{\theta}_t$, $\theta_{out,t}$, $\tilde{u}$] and $\tilde{\theta}_{t+1}$ separately;
11	**end for**
12	**end for**
13	**Least squares parameter estimation:**
14	Obtain the aggregated parameters:
15	$\boldsymbol{x} = \left(\boldsymbol{A}^T \boldsymbol{A}\right)^{-1} \boldsymbol{A}^T \boldsymbol{c}$

$$0 \le P_{i,t}^{PV} \le P_{i,t}^{PV,fore} \tag{3.20}$$

$$-P_{i,t}^{PV} \tan(\arccos \alpha_i) \le Q_{i,t}^{PV} \le P_{i,t}^{PV} \tan(\arccos \alpha_i) \tag{3.21}$$

Static Var compensator (SVC) is induced to help maintain the voltage due to three attributes: 1) can generate or absorb reactive power, 2) output power can be adjusted continuously, 3) a good tradeoff between cost and performance [8].

$$Q_{i,t}^{SVC,\min} \le Q_{i,t}^{SVC} \le Q_{i,t}^{SVC,\max} \tag{3.22}$$

3.3 Tri-level Model

As discussed in the previous section, aggregators and the DSO are different entities with different interests, meanwhile, an aggregator's load demand and the system DLMP are coupled variables, which means any change in one variable will cause changes in the other one and vice versa. Therefore, a bilevel model is formulated to represent this relationship. Next, since the aggregator and residents follow a vertical dispatcher-receiver structure, the third level model will allocate the demand to all participating residents after the aggregator's optimal load demand is determined.

3.3.1 First Level

The first level is to minimize aggregators' power purchasing costs while satisfying comforts and charging requirements.

$$\min \sum_{t \in T} \left(\sum_{i \in H} \pi_{i,t}^{p} \cdot P_{i,t}^{H} + \sum_{i \in E} \pi_{i,t}^{p} \cdot P_{i,t}^{C} \right) \tag{3.23}$$

$$s.t.\ Constraints\ (3.1) - (3.5), (3.11) - (3.17) \tag{3.24}$$

3.3.2 Second Level

The second level is a market clearing model which has the objective to minimize system generation cost while maintaining all operational constraints. Note that the power congestion constraint is neglected in this study because congestion rarely happens in real distribution systems with radial topologies.

$$\min \sum_{t\in T}\left(\sigma_{S,t}^{p}\cdot P_{S,t}^{G}+\sigma_{S,t}^{q}\cdot \widehat{Q}_{S,t}^{G}+\sum_{i\in G}\left(\sigma_{i,t}^{p}\cdot P_{i,t}^{G}+\sigma_{i,t}^{q}\cdot \widehat{Q}_{i,t}^{G}\right)\right) \quad (3.25)$$
$$where\ G=\{PV,MT,SVC\}$$

$$s.t.\ \sum_{i\in\{S,G\}}P_{i,t}^{G}-\sum_{i\in B}P_{i,t}^{D}-\sum_{i\in H}P_{i,t}^{H}-\sum_{i\in E}P_{i,t}^{C}-P_{t}^{loss}=0:\lambda_{t}^{p},\forall t\in T \quad (3.26)$$

$$\sum_{i\in\{S,G\}}Q_{i,t}^{G}-\sum_{i\in B}Q_{i,t}^{D}-Q_{t}^{loss}=0:\lambda_{t}^{q},\forall t\in T \quad (3.27)$$

$$V_{j,t}=V_{1,t}+\sum_{i\in B}Z_{j,i}^{p}\left(P_{i,t}^{G}-P_{i,t}^{D}-P_{i,t}^{H}-P_{i,t}^{C}\right)+\sum_{i\in B}Z_{j,i}^{q}\left(Q_{i,t}^{G}-Q_{i,t}^{D}\right) \quad (3.28)$$

$$V^{\min}\le V_{j,t}\le V^{\max}:\omega_{j,t}^{v,\min},\omega_{j,t}^{v,\max},\forall j\in B,\forall t\in T \quad (3.29)$$

$$P_{i,t}^{G,\min}\le P_{i,t}^{G}\le P_{i,t}^{G,\max}:\omega_{i,t}^{p,\min},\omega_{i,t}^{p,\max},\forall i\in S,\forall t\in T \quad (3.30)$$

$$Q_{i,t}^{G,\min}\le Q_{i,t}^{G}\le Q_{i,t}^{G,\max}:\omega_{i,t}^{q,\min},\omega_{i,t}^{q,\max},\forall i\in S,\forall t\in T \quad (3.31)$$

$$(3.18)(3.20):\omega_{i,t}^{p,\min},\omega_{i,t}^{p,\max},\forall i\in\{MT,PV\},\forall t\in T \quad (3.32)$$

$$(3.19)(3.21)(3.22):\omega_{i,t}^{q,\min},\omega_{i,t}^{q,\max},\forall i\in\{G\},\forall t\in T \quad (3.33)$$

$$-Q_{i,t}^{G}\le\widehat{Q}_{i,t}^{G},Q_{i,t}^{G}\le\widehat{Q}_{i,t}^{G}:\kappa_{i,t}^{-},\kappa_{i,t}^{+},\forall i\in\{S,G\},\forall t\in T \quad (3.34)$$

where (3.26) and (3.27) represent the active and reactive power balance constraints, the substation is regarded as a generator with a large capacity; (3.28) is the voltage expression derived from linearized power flow for distribution (LPF-D) [36], in which Z^p and Z^q are matrices of nodal voltage change with respect to net power injections that can be derived from [36][166]; (3.29) is the voltage limit, Node 1 is the reference bus that connects to the substation; (3.30) - (3.31) are generators' active and reactive power output limits; in (3.34), $\widehat{Q}_{i,t}^{G}=\left|Q_{i,t}^{G}\right|$ since both absorbing and generating reactive power will induce cost [8]. The power loss and power loss factors are obtained by the loss factors for distribution (LF-D) in [36], then the power loss is linearized by Taylor's series:

$$P_{t}^{loss}\approx P_{t}^{loss*}+\sum_{i\in B}\frac{\partial P_{t}^{loss}}{\partial P_{i,t}^{G}}\left(\Delta P_{i,t}^{G}-\Delta P_{i,t}^{D}\right)+\sum_{i\in B}\frac{\partial P_{t}^{loss}}{\partial Q_{i,t}^{G}}\left(\Delta Q_{i,t}^{G}-\Delta Q_{i,t}^{D}\right) \quad (3.35)$$

$$Q_{t}^{loss}\approx Q_{t}^{loss*}+\sum_{i\in B}\frac{\partial Q_{t}^{loss}}{\partial P_{i,t}^{G}}\left(\Delta P_{i,t}^{G}-\Delta P_{i,t}^{D}\right)+\sum_{i\in B}\frac{\partial Q_{t}^{loss}}{\partial Q_{i,t}^{G}}\left(\Delta Q_{i,t}^{G}-\Delta Q_{i,t}^{D}\right) \quad (3.36)$$

where $\Delta P_{i,t}^{G} = P_{i,t}^{G} - P_{i,t}^{G*}$ represents the power difference between two close operating points, $\Delta Q_{i,t}^{G}$, $\Delta P_{i,t}^{D}$ and $\Delta Q_{i,t}^{D}$ have similar expressions.

The decision variables are $P_{i,t}^{H}$ and $P_{i,t}^{C}$ in the first level objective function, $P_{S,t}^{G}$, $Q_{S,t}^{G}$, $P_{i,t}^{MT}$, $Q_{i,t}^{MT}$, $P_{i,t}^{PV}$, $Q_{i,t}^{PV}$, and $Q_{i,t}^{SVC}$ in the second level objective function. The Lagrange function can be written as follows.

$$\begin{aligned} L = & \sum_{t\in T}\left(\sigma_{S,t}^{p}\cdot P_{S,t}^{G} + \sigma_{S,t}^{q}\cdot \widehat{Q}_{S,t}^{G} + \sum_{i\in G}\left(\sigma_{i,t}^{p}\cdot P_{i,t}^{G} + \sigma_{i,t}^{q}\cdot \widehat{Q}_{i,t}^{G}\right)\right) \\ & - \sum_{t\in T}\lambda_{t}^{p}\left(\sum_{i\in\{S,G\}} P_{i,t}^{G} - \sum_{i\in B} P_{i,t}^{D} - \sum_{i\in H} P_{i,t}^{H} - \sum_{i\in E} P_{i,t}^{C} - P_{t}^{loss}\right) \\ & - \sum_{t\in T}\lambda_{t}^{q}\left(\sum_{i\in\{S,G\}} Q_{i,t}^{G} - \sum_{i\in B} Q_{i,t}^{D} - Q_{t}^{loss}\right) \\ & - \sum_{t\in T}\sum_{j\in B}\omega_{j,t}^{v,\min}\left(V_{j,t} - V^{\min}\right) - \sum_{t\in T}\sum_{j\in B}\omega_{j,t}^{v,\max}\left(V^{\max} - V_{j,t}\right) \\ & - \sum_{t\in T}\sum_{i\in\{S,G\}}\omega_{i,t}\cdot g_{i,t}(x) \end{aligned} \tag{3.37}$$

where $g_{i,t}(x)$ represents the power output limits in (3.30) - (3.34).

The active DLMP is the first-order partial derivative of the Lagrange function with respect to the active power. Based on (3.37), the active DLMP can be expressed as the following expression:

$$\pi_{i,t}^{p} = \frac{\partial L}{\partial P_{i,t}^{D}} = \lambda_{t}^{p} + \lambda_{t}^{p}\cdot\frac{\partial P_{t}^{loss}}{\partial P_{i,t}^{D}} + \lambda_{t}^{q}\cdot\frac{\partial Q_{t}^{loss}}{\partial P_{i,t}^{D}} + \sum_{j\in B}\left(\omega_{j,t}^{v,\min} - \omega_{j,t}^{v,\max}\right)Z_{j,i}^{p} \tag{3.38}$$

3.3.3 Third Level

The third level is to dispatch the optimal load demand for all individual end residents. Based on the priority list control, the load dispatching algorithm for HVACs, with a 10-min time step (i.e., K time slots in one hour, K = 6) to achieve more accurate control, is presented in Table 3.2.

To make the EV charging close to practical situations, the individual EV is assumed to charge every few days with a longer charging time until reaching its upper SOC boundary. Based on this assumption, load dispatching for EV is similar to Algorithm 2, thus it is not shown here.

Table 3.2. HVAC aggregator load dispatching algorithm.

Algorithm 2: HVAC Load Dispatching for Aggregator i	
Input	Optimal load $P_{i,t}^{H}$, HVACs' initial conditions and parameters $\theta_{j,t=0}$, R_j, C_j
Output	ON/OFF status $u_{s,t}$, dispatching error $e_{i,t}$
1	**for** $t = 1, \ldots T$ **do**
2	**for** $k = 1, \ldots K$ **do**
3	$s = (t\text{-}1)\cdot K + k$;
4	Get the number of devices to be turned on: $N_{k,on} = \text{round}(P_{i,t}^{H}/P^{rated})$;
5	Update the ON/OFF status $u_{j,s}$ based on $N_{k,on}$ and the descending order of $\theta_{j,s\text{-}1}$;
6	**for** $j = 1, \ldots N_i^h$ **do**
7	Update $\theta_{j,s}$ by (3.9);
8	**if** $\theta_{j,s} > \theta^{max}$, **then** $u_{j,s} = 1$, $N_{k,on} = N_{k,on} + 1$
9	**if** $\theta_{j,s} < \theta^{min}$, **then** $u_{j,s} = 0$, $N_{k,on} = N_{k,on} - 1$
10	**end for**
11	**end for**
12	Calculate the accumulated dispatching error at t: $e_{i,t} = \left(P_{i,t}^{H} - \sum_{k=1}^{K} P^{rated} \cdot N_{k,on} / K \right) / P_{i,t}^{H} \cdot 100\%$
13	**end for**

3.3.4 Solution Method of the Coupled First Two Levels

The first level and the second level are coupled due to the inter-dependent variables $P_{i,t}^{H}$, $P_{i,t}^{C}$ and $\pi_{i,t}^{p}$. The solution method for such a coupled bilevel model is described below.

1) MPEC model: Since the second level is a linear programming problem, the KKT optimality conditions are the necessary and sufficient conditions of its optimal solution. Therefore, the bi-level optimization problem is transformed into a single level problem with the KKT conditions added to the first level. The new model is a single-level MPEC as:

$$\min\ (3.23) \tag{3.39}$$

$$s.t.\ \ Constraints\ (3.24),(3.26)-(3.28) \tag{3.40}$$

$$\begin{aligned}&\sigma_{i,t}^{p}-\lambda_{t}^{p}\left(1-\frac{\partial P_{t}^{loss}}{\partial P_{i,t}^{G}}\right)+\lambda_{t}^{q}\frac{\partial Q_{t}^{loss}}{\partial P_{i,t}^{G}}-\sum_{j\in B}\left(\omega_{j,t}^{v,\min}-\omega_{j,t}^{v,\max}\right)Z_{j,i}^{p}\\&-\omega_{i,t}^{p,\min}+\omega_{i,t}^{p,\max}=0,\quad \forall i\in\{S,G\},\forall t\in T\end{aligned} \tag{3.41}$$

$$\sigma_{i,t}^{q}-\kappa_{i,t}^{-}-\kappa_{i,t}^{+}=0,\quad \forall i\in\{S,G\},\forall t\in T \tag{3.42}$$

$$\begin{aligned}&\lambda_{t}^{p}\frac{\partial P_{t}^{loss}}{\partial Q_{i,t}^{G}}-\lambda_{t}^{q}\left(1-\frac{\partial Q_{t}^{loss}}{\partial Q_{i,t}^{G}}\right)-\sum_{j\in B}\left(\omega_{j,t}^{v,\min}-\omega_{j,t}^{v,\max}\right)Z_{j,i}^{q}\\&-\omega_{i,t}^{q,\min}+\omega_{i,t}^{q,\max}-\kappa_{i,t}^{-}+\kappa_{i,t}^{+}=0,\quad \forall i\in\{S,G\},\forall t\in T\end{aligned} \tag{3.43}$$

$$0\le\omega_{j,t}^{v,\min}\perp\left(V_{j,t}-V^{\min}\right)\ge 0,\quad \forall j\in B,\forall t\in T \tag{3.44}$$

$$0\le\omega_{j,t}^{v,\max}\perp\left(V^{\max}-V_{j,t}\right)\ge 0,\quad \forall j\in B,\forall t\in T\text{`} \tag{3.45}$$

$$0\le\omega_{i,t}^{p,\min}\perp\left(P_{i,t}^{G}-P_{i,t}^{G,\min}\right)\ge 0,\quad \forall i\in\{S,G\},\forall t\in T \tag{3.46}$$

$$0\le\omega_{i,t}^{p,\max}\perp\left(P_{i,t}^{G,\max}-P_{i,t}^{G}\right)\ge 0,\quad \forall i\in\{S,G\},\forall t\in T \tag{3.47}$$

$$0\le\omega_{i,t}^{q,\min}\perp\left(Q_{i,t}^{G}-Q_{i,t}^{G,\min}\right)\ge 0,\quad \forall i\in\{S,G\},\forall t\in T \tag{3.48}$$

$$0\le\omega_{i,t}^{q,\max}\perp\left(Q_{i,t}^{G,\max}-Q_{i,t}^{G}\right)\ge 0,\quad \forall i\in\{S,G\},\forall t\in T \tag{3.49}$$

$$0\le\kappa_{i,t}^{-}\perp\left(\widehat{Q}_{i,t}^{G}+Q_{i,t}^{G}\right)\ge 0,\quad \forall i\in\{S,G\},\forall t\in T \tag{3.50}$$

$$0\le\kappa_{i,t}^{+}\perp\left(\widehat{Q}_{i,t}^{G}-Q_{i,t}^{G}\right)\ge 0,\quad \forall i\in\{S,G\},\forall t\in T \tag{3.51}$$

where (3.41) - (3.43) are stationary conditions, (3.44) - (3.51) are complementary slackness conditions which deal with the inequality constraints. The formulation of $0 \le \omega_{i,t} \perp h_{i,t}(x) \ge 0$ means both $\omega_{i,t}$ and $h_{i,t}(x)$ are no less than 0, and satisfy $\omega_{i,t} \cdot h_{i,t}(x) = 0$.

Noted that (3.48) and (3.49) including all DGs are written in the same generic expression for simplicity. They can be further elaborated based on constraints (3.19), (3.21) and (3.22) for specific DGs.

$$
\begin{aligned}
&\sum_{t\in T}\left(\sum_{i\in H}\pi_{i,t}^{p}\cdot P_{i,t}^{H}+\sum_{i\in E}\pi_{i,t}^{p}\cdot P_{i,t}^{C}\right)\\
&=\sum_{t\in T}\sum_{i\in H}\left(\lambda_t^{p}+\lambda_t^{p}\frac{\partial P_t^{loss}}{\partial P_{i,t}^{D}}+\lambda_t^{q}\frac{\partial Q_t^{loss}}{\partial P_{i,t}^{D}}+\sum_{j\in B}(\omega_{j,t}^{v,\min}-\omega_{j,t}^{v,\max})Z_{j,i}^{p}\right)P_{i,t}^{H}\\
&+\sum_{t\in T}\sum_{i\in E}\left(\lambda_t^{p}+\lambda_t^{p}\frac{\partial P_t^{loss}}{\partial P_{i,t}^{D}}+\lambda_t^{q}\frac{\partial Q_t^{loss}}{\partial P_{i,t}^{D}}+\sum_{j\in B}(\omega_{j,t}^{v,\min}-\omega_{j,t}^{v,\max})Z_{j,i}^{p}\right)P_{i,t}^{C}\\
&=\sum_{t\in T}\left(\sigma_{S,t}^{p}\cdot P_{S,t}^{G}+\sigma_{S,t}^{q}\cdot\hat{Q}_{S,t}^{G}+\sum_{i\in G}\left(\sigma_{i,t}^{p}\cdot P_{i,t}^{G}+\sigma_{i,t}^{q}\cdot\hat{Q}_{i,t}^{G}\right)\right)\\
&-\left\{\begin{array}{l}
\sum_{t\in T}\lambda_t^{p}\left(\sum_{i\in B}\left(1+\frac{\partial P_t^{loss}}{\partial P_{i,t}^{D}}\right)P_{i,t}^{D}+\sum_{i\in B}\frac{\partial P_t^{loss}}{\partial Q_{i,t}^{D}}Q_{i,t}^{D}+P_t^{loss0}\right)\\
+\sum_{t\in T}\lambda_t^{q}\left(\sum_{i\in B}\left(1+\frac{\partial Q_t^{loss}}{\partial Q_{i,t}^{D}}\right)Q_{i,t}^{D}+\sum_{i\in B}\frac{\partial Q_t^{loss}}{\partial P_{i,t}^{D}}P_{i,t}^{D}+Q_t^{loss0}\right)\\
+\sum_{t\in T}\sum_{j\in B}\omega_{j,t}^{v,\min}\left(V^{\min}-V_{1,t}+\sum_{i\in B}Z_{j,i}^{p}P_{i,t}^{D}+\sum_{i\in B}Z_{j,i}^{q}Q_{i,t}^{D}\right)\\
-\sum_{t\in T}\sum_{j\in B}\omega_{j,t}^{v,\max}\left(V^{\max}-V_{1,t}+\sum_{i\in B}Z_{j,i}^{p}P_{i,t}^{D}+\sum_{i\in B}Z_{j,i}^{q}Q_{i,t}^{D}\right)\\
+\sum_{t\in T}\sum_{i\in\{S,G\}}\left(\omega_{i,t}^{p,\min}P_{i,t}^{G,\min}-\omega_{i,t}^{p,\max}P_{i,t}^{G,\max}\right)\\
+\sum_{t\in T}\sum_{i\in\{S,G\}}\left(\omega_{i,t}^{q,\min}Q_{i,t}^{G,\min}-\omega_{i,t}^{q,\max}Q_{i,t}^{G,\max}\right)
\end{array}\right\}
\end{aligned}
\tag{3.52}
$$

2) MILP model: From the above formulation, it can be seen that MPEC is a nonlinear model with nonlinearities in two parts: 1) $\pi_{i,t}^{p}\cdot P_{i,t}^{H}+\pi_{i,t}^{p}\cdot P_{i,t}^{C}$ in the objective function (3.39); 2) complementary slackness constraints (3.44) - (3.51). The methods for dealing with these nonlinearities are described below [167][168].

For $\pi^{p}_{i,t} \cdot P^{H}_{i,t} + \pi^{p}_{i,t} \cdot P^{C}_{i,t}$, the strong duality theory states that the primal problem and its dual problem have the same optimal value if the problem is convex. The original second level is a linear optimization model, thus (3.39) can be substituted by (3.52).

For the complementary constraints, the big-M approach is adopted. Then, each formulation of $0 \le \omega_{i,t} \perp h_{i,t}(x) \ge 0$ can be substituted as:

$$0 \le \omega_{i,t} \le M_{i,t} v_{i,t}, 0 \le h_{i,t}(x) \le M_{i,t}(1 - v_{i,t}) \tag{3.53}$$

where $M_{i,t}$ is a big number and $v_{i,t}$ is a binary variable.

Now, the completed MILP model is presented as:

$$\min (3.52) \tag{3.54}$$

$$s.t.\ \textit{Constraints}\ (3.40) - (3.43), (3.53) \tag{3.55}$$

After the MILP model is solved**,** Algorithm 2 is applied to dispatch the aggregated load to all end residents, as discussed in the previous Subsection 3.3.3.

It should be noted that the proposed tri-level approach is based on a competitive DLMP model, which is aligned with the increasing interests in industrial practices toward competitive distribution or retail markets [169].

3.4 Case Studies

In this section, the proposed tri-level model is tested on a modified IEEE 33-Bus distribution system. Simulations are performed on a laptop with Intel (R) Core™ i7-8650U 2.11GHz CPU, and 16GB RAM. The coding work is carried out in MATLAB R2019a, YALMIP and CPLEX 12.9.

3.4.1 IEEE 33-Bus Distribution System

The topology of the modified IEEE 33-Bus system is shown in Figure 3.2, in which two 500 kW PVs are installed at nodes 12 and 28, respectively; two 500 kW MTs are located at nodes 18 and 33, respectively; and three 500 kVar SVCs are installed at nodes 10, 16 and 30, respectively. The parameters of a single EV and HVAC, EV aggregators and HVAC aggregators are shown in Table 3.3 and Table 3.4 respectively. Here, it is assumed that HVAC units in their corresponding aggregator have similar thermal parameters, and have a big difference with HVAC units in other aggregators.

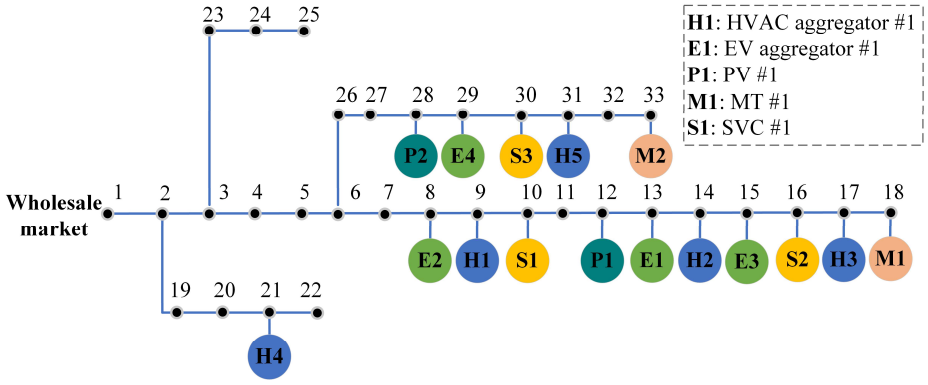


Figure 3.2. Modified IEEE 33-Bus system.

Table 3.3. Parameters of single EV and HVAC.

EV	Parameter	HVAC	Parameter
E_j^{rated}	N (50, 1^2) (kWh)	P^{rated}	5 (kW)
p_j^C	N (7.2, 0.2^2) (kW)	R_j	N (R_A, 0.2^2) (°C/kW)
e_j^d	N (0.23, 0.01^2) (kWh/mile)	C_j	N (C_A, 0.2^2) (kWh/°C)
η^C/η^D	0.98	η^H	3
$E_{j,t=0}$	$E_j^{rated} \cdot U$ [0.4,0.6] (kWh)	θ^{max}	21 (°C)
d_j	U [30, 50] (miles)	θ^{min}	19 (°C)

Table 3.4. Parameters of Aggregators.

Aggregators	Parameter	Typical Value
HVAC Aggregators	Location	Node 9, 11, 17, 21, 31
	Number of HVACs	160, 160, 320, 320, 320
	R_A (°C/kW)	3.96, 3.6, 3.96, 4.32, 4.68
	C_A (kWh/°C)	3.75
	Synchronization limit	[0.1, 0.7]
	SOC limit	[0.15, 0.8]
	Ramp up/down rate	0.1
EV Aggregators	Location	Node 8, 13, 15, 29
	Number of EVs	300, 300, 300, 300
	Number of chargers	25, 25, 25, 25
	SOC limit	[0.2, 0.8]

The day-ahead active LMP of the wholesale market, scaled forecasted mean power output of PV and scaled fixed load are obtained from PJM [170], as depicted in Figure 3.3 (a). The system peak fixed load is 3.715MW + j1.78MVar. The active power bidding prices of PV and MT are set at \$15/MWh and \$70/MWh, respectively. Reactive LMP, reactive power prices of PV, MT and SVC are set to 0. The outdoor temperature on a summer day is shown in Figure 3.3 (b).

Aggregators can choose to participate in the market or not. If they participate in the market, their loads become flexible; otherwise, they are only price takers and are regarded as fixed loads. Five cases with different flexible load ratios are established in Table 3.5. The flexible load ratio is defined as the maximum ratio of flexible load divided by the system load.

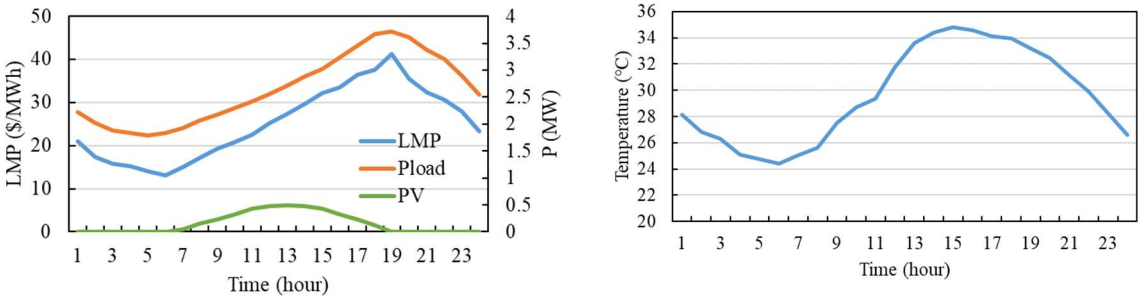
3.4.2 Analysis of Case 1

1) DLMP and voltage profiles: The DLMP and voltage profiles of all nodes for 24 hours are shown in Figure 3.4. It can be seen in Figure 3.4 (a) that DLMP increases as the node number increases. This is due to the radial topology and power loss is a component of DLMP. The farther away from Node 1, the larger the power loss factor will be. Figure 3.4 (b) shows that voltages are maintained within the voltage boundary.

2) HVAC aggregator: H2's load demand and its corresponding buildings' indoor temperatures are shown in Figure 3.5. From Figure 3.5 (a), it can be seen that load shift happens. Combined with Figure 3.4 (a), it is revealed that incentivized by DLMP, an aggregator consumes more energy before price arises. According to the indoor temperatures in Figure 3.5 (b), this load shifting is the precooling for HVACs.

3) EV aggregator: E1's load profile under Case 0 and Case 1 are shown in Figure 3.6 (a). In Case 0, it is assumed EV owners choose to charge during daytime and charging power is evenly distributed at different hours to simplify the charging process. While in Case 1, the EV aggregator makes the optimal charging schedule, such that the charging process happens during 1:00 - 14:00 and 23:00 - 24:00 when DLMP is not high.

4) Load dispatching error analysis: The load dispatching errors of H2 and E1 in Case 1 are shown in Figure 3.6 (b). The accumulated dispatching errors (i.e., $e_{i,t}$ in Step 12, Algorithm 2) are within ±3% at each hour.

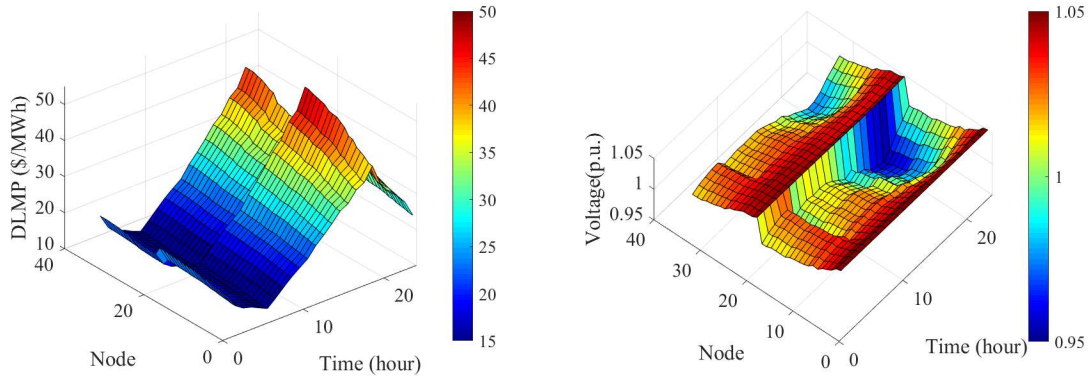


(a) LMP, fixed load and PV profiles (b) Outdoor temperature

Figure 3.3. LMP, fixed load, PV, and outdoor temperature on a summer day.

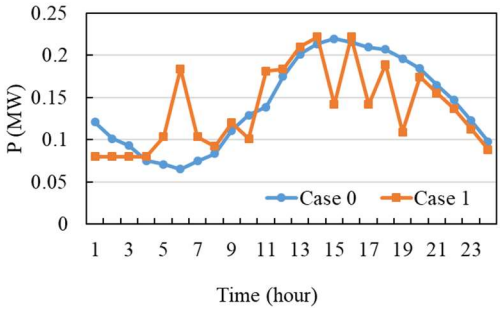
Table 3.5. Different Cases.

Case	Flexible ratio	Load composition		
		Flexible load	Total fixed loads	
0	0%	None	H1 - H5, E1 - E4	Other fixed loads
1	10%	H1 - H2, E1	H3 - H5, E2 - E4	Other fixed loads
2	20%	H1 - H3, E1 - E2	H4 -H5, E3 - E4	Other fixed loads
3	30%	H1 - H4, E1 - E3	H5, E4	Other fixed loads
4	40%	H1 - H5, E1 - E4	None	Other fixed loads

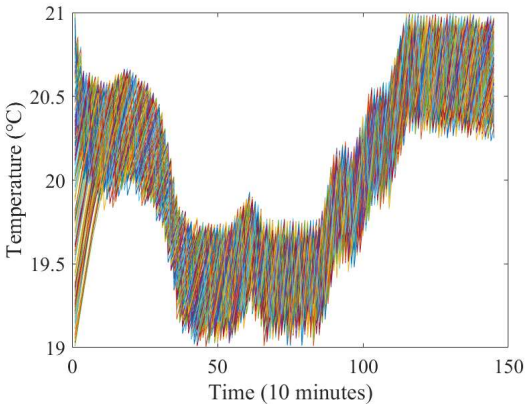


(a) DLMP (b) Voltage

Figure 3.4. Spatial and temporal distribution of DLMPs and voltages.

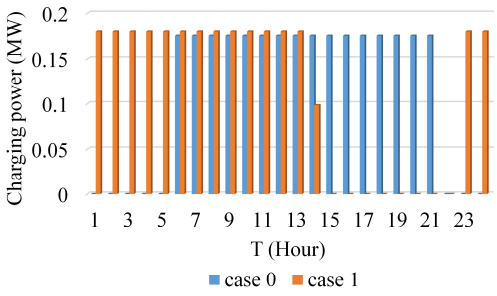


(a) Load demand

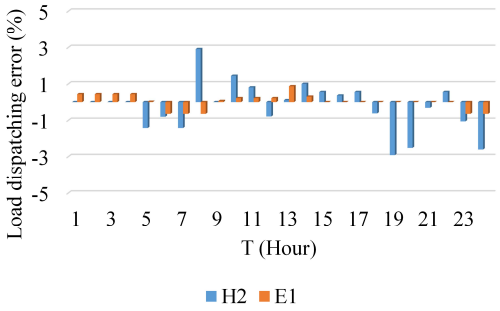


(b) Indoor temperatures of H2

Figure 3.5. H2's load demand and indoor temperatures.



(a) Load profile of E1



(b) Load dispatching error

Figure 3.6. Load profile of E1 and load dispatching error of H2 and E1.

In Table 3.3, parameters of individual HVACs and EVs are assumed to follow the Gaussian distribution. To provide an in-depth analysis of the impacts of Gaussian distribution on the dispatching error, additional simulations are shown next. For simplicity, we may have HVAC as the research target, and assume that R_j and C_j satisfy the following Gaussian parameters: 1) no skewness (Sk=0), different standard deviation (σ); 2) fixed standard deviation (σ=0.2), different skewness. The simulation results are shown in Table 3.6.

From Table 3.6, it can be observed that: 1) with the increase of standard deviation, the absolute maximum dispatch error in the 24-hour time scale is in an increasing trend. This indicates that a higher difference level will result in a higher maximum absolute dispatch error, however, it is under 8% which is acceptable; 2) when fixing the standard deviation and varying the skewness of the Gaussian distribution, the scale of the maximum absolute dispatch error keeps at the same level, this shows that the skewness does not impact the dispatch error. This is reasonable because Algorithm 1 is a generic method that can deal with the skewness distribution and can reflect the skewness into the aggregated parameters and then Algorithm 2 can well dispatch the load.

It should be noted that the different max $|e_{i,t}|$ in each simulation is due to the random sampling of R_j and C_j according to the different Gaussian distribution parameters.

3.4.3 Operation and Economic Analysis under Different Flexible Load Ratios

System load profiles under different flexible ratios in 24 hours are shown in Figure 3.7, and voltage profiles at t = 19:00 are shown in Figure 3.8. From Figure 3.7 and Figure 3.8, it can be observed that with the increase of flexible load ratio, peak load is further reduced, more load is shifted from peak hours to off-peak hours, and the voltage profiles at peak hours are improved.

Part of the numerical results are shown in Table 3.7, in which P^* refers to the system load at t = 19:00; V^* refers to the voltage at node 18 at t = 19:00; GC is the total system generation cost; Enr., Vol., and Loss are energy cost, voltage support cost and power loss cost of HVAC and EV payment, respectively. When comparing Case 4 with Case 0, it can be seen that peak load, total generation cost, total HVAC and EV electricity payment are reduced by 22.05%, 6.87% and 23.84%, and voltage is improved by 3.90%, respectively.

Table 3.6. Absolute maximum dispatch error under different gaussian parameters.

σ (Sk=0)	0	0.1	0.2	0.3	0.4	0.5	0.6
max $\lvert e_{i,t} \rvert$	2.438	2.064	2.663	1.996	2.573	3.778	7.109
Sk (σ=0.2)	-0.6	-0.4	-0.2	0	0.2	0.4	0.6
max $\lvert e_{i,t} \rvert$	1.671	2.174	2.595	2.663	3.34	2.283	3.625

Table 3.7. Benefits of DLMP to the system.

Case	Operation		GC ($)	Economy			
	P^* (MW)	V^* (p.u.)		HVAC and EV Payment ($)			
				Total	Enr.	Vol.	Loss
0	5.76	0.95	2712.4	1163.7	964.8	40.2	158.7
1	5.43	0.954	2660.3	1043.8	931.5	0	112.2
2	5.06	0.973	2609.5	976.5	900.9	0	75.6
3	4.80	0.983	2568.3	932.3	870.7	0	61.7
4	4.49	0.987	2526.2	886.3	840.2	0	46.1

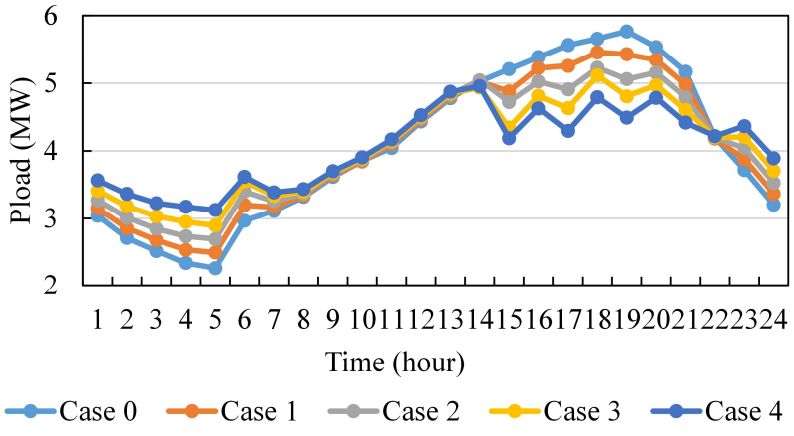


Figure 3.7. System load profiles under different flexible ratios.

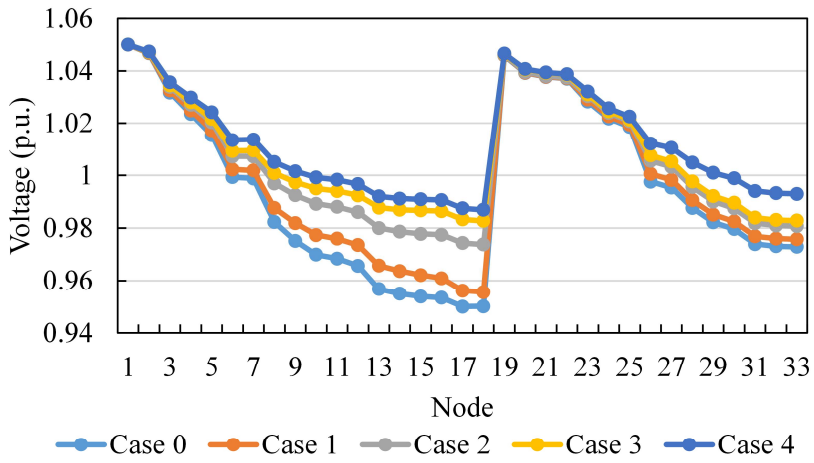


Figure 3.8. Voltage profiles of at t = 19:00 under different flexible ratios.

Due to load shift, the DSO reduces the cost of purchasing electricity from the wholesale market and the cost of scheduling peaking DG units (MT in this chapter) at high LMP hours. The analysis of HVAC and EV payment reduction is presented in detail in Subsection 3.4.4.

Regarding the computational aspects, in Case 4 with all HVACs and EVs are considered, the MILP formulation has 6698 constraints, 5697 continuous variables, and 2736 binary variables in total. The average calculation time of 10 simulation runs is 24.246s, where Algorithm 1 takes 0.035s, MILP takes 24.189s, and Algorithm 2 takes 0.022s. Since the MILP is a large-scale optimization problem, it takes much more calculational time than that of Algorithm 1 and Algorithm 2.

3.4.4 Economic Analysis under Different System Load Levels

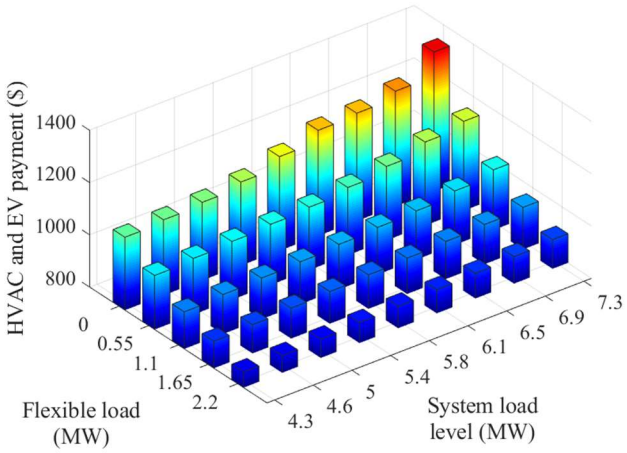
In this subsection, simulations are carried out to investigate the impacts of the system load level. The fixed load varies from 0.6 to 1.4 times the original fixed load shown in Figure 3.3. The number of HVACs and EVs are kept the same as in Table 3.4. The system load level is defined as the peak load in Case 0. As illustrated in Figure 3.9, the system load level ranges from 4.3 MW to 7.3 MW, the flexible load of the five cases is between 0 and 2.2 MW.

From Figure 3.9, we have three findings regarding the economic benefits from demand flexibility:

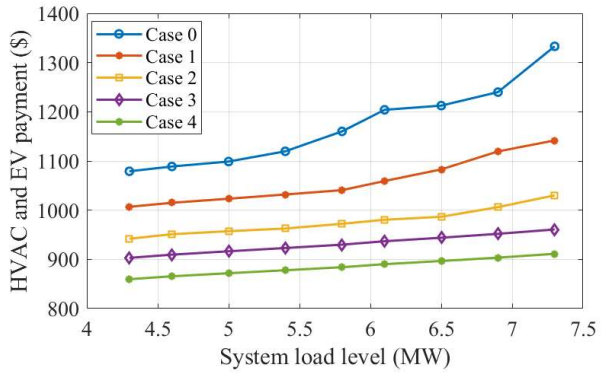
- **F1**: At the same system load level, a higher flexible load can significantly reduce the payment which has the same pattern as in Table 3.7.
- **F2**: With the same flexible load, HVACs and EVs payment increases as the system total load increases (i.e., fixed load increases).
- **F3**: In addition to **F2**, the increased payments between 4.3 and 7.3 MW system load levels are different for five cases. The increasing rates are 23.54%, 13.39%, 9.31%, 6.39%and 6.00%, respectively, which indicates a higher flexible load can slow down the payment increase rate. This is shown by the payment curves of the five cases in Figure 3.9 (b). The detailed increment can be found in Table 3.8.

Table 3.8. Payment increase and its decomposition between 4.3 and 7.3 MW system load level.

Case	ΔPayment ($)	Inc. ratio (%)	Decomposition ($)		
			ΔEnr.	ΔVol.	ΔLoss
0	253.99	23.54%	0	167.06	86.93
1	134.85	13.39%	0.39	62.58	71.89
2	87.92	9.31%	3.15	24.89	59.88
3	57.72	6.39%	2.4	0	54.69
4	51.55	6.00%	1.78	0	48.70



(a) HVAC and EV payment in the 3-dimension view



(b) HVAC and EV payment in the 2-dimension view

Figure 3.9. HVAC and EV payment versus different load levels with various flexible loads.

As equation (3.38) shows, DLMP consists of three parts: energy price, voltage support price and power loss price. Accordingly, HVAC and EV electricity payments can also be decomposed into three components as shown in Table 3.7 and Table 3.8. Based on observations from these two tables, the fundamental reasons of the three findings can be summarized as follows.

Load shifts: In general, if shifting loads from peak DLMP hours to off-peak DLMP hours, the energy cost can be reduced. Table 3.7 and the discussion in Subsection 3.4.3 demonstrate that with more flexible loads, the load-shifting quantity increases and energy cost decreases. This is an important reason for finding **F1**. Also, with the same flexible load and an increasing total system load, the load-shifting quantity stays almost the same. As can be found in Table 3.8, ΔEnr. is close to 0 for five cases, thus energy cost contributes little to the findings **F2** and **F3**.

DLMP step changes: To illustrate this, Figure 3.10 shows the DLMP at node 18 at t = 19:00 under different system load levels. The simulation for each case ends at its own operation capacity. It can be seen that DLMP spikes up at a certain load level. In this study, the step change of DLMP is similar to that of LMP in [171]. However, the difference is that the former is caused by the binding voltage limit while the latter is the binding congestion limit. Taking Case 0 as an example, when the system load is beyond 5.3 MW, DLMP has a sudden increase because the voltage limit at node 18 binds, and M1 is activated to support the voltage at node 18. The comparison in Table 3.7 and Table 3.8 clearly shows that at the same system load level, the more flexible loads, the less likely having binding voltage limits, thus less voltage support cost. More importantly, when the system load increases from 4.3 to 7.3 MW, Cases 0, 1 & 2 have a sharper increase than Cases 3 & 4 because DLMP step changes of Cases 0-2 come quicker as shown in Figure 3.10. This DLMP step change is a hidden reason related to all the findings **F1**~**F3**.

Power losses: As shown in Figure 3.10, before reaching the step change, DLMP has a slight but consistent increase which is because of power losses. Equation (3.38) shows that the power loss price is proportional to power loss factors, which are generally higher in peak hours than that in off-peak hours.

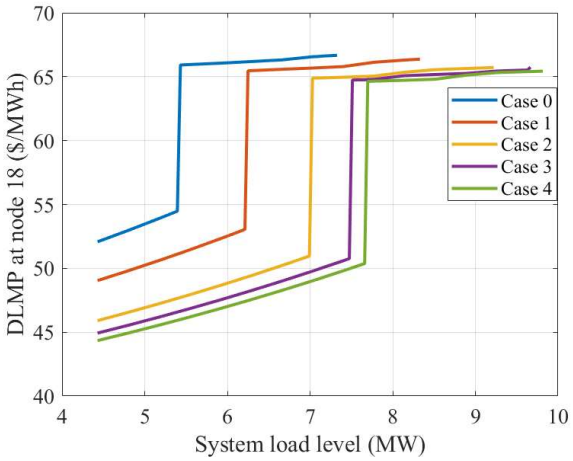


Figure 3.10. DLMP at node 18 with step changes under different system load levels.

Therefore, the loss prices in peak hours are higher than in off-peak hours, and the power loss cost can be reduced by load shifting as well. All three findings **F1**~**F3** are related to power losses.

The above three reasons can serve as general guidelines for decision-makers to carefully choose the appropriate time and location of HVACs and EVs to potentially gain high benefits.

3.5 Conclusions

In this chapter, DLMP is used as price signals to guide the electricity consumption of residential customers. In the day-ahead distribution market environment, a tri-level scheduling model is proposed to minimize residents' electricity bills. Two algorithms are designed to aggregate and dispatch individual customers. KKT optimality conditions, big-M method and strong duality theory are utilized to solve the coupled first two levels. Numerical studies draw the following conclusions:

- The proposed DG-LSPE algorithm can estimate the aggregated HVAC parameters under different Gaussian distribution parameters, and the collaboration with the subsequent load dispatching algorithm can control the dispatching error to a limited range.
- The tri-level scheduling model quantitively demonstrates the potential of operational and economic benefits for both the distribution system and aggregators, especially in different flexible load ratios.
- By the in-depth analysis of DLMP components and payment components, three generalized reasons leading to the benefit from flexible HVAC and EV demands are summarized, namely, load shifts, DLMP step changes, and power losses. This can be used by stakeholders for better decision-making.

Chapter 4 Tri-level Hybrid Interval-Stochastic Optimal Scheduling for Flexible Residential Loads under Multiple Uncertainties

Various building loads, such as heating, ventilation, and air conditioners (HVACs), electric water heaters (EWHs), and electric vehicles (EVs), can introduce opportunities for improving the flexibility of electricity consumption while satisfying the needs of building owners as well as benefiting the resilience of distribution system. To utilize such flexibility, a tri-level distribution market framework is established, including residential consumers, load aggregators (LAs), and the distribution system operator (DSO). The uncertainties from all three levels are considered. The random consumption behavior at the consumer level is modeled as a Gaussian noise that is also aggregated and transmitted to the LA level. The weather temperature in the LA level is forecasted as an interval, and the photovoltaic (PV) power in the market-clearing level is modeled by a set of power scenarios generated by Generative Adversarial Networks (GANs). Then, a hybrid interval-stochastic programming is proposed to transform the uncertain problems in the first two levels into deterministic ones. For real-time implementations, a rolling horizon optimization (RHO) scheme is employed to continuously optimize the power consumption based on the latest operating information. Finally, case studies on a modified IEEE 69-bus system validate the effectiveness of the proposed uncertainty modeling strategies and the RHO scheme.

4.1 Introduction

Grid-interactive efficient buildings (GEBs) have been receiving wide attention in recent years. They can introduce opportunities for improving the flexibility and efficiency of electricity consumption while satisfying the needs of building owners, as well as benefiting the distribution system [172].

Buildings account for over 70% of all U.S. electricity consumption. Among all residential loads, heating, ventilation, and air conditioners (HVACs), electric water heaters (EWHs), and electric vehicles (EVs) share most of the electricity consumption and have similar energy storage characteristics that render them high energy flexible loads [173].

Such characteristics make these building loads the research focus to satisfy grid requirements, such as load shifting, load shedding, frequency regulation [174], and voltage control [175][176].

On the other hand, to keep pace with the deregulation process in distribution systems, the concept of a distribution market or local market has been proposed as well as the distribution locational marginal price (DLMP) [36]. As an extension to the transmission-level locational marginal price (LMP), DLMP can reflect the physical characteristics and operating conditions of distribution systems. It can also provide price incentives for residential loads to improve their energy efficiency.

However, individual end-users do not have the capability to participate directly in the electricity market. Thus, load aggregators (LAs) are proposed as agents to aggregate a large number of residential loads to provide grid-scale services and participate in electricity markets.

Multiple studies have been conducted to aggregate individual end-users into LA. The aggregator in [33] is modeled as an intermediary to transmit load quantity and dual variables between end-users and utility. Reference [4] averages the first-order heat transfer function of all HVACs/EWHs to obtain the aggregator's heat transfer function and validate its effectiveness. The authors in [177] aggregate thermostatically controlled loads to provide synthetic inertia and primary frequency regulation services to the grid. In [100], a data generation and least-square parameter estimation (DG-LSPE) algorithm is proposed to estimate aggregator parameters for heterogeneous HVACs.

In the research community, to model the interdependence between LAs and a distribution system operator (DSO), one commonly used formulation is bilevel programming. In this formulation, LAs and the DSO are at different levels and have respective objectives. They are coupled due to the coupled variables, such as the DLMP and load quantity. In [83], LAs and the DSO are represented using a bilevel formulation with the objectives to minimize payments for LAs in the upper level and minimize the operating cost for the DSO in the lower level. References [81][178] follow a similar bilevel structure but for different types of aggregators, such as EV aggregators, virtual power plants, and microgrids. In [100], a three-layer hierarchical market structure is established

to integrate the three entities: residential consumers, LAs, and the DSO. Based on these aforementioned studies, two essential enhancements can be made.

1) Uncertainties can impact system flexibility and induce unexpected economic losses. In [180] [181], stochastic and robust optimizations, respectively, are utilized to handle the uncertainty of renewable energy and electricity price respectively. However, only one or two uncertainty sources are considered. In a three-layer structure, uncertainties can come from multiple sources, such as renewable energies, temperature forecasts, and consumer behaviors. Thus, the appropriate modeling of these uncertainties as well as maintaining tractability are of high value.

2) As time goes by, more latest operating and forecast information are updated. Thus, the day-ahead (DA) power consumption schedule may not be optimal. In order to benefit from the released information over time and improve the radical or conservative DA schedule, the schedule can be modified in real-time (RT).

In this context, this chapter adopts our previous proposed three-layer market structure in [100], which is to minimize the total electricity cost for residential consumers as well as maintain occupant comfort and the distribution system operating constraints. Then, several enhancements and new models are proposed to address uncertainties. The detailed motivations and technical contributions can be summarized as:

- Uncertainties from all three layers and multiple sources are modeled, namely, the PV power output, outdoor temperature, and the random consumption behaviors of individual users. Especially, for the first time, the uncertainty of individual users is aggregated and transmitted to the load aggregator level.
- A feasible hybrid interval-stochastic bilevel programming model is established to simulate the interdependence of the first two levels with uncertainties, in which state-space representations and Generative Adversarial Networks (GANs) are utilized to handle the uncertainties in the first level and second level, respectively.
- A rolling horizon optimization (RHO) scheme is employed to continuously optimize the consumption schedule for consumers based on the latest operating information which makes the tri-level model schedule realistic.

The rest of this chapter is organized as follows. Section 4.2 describes the modeling and uncertainty sources for the various residential loads. Section 4.3 establishes the aggregator model and the three-level optimization model. Uncertainty handling and solution methods are presented in Section 4.4. Section 4.5 introduces the RHO scheme. Case studies are performed in Section 4.6 to verify the proposed modeling methods and analyze the impact of uncertainties. Finally, Section 4.7 concludes the chapter.

4.2 Modeling Residential Loads with Uncertainties

In this section, the mathematical models and uncertainty sources of the various building loads are presented, including HVACs, EWHs, and EVs.

4.2.1 HVAC Model

An HVAC maintains the room temperature through a thermostat. The first-order thermal transfer function is utilized to model a building's varied indoor temperature [6]. However, the indoor temperature may not strictly follow this heat transfer function due to the inherent inaccuracy and householder's random behavior, e.g., opening windows, cooking, having guests in the house, etc. To account for such uncertainties, a Gaussian noise is added to the original HVAC model. Without loss of generality, we consider a cooling HVAC mode in this study. Then, each HVAC can be modeled with the following expressions:

$$\theta^h_{i,j,t+1} = a^h_{i,j}\theta^h_{i,j,t} + b^h_{i,j}\tilde{\theta}^{out}_t + g^h_{i,j}u^h_{i,j,t} + \tilde{\varepsilon}^h_{i,j,t} \tag{4.1}$$

$$\theta^{h,\min} \le \theta^h_{i,j,t} \le \theta^{h,\max} \tag{4.2}$$

where $\theta^h_{i,j,t}$ is the indoor temperature of building j in aggregator i at time t; $\tilde{\theta}^{out}_t$ is the forecasted outdoor temperature; $u^h_{i,j,t}$ is the ON/OFF status of HVAC j at time t; $\tilde{\varepsilon}^h_{i,j,t}$ is the Gaussian noise, $\tilde{\varepsilon}^h_{i,j,t} \sim N\left(0, \left(\alpha^h\theta^{h,mid}\right)^2\right)$, $\theta^{h,mid} = \left(\theta^{h,\min} + \theta^{h,\max}\right)/2$, α^h is a scaler to control the uncertainty level; $a^h_{i,j}$, $b^h_{i,j}$, $g^h_{i,j}$ are the coefficients of the thermal function of HVAC j; $\theta^{h,\min}$ and $\theta^{h,\max}$ are the consumer's preferable temperature boundaries. The typical parameters of a single HVAC can be found in [100].

4.2.2 EWH Model

For an EWH, the uncertainty is the forecasted water usage. Then, similar to HVAC, each EWH can be represented as:

$$\theta^{w}_{i,j,t+1} = a^{w}_{i,j}\theta^{w}_{i,j,t} - b^{w}_{i,j}\tilde{W}^{D}_{i,j,t} + g^{w}_{i,j}u^{w}_{i,j,t} + c^{w}_{i,j} \tag{4.3}$$

$$\theta^{w,\min} \le \theta^{w}_{i,j,t} \le \theta^{w,\max} \tag{4.4}$$

where $\theta^{w}_{i,j,t}$ is the water temperature in the water tank; $b^{w}_{i,j}$ represents the temperature drop when consuming 1-liter hot water; $g^{w}_{i,j}$ is the water temperature rise after heating 1 hour; $u^{w}_{i,j,t}$ is the ON/OFF status of the EWH; $\tilde{W}^{D}_{i,j,t} \sim N\left(\bar{W}^{D}_{i,j,t}, \left(\alpha^{w}\bar{W}^{D}_{i,j,t}\right)^2\right)$, $\bar{W}^{D}_{i,j,t}$ is the forecasted water usage at time *t*, α^{w} is a scaler. The derivation of these parameters can be found in Appendix B.

4.2.3 EV Model

For an EV, the uncertainty is the forecasted daily driving distance. Then, the state-of-charge (SOC) of an EV can be presented as:

$$E_{i,j,t+1} = E_{i,j,t} - P^{c}_{i,j,t}\Big/\sqrt{\eta_i} + \sqrt{\eta_i}P^{dri}_{i,j,t} \tag{4.5}$$

$$SOC^{E,\min}\cdot E^{r}_{i,j} \le E_{i,j,t+1} \le SOC^{E,\max}\cdot E^{r}_{i,j} \tag{4.6}$$

$$\sum\nolimits_{t=1}^{T} P^{dri}_{i,j,t} = e^{d}\cdot\tilde{d}_{i,j} \tag{4.7}$$

where $E_{i,j,t}$ is the stored energy of EV *j* in aggregator *i*; $P^{c}_{i,j,t}$ is the charging power; $P^{dri}_{i,j,t}$ is the driving consumption power; η_i is the round-trip efficiency; $E^{r}_{i,j}$ is the rated energy of EV *j*; $SOC^{E,\min}$ and $SOC^{E,\max}$ are the consumer's preferable SOC boundaries; e^{d} is the driving energy consumption per mile, $\tilde{d}_{i,j} \sim N\left(\bar{d}_{i,j}, \left(\alpha^{e}\bar{d}_{i,j}\right)^2\right)$, $\bar{d}_{i,j}$ is the forecasted daily driving distance, α^{e} is a scaler. The typical parameters of a single EV can be found in [100].

4.3 Day-Ahead: Tri-Level Market Framework

In this section, a tri-level market framework is established to represent the relationship between residential consumers, LAs, and the DSO. In this structure, each entity has its

objective and operating constraints which are considered separately. The LA collects all operation and preference information from the contracted residential users. Then, the aggregated model is established and the LA bids in the distribution market. After collecting bids and offers from all market participants, the DSO clears the market and broadcasts generation/load capacity and DLMP to all participants. At last, LAs dispatch the optimal aggregated loads to end-users.

4.3.1 First Level: LAs

The first level minimizes the total electricity payments for LAs that include HVAC aggregator, EWH aggregator, and EV aggregator.

$$\min \sum_{t\in T}\left(\sum_{i\in H}\pi_{i,t}^{p}\cdot P_{i,t}^{H}+\sum_{i\in W}\pi_{i,t}^{p}\cdot P_{i,t}^{W}+\sum_{i\in E}\pi_{i,t}^{p}\cdot P_{i,t}^{C}\right) \tag{4.8}$$

where $\pi_{i,t}^{p}$ is the DLMP; $P_{i,t}^{H}$, $P_{i,t}^{W}$ and $P_{i,t}^{C}$ are respectively the power consumption of HVAC, EWH and EV aggregators; H, W and E are the set of aggregators.

1) HVAC aggregator model: By utilizing the DG-LSPE algorithm proposed in [100], the HVAC aggregator's thermal transfer function in a cooling mode can be obtained. The operating constraints are shown below, the uncertainties are the forecasted outdoor temperature $\tilde{\theta}_{t}^{out}$ and the aggregated noise $\tilde{\varepsilon}_{i,t}^{h}$.

$$\theta_{i,t+1}^{h}=a_{i}^{h}\theta_{i,t}^{h}+b_{i}^{h}\tilde{\theta}_{t}^{out}+g_{i}^{h}u_{i,t}^{h}+\tilde{\varepsilon}_{i,t}^{h} \tag{4.9}$$

$$\theta^{h,\min}\le\theta_{i,t}^{h}\le\theta^{h,\max} \tag{4.10}$$

$$syn_{i}^{h,\min}\le u_{i,t}^{h}\le syn_{i}^{h,\max} \tag{4.11}$$

$$-\Delta u_{i}^{h,dr}\le u_{i,t+1}^{h}-u_{i,t}^{h}\le\Delta u_{i}^{h,ur} \tag{4.12}$$

$$SOC_{i,t}^{h}=\frac{\theta^{h,\max}-\theta_{i,t}^{h}}{\theta^{h,\max}-\theta^{h,\min}} \tag{4.13}$$

$$SOC_{i}^{h,\min}\le SOC_{i,t}^{h}\le SOC_{i}^{h,\max} \tag{4.14}$$

$$P_{i,t}^{H}=u_{i,t}^{h}\cdot N_{i}^{h}\cdot P^{h,rated} \tag{4.15}$$

$$\tilde{\theta}_{t}^{out}\in\left[\underline{\theta}_{t}^{out},\overline{\theta}_{t}^{out}\right]=\left[\theta_{t}^{out}-\alpha^{temp}\theta_{t}^{out},\theta_{t}^{out}+\alpha^{temp}\theta_{t}^{out}\right] \tag{4.16}$$

where (4.9) represents the varied indoor temperature; $\theta_{i,t}^{h}$ is the indoor temperature of aggregator *i* at time *t*; a_i^h, b_i^h and g_i^h are the coefficients of the aggregator; $u_{i,t}^{h}$ is an approximate continuous variable in [0, 1] indicating the ON status ratio in HVAC aggregator *I*; $\tilde{\varepsilon}_{i,t}^{h}$ is the aggregated noise in the end users, $\tilde{\varepsilon}_{i,t}^{h} \sim N\left(0, \sigma_{i,t}^{h\,2}\right)$, $\sigma_{i,t}^{h} = \sqrt{\sum_{j=1}^{N_i^h}\left(\alpha^h \theta^{mid}\right)^2} \Big/ N_i^h$; N_i^h is the number of HVACs in aggregator *i*, (4.10) is the indoor temperature setting boundary; (4.11) is the synchronous constraint which limits the number of HVACs to be turned ON at time step *t*; (4.12) is the ramp constraints to limit the status transformation rate; (4.13) and (4.14) are energy constraints to avoid the situation that indoor temperatures centering at the setting temperature boundaries [182]; (4.15) is to obtain the active power of the HVAC aggregator; (4.16) is the outdoor temperature forecasting interval; and α^{temp} is a scaler to control the uncertainty interval.

2) EWH aggregator model: Similar to the HVAC aggregator model, the EWH aggregator model and operating constraints are shown as follows:

$$\theta_{i,t+1}^{w} = a_i^w \theta_{i,t}^{w} - b_i^w \tilde{W}_{i,t}^{D} + g_i^w u_{i,t}^{w} + c_i^w \tag{4.17}$$

$$\theta^{w,\min} \le \theta_{i,t}^{w} \le \theta^{w,\max} \tag{4.18}$$

$$syn_i^{w,\min} \le u_{i,t}^{w} \le syn_i^{w,\max} \tag{4.19}$$

$$-\Delta u_i^{w,dr} \le u_{i,t+1}^{w} - u_{i,t}^{w} \le \Delta u_i^{w,ur} \tag{4.20}$$

$$SOC_{i,t}^{w} = \frac{\theta^{w,\max} - \theta_{i,t}^{w}}{\theta^{w,\max} - \theta^{w,\min}} \tag{4.21}$$

$$SOC_i^{w,\min} \le SOC_{i,t}^{w} \le SOC_i^{w,\max} \tag{4.22}$$

$$P_{i,t}^{W} = u_{i,t}^{w} \cdot N_i^w \cdot P^{w,rated} \tag{4.23}$$

where the aggregated coefficients a_i^w, b_i^w, g_i^w and c_i^w can also be obtained by the DG-LSPE algorithm; the uncertainty is the aggregated water usage $\tilde{W}_{i,t}^{D}$, $\tilde{W}_{i,t}^{D} \sim N\left(\bar{W}_{i,t}^{D}, \sigma_{i,t}^{w\,2}\right)$, $\bar{W}_{i,t}^{D} = \sum_{j=1}^{N_i^w} \bar{W}_{i,j,t}^{D} \Big/ N_i^w$, $\sigma_{i,t}^{w} = \sqrt{\sum_{j=1}^{N_i^w}\left(\alpha^w \bar{W}_{i,j,t}^{D}\right)^2} \Big/ N_i^w$, and N_i^w is the number of EWHs in aggregator *i*.

3) EV aggregator model: The EV aggregator and operating constraints can be modeled as:

$$E_{i,t+1} = E_{i,t} + \sqrt{\eta_i} P_{i,t}^{C} - P_{i,t}^{Dri} \Big/ \sqrt{\eta_i} \tag{4.24}$$

$$SOC_i^{e,\min} \cdot E_i^R \le E_{i,t+1} \le SOC_i^{e,\max} \cdot E_i^R \tag{4.25}$$

$$0 \le P_{i,t}^{C} \le P_i^{C,\max} \tag{4.26}$$

$$E_{i,t=0} \le E_{i,t=T} \tag{4.27}$$

$$\sum_{t=1}^{T} P_{i,t}^{Dri} = e^d \tilde{d}_i \tag{4.28}$$

$$E_i^R = \sum_j^{N_i^e} E_{i,j}^r \tag{4.29}$$

where (4.24) is the energy of EV aggregator *i*; it is assumed all EVs have the same round-trip efficiency η_i; (4.25) represents the aggregator's SOC limits; (4.26) is the charging power limit; (4.27) ensures the total charging energy is no less than the total consumption energy; (4.28) describes the driving consumption power; (4.29) refers to the rated energy of an aggregator which equals to the summation of the rated energy of multiple EVs, the uncertainty is the aggregated daily driving distance $\tilde{d}_i, \tilde{d}_i \sim N\left(\overline{d}_i, \sigma_i^{e2}\right)$, $\overline{d}_i = \sum_{j=1}^{N_i^e} \overline{d}_{i,j}$, and $\sigma_i^e = \sqrt{\sum_{j=1}^{N_i^e} \left(\alpha^e \overline{d}_{i,j}\right)^2}$.

4.3.2 Second Level: DSO

In the second level, the DSO clears the market, its objective is to minimize the system's generation cost. The uncertainty is PV's power output $\tilde{P}_{i,t}^{PV}$.

$$\min \sum_{t \in T} \sum_{i \in G} c_{i,t} \cdot P_{i,t}^{G} \tag{4.30}$$

s.t.

$$\sum_{i \in G} P_{i,t}^{G} + \sum_{i \in PV} \tilde{P}_{i,t}^{PV} = \sum_{i \in B} P_{i,t}^{D} + \sum_{i \in H} P_{i,t}^{H} + \sum_{i \in W} P_{i,t}^{W} + \sum_{i \in E} P_{i,t}^{C} + P_t^{loss} : \lambda_t^p \tag{4.31}$$

$$\sum_{i \in G} Q_{i,t}^{G} = \sum_{i \in B} Q_{i,t}^{D} + Q_t^{loss} : \lambda_t^q \tag{4.32}$$

$$V^{\min} \le V_{sub,t} + \sum_{i\in B} Z^{p}_{j,i}\left(P^{G}_{i,t} + \tilde{P}^{PV}_{i,t} - P^{D}_{i,t} - P^{H}_{i,t} - P^{W}_{i,t} - P^{C}_{i,t}\right) + \sum_{i\in B} Z^{q}_{j,i}\left(Q^{G}_{i,t} - Q^{D}_{i,t}\right) \le V^{\max} : \omega^{v,\min}_{j,t}, \omega^{v,\max}_{j,t} \tag{4.33}$$

$$P^{G,\min}_{i,t} \le P^{G}_{i,t} \le P^{G,\max}_{i,t} : \omega^{p,\min}_{i,t}, \omega^{p,\max}_{i,t} \tag{4.34}$$

$$Q^{G,\min}_{i,t} \le Q^{G}_{i,t} \le Q^{G,\max}_{i,t} : \omega^{q,\min}_{i,t}, \omega^{q,\max}_{i,t} \tag{4.35}$$

$$\pi^{p}_{i,t} = \frac{\partial L}{\partial P^{D}_{i,t}} = \lambda^{p}_{t} + \left(\lambda^{p}_{t} \cdot \frac{\partial P^{loss}_{t}}{\partial P^{D}_{i,t}} + \lambda^{q}_{t} \cdot \frac{\partial Q^{loss}_{t}}{\partial P^{D}_{i,t}}\right) + \sum_{j\in B}\left(\omega^{v,\min}_{j,t} - \omega^{v,\max}_{j,t}\right) Z^{p}_{j,i} \tag{4.36}$$

where (4.31) and (4.32) are the active and reactive power balance constraints; $P^{G}_{i,t}$, $P^{D}_{i,t}$, $P^{H}_{i,t}$, $P^{W}_{i,t}$, $P^{C}_{i,t}$, P^{loss}_{t}, $Q^{G}_{i,t}$, $Q^{D}_{i,t}$ and Q^{loss}_{t} are the active/reactive generation/load/power loss respectively; (4.33) represents the voltage limit which is derived from linearized power flow for distribution (LPF-D) [36]; Z^{p} and Z^{q} are matrices of nodal voltage change to net power injections, where the substation is the reference bus that connects to the transmission system; (4.34) and (4.35) are generators' active and reactive power output limits; (4.36) is the expression of the DLMP which is derived from the Lagrangian function of the second level problem, it can be seen that the DLMP includes three components: the marginal energy price, the marginal loss price (including real and reactive power), and the marginal voltage support price; λ^{p}_{t}, λ^{q}_{t}, $\omega^{v,\min}_{j,t}$, $\omega^{v,\max}_{j,t}$, $\omega^{p,\min}_{i,t}$, $\omega^{p,\max}_{i,t}$, $\omega^{q,\min}_{i,t}$ and $\omega^{q,\max}_{i,t}$ are dual variables. The power loss is linearized by using the first order Taylor's series.

$$P^{loss}_{t} \approx P^{loss*}_{t} + \sum_{i\in B} \frac{\partial P^{loss}_{t}}{\partial P^{G}_{i,t}}\left(\Delta P^{G}_{i,t} - \Delta P^{D}_{i,t}\right) + \sum_{i\in B} \frac{\partial P^{loss}_{t}}{\partial Q^{G}_{i,t}}\left(\Delta Q^{G}_{i,t} - \Delta Q^{D}_{i,t}\right) \tag{4.37}$$

$$Q^{loss}_{t} \approx Q^{loss*}_{t} + \sum_{i\in B} \frac{\partial Q^{loss}_{t}}{\partial P^{G}_{i,t}}\left(\Delta P^{G}_{i,t} - \Delta P^{D}_{i,t}\right) + \sum_{i\in B} \frac{\partial Q^{loss}_{t}}{\partial Q^{G}_{i,t}}\left(\Delta Q^{G}_{i,t} - \Delta Q^{D}_{i,t}\right) \tag{4.38}$$

where power losses P^{loss*}_{t} and Q^{loss*}_{t}, power output $P^{G*}_{i,t}$ and $Q^{G*}_{i,t}$, and load demand $P^{D*}_{i,t}$ and $Q^{D*}_{i,t}$ refer to the power flow results at an initial operating point; $\frac{\partial P^{loss}_{t}}{\partial P^{G}_{i,t}}$ and $\frac{\partial P^{loss}_{t}}{\partial Q^{G}_{i,t}}$ are the partial derivatives of P^{loss}_{t} to bus injection $P^{G}_{i,t}$ and $Q^{G}_{i,t}$ at every bus and every time step, and they are opposite in sign with the partial derivatives of P^{loss}_{t} to bus demand $P^{D}_{i,t}$ and $Q^{D}_{i,t}$; $\Delta P^{G}_{i,t}$

$= P_{i,t}^{G} - P_{i,t}^{G^*}$ is the power difference between the to-be-determined operating point and the initial operating point; $\Delta Q_{i,t}^{G}$, $\Delta P_{i,t}^{D}$ and $\Delta Q_{i,t}^{D}$ can be expressed similarly.

The related linearization discussion can also be found in [36]. The main difference between [36] and this work is that P^D and Q^D are assumed constant in the former but considered flexible loads in this work. So $\Delta P_{i,t}^{D} = P_{i,t}^{D} - P_{i,t}^{D^*}$ is also one item in (4.37).

4.3.3 Third Level: Individual End Users

In the third level, each LA dispatches the corresponding optimal load obtained in the first level to individual end-users. The priority-control-based load dispatching algorithm for HVACs, EWHs, and EVs in [100] is used in this study for dispatching the end-users.

4.4 Uncertainty Modeling and Solution Methods

The proposed trilevel problem with uncertainties in each level is hard to solve directly. Thus, two methods are applied to transform the original problem into a tractable one. 1) Decoupling: the first two levels are within a bilevel structure, and they have a leader-follower structure with the third level. Thus, the trilevel problem can be decoupled and solved sequentially, which means the first two levels are solved first, then the optimal aggregated load is dispatched to individual consumers in the third level. 2) Uncertainty handling: to solve the bilevel problem with uncertainties, the first step is to transform the uncertainty models into the equivalent deterministic ones by interval or stochastic optimization. Then, mature bilevel solution methods can be used to solve the deterministic bilevel problems.

4.4.1 Uncertainty Handling

Interval optimization and stochastic programming are the two widely used uncertainty handling methods. How to handle uncertainties to ensure the solvability and maintain decision-maker's objective is a key point. In this chapter, in the first level, interval optimization is utilized to model the uncertainty of the forecasted temperature and the aggregated random power consumption behaviors to obtain the best and worst payment for aggregators. In the second level, stochastic programming is adopted to simulate the volatility of PV power output.

There are three considerations for these different handling strategies. 1) From the perspective of LAs in the first level, they may care more about the best and worst payment range rather than the expected payment, thus interval optimization is appropriate. 2) Based on the available PV historical data, possible PV scenarios can be generated, then stochastic modeling is more effective as a risk measure [183]. 3) Another advantage is that stochastic programming can maintain the convexity of the second level which ensures the bilevel problem is tractable.

1) Uncertainty transformation in the first level: State-space representation

The variable $\theta_{i,t}^{h}$ in (4.9) is a time-dependent variable, thus the state-space structure is proper to represent the dependent relationship. Constraint (4.9) can be written as below:

$$\boldsymbol{\theta} = \boldsymbol{A}^{-1}\left(\boldsymbol{B}\tilde{\boldsymbol{\theta}}^{out} + \boldsymbol{G}\boldsymbol{u} + \boldsymbol{C} + \tilde{\boldsymbol{\varepsilon}}\right) \tag{4.39}$$

where $\boldsymbol{A}$ is a diagonal matrix with diagonal elements 1 and sub-diagonal elements -a; $\boldsymbol{B}$ and $\boldsymbol{G}$ are diagonal matrices with diagonal elements b and g respectively; $\boldsymbol{C}$ is the vector with initial conditions, and $\boldsymbol{C} = [a\theta_0, 0, \ldots, 0]^{\mathrm{T}}$. By setting 95% confidence interval, the uncertainty interval is $\tilde{\boldsymbol{\varepsilon}} \in \left[-2\boldsymbol{\sigma}, 2\boldsymbol{\sigma}\right]$. Note that (4.39) is a general formulation of the indoor temperature for each HVAC aggregator.

Next, by merging constraints (4.9) and (4.10), we have:

$$\boldsymbol{\theta}^{\min} \le \boldsymbol{A}^{-1}\left(\boldsymbol{B}\tilde{\boldsymbol{\theta}}^{out} + \boldsymbol{G}\boldsymbol{u} + \boldsymbol{C} + \tilde{\boldsymbol{\varepsilon}}\right) \le \boldsymbol{\theta}^{\max} \tag{4.40}$$

The interval optimization model can be converted to an optimistic model and a pessimistic model [184]. The robust counterpart for the optimistic model is:

$$\boldsymbol{A}^{-1}\left(\boldsymbol{B}\underline{\boldsymbol{\theta}}_{out} + \boldsymbol{G}\boldsymbol{u} + \boldsymbol{C} + \underline{\boldsymbol{\varepsilon}}\right) \le \boldsymbol{\theta}^{\max} \tag{4.41}$$

$$\boldsymbol{\theta}^{\min} \le \boldsymbol{A}^{-1}\left(\boldsymbol{B}\overline{\boldsymbol{\theta}}_{out} + \boldsymbol{G}\boldsymbol{u} + \boldsymbol{C} + \overline{\boldsymbol{\varepsilon}}\right) \tag{4.42}$$

While the robust counterpart for the pessimistic model is:

$$\boldsymbol{A}^{-1}\left(\boldsymbol{B}\overline{\boldsymbol{\theta}}_{out} + \boldsymbol{G}\boldsymbol{u} + \boldsymbol{C} + \overline{\boldsymbol{\varepsilon}}\right) \le \boldsymbol{\theta}^{\max} \tag{4.43}$$

$$\boldsymbol{\theta}^{\min} \le \boldsymbol{A}^{-1}\left(\boldsymbol{B}\underline{\boldsymbol{\theta}}_{out} + \boldsymbol{G}\boldsymbol{u} + \boldsymbol{C} + \underline{\boldsymbol{\varepsilon}}\right) \tag{4.44}$$

Constraints (4.13) and (4.14) can be merged in the same way.

The state-space representation for EWHs and EVs can also be obtained in a similar way. Now, the uncertainties in the first level have been transformed into deterministic ones.

2) Uncertainty transformation in the second level: GANs scenario generation

To simulate the uncertainty of PV power output, a widely used approach is to generate a finite number of possible PV scenarios. Then, the second level becomes a stochastic programming problem.

In addition to the traditional probability-based scenario generation methods, a series of machine learning related methods have been proposed in power systems in recent years. In [185], the k-means, as an unsupervised learning method, is utilized to classify the historical data and reduce the number of the generated scenarios. In [186], the long short-term memory is proposed to characterize the stochasticity of the electricity price. GANs have been extended to generate power scenarios for renewable resources in [187][188]. Compared to the traditional methods, GANs have two advantages: 1) they can generate scenarios only according to historical data, without assuming or fitting probability distributions; 2) they belong to unsupervised learning, which can avoid labeling work that sometimes is impossible and inaccurate. Thus, the GANs approach is selected for scenario generation in this study.

The detailed scenario generation procedures are elaborated in [187]. These huge number of generated scenarios cover most if not all possible PV outputs. However, only a fraction of scenarios has a similar pattern with the day-ahead PV point-forecast power. Based on all scenarios and the forecasted power, a candidate scenario set can be obtained, and then a scenario reduction strategy is introduced to reduce the computational burden.

The main idea of scenario reduction is to minimize the Kantorovich probability distance between reduced scenarios and the candidate scenario set. The detailed mathematical derivations can be found in [189]. The procedures of obtaining the candidate scenario set and scenarios reduction are illustrated in Table 4.1.

3) Compact notation

Based on the uncertainty modeling, the unified compact notation of the first two levels for the optimistic model or the pessimistic model can be presented as follows [150].

Table 4.1. Scenario reduction algorithm.

Algorithm 1: Scenario Reduction

1. Initialization: Calculate the Euclidean distance between point forecast profile and all scenarios.

$$d(\overline{\boldsymbol{P}}^{PV}, \boldsymbol{P}^{PV,s}) = \left\| \overline{\boldsymbol{P}}^{PV} - \boldsymbol{P}^{PV,s} \right\|_2, \ s = 1,2,...,S$$

where $\overline{\boldsymbol{P}}^{PV}$ is the point-forecast power, and $\boldsymbol{P}^{PV,s}$ is the generated scenario.

2. Candidate Scenario set: Choose the closest 30% of all scenarios as the candidate scenario set S_C, with the probability of each candidate scenario $p = 1/|S_C|$;

3. Kantorovich probability distance-based scenario reduction:

3.1 Eliminate scenario s_m if it meets the following condition.

$$d_m = \min \left\{ p(m) \cdot p(n) \cdot d(\boldsymbol{P}^{PV,m}, \boldsymbol{P}^{PV,n}) \right\} \ m, n \in \{1,..., S_C\}, n \neq m$$

3.2 Update the probability of s_n and the number of scenarios.

$$S_C = S_C - 1, \ p(n) = p(n) + p(m)$$

3.3 If $S_C > S_0$ (S_0 is the preferred scenario number), go back to **Step 3.1**; otherwise, terminate the algorithm.

$$\min_{\boldsymbol{y}} \sum_{s\in S_0} p(s)\boldsymbol{\pi}^T(\mathrm{s})\boldsymbol{y} \tag{4.45}$$

$$s.t. \quad \boldsymbol{A}\boldsymbol{y} \le \boldsymbol{b} \tag{4.46}$$

$$\boldsymbol{\pi}(s) \in \arg\min_{\boldsymbol{x}} \sum_{s\in S_0} p(s)\boldsymbol{c}^T\boldsymbol{x}(s) \tag{4.47}$$

$$s.t. \quad \boldsymbol{W}(s)\boldsymbol{x}(s) \le \boldsymbol{r}(s) - \boldsymbol{T}(s)\boldsymbol{y} \tag{4.48}$$

where (4.45)-(4.46) represent the objective and constraints of the optimistic model or the pessimistic model in the first level, and (4.47)-(4.48) represent the stochastic model in the second level.

4.4.2 Solution Method

The solution methods of the bilevel problem have been widely studied [190]. Due to the convexity in the second level, the equivalent transformation via Karush-Kuhn-Tucker (KKT) optimal conditions is adopted. The coupled first two levels can be solved into two steps which are presented below.

1) Mathematical program with equilibrium constraints (MPEC) model: The second level is a deterministic linear programming problem with a finite number of scenarios, it can be transformed into a set of constraints adding to the first level by obtaining the KKT optimality conditions. Then, the bilevel problem becomes a single-level problem which is called MPEC.

2) Mixed-integer linear programming (MILP) model: The MPEC model is non-convex due to the bilinear objective function and the complementary slackness constraints. Therefore, the strong duality theory and big-M approach can be utilized to transform the MPEC to a MILP which is tractable. The detailed derivation of MPEC and MILP can be found in [168] and is neglected here.

4.5 Real-Time: Rolling Horizon Optimization

In this section, to reflect the continuous clearing nature of the RT market and integrate the latest operating information, RHO is applied to allow the re-scheduling and re-dispatching [191].

In general, the closer to the real-time *t*, the less prediction errors of the PV power output and outdoor temperature, and the more accurate end users' housing/EV conditions. In this context, aggregators are willing to adjust their schedules and the DSO can make a precise DA market clearing. By incorporating the latest released information, the radicalness and conservativeness of the interval optimization in the DA market can also be reduced.

The diagram of the RHO scheme is illustrated in Figure 4.1. The procedures of the RHO scheme are described in Table 4.2. The first two levels are highly coupled due to the coupled decision variables: Utilizing less data is indeed an advantage for some methods. They form a Stackelberg model: LAs bid in the distribution market with load demands, DSO clears the market and sends the DLMP back to LAs, then LAs make their decisions based on DLMP and resubmit their bids, and so on. The complicated process in these two levels can be solved by the typical bilevel solution described in subsection 4.4.2. After that, LAs can obtain the aggregated demand $P_{i,t}^{H}$, $P_{i,t}^{W}$ and $P_{i,t}^{C}$. As shown in Figure 4.1, the time step in the first two levels is 1 hour, while the third level utilizes a high-resolution control interval which is 10 minutes. In the third level, LAs dispatch the aggregated demand to all the contracted consumers based on the priority-based dispatching algorithm. LAs send control signals (e.g., $u_{i,j,t}^{h}$, $u_{i,j,t}^{w}$, $P_{i,j,t}^{c}$) to consumers at the beginning of every 10 minutes, collect operating information (e.g., $\theta_{i,j,t}^{h}$, $\theta_{i,j,t}^{w}$, $E_{i,j,t}$, $\tilde{\theta}_{t}^{out}$) at the end of every 10 minutes, and calculate the control signals and resend them to consumers for the next 10 minutes. At the end of the 1-hour time step, LAs update $\theta_{i,t+1}^{h}$, $\theta_{i,t+1}^{w}$, $E_{i,t+1}$, and $\tilde{\theta}_{t+1}^{out}$ for the next RHO schedule.

4.6 Case Studies

This section mainly focusses on analysis of the simulation results. The proposed hybrid interval-stochastic tri-level model with multiple uncertainty sources is tested on a modified IEEE 69-bus distribution system. Simulations are performed on a laptop with an Intel Core i7-8650U CPU and 16GB RAM. Problems are formulated in MATLAB R2020a and YALMIP and solved by GUROBI 9.0.0.

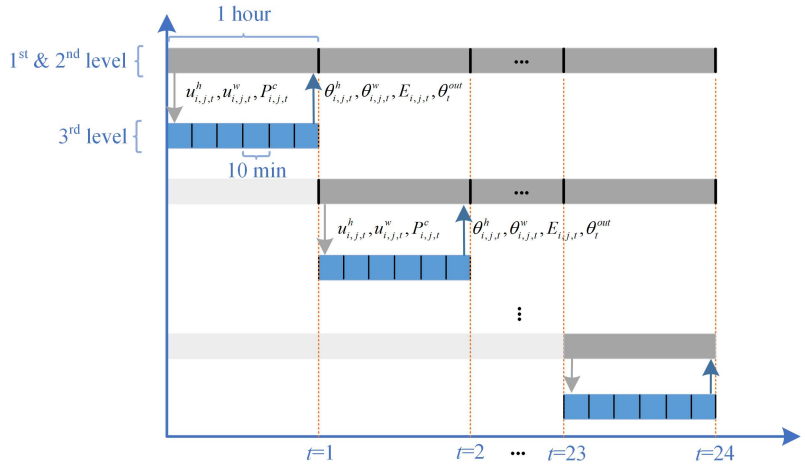


Figure 4.1. Illustration of the rolling horizon optimization scheme.

Table 4.2. Procedure of RHO algorithm.

Algorithm 2: Procedures of RHO
1. Aggregator level: At t, LAs collect the forecasted outdoor temperature $\tilde{\theta}_t^{out}$ and indoor temperatures $\theta_{i,j,t}^h$, water temperatures $\theta_{i,j,t}^w$, EV SOCs of individual users, then update the aggregated indoor temperature $\theta_{i,t}^h$, water temperature $\theta_{i,t}^w$ and EV energy $E_{i,t}$;
2. DSO level: The DSO collects the latest forecasted PV power output, then updates the PV power scenarios by Algorithm 1;
3. Solve the first bi-level model: Solve the rest (24 - t) hours interval-stochastic bi-level model, obtain the optimal load demand schedule, the time step is 1 hour;
4. Residential level: LAs dispatch the optimal demand schedule of hour t + 1 to individual users;
5. Termination checking: $t = t + 1$, check whether $t <= T$ or not. If yes, go back to **Step 1**; otherwise, the algorithm terminates.

4.6.1 Modified IEEE 69-bus Distribution System

The modified IEEE 69-bus system is shown in Figure 4.2. Microturbines (MTs), static Var compensators (SVCs), and PVs are installed in the system. The parameters of the distribution system, HVAC aggregators, EWH aggregators, and EV aggregators are listed in Table 4.3.

For simplicity, it is assumed that each house has both HVAC and EWH, and if the owner is willing to participate in LA, both HVAC and EWH are included. While the EV charging stations are located at some specific buses; they act as EV aggregators.

4.6.2 PV Scenarios

The historical PV dataset is obtained from NREL Solar Integration Datasets [192]. The normalized power profiles over one year are illustrated in Figure 4.3 (a). Based on GANs, 1200 PV power scenarios are generated as shown in Figure 4.3 (b). These scenarios cover the most possible PV power outputs in one year, but they are not proper for the schedule of a specific day. Thus, according to Algorithm 1, 360 scenarios are selected as the candidate scenario set, which is shown in Figure 4.3 (c). However, the candidate set still has too many scenarios. Then, they are further reduced, and finally 10 scenarios are kept, which are shown in Figure 4.3 (d). In these figures, green curves are generated scenarios, and the red curve is the forecasted day-ahead PV curve in a specific day.

If Figure 4.3 (a) and Figure 4.3 (b) are compared, we may observe that the scenarios generated by GANs can well follow the distribution of the historical set. From Figure 4.3 (c) and Figure 4.3 (d), it can be seen that the candidate set and the reduced set can cover the forecasted curve and maintain the ramp trend with the forecasted one. These findings demonstrate the power and effectiveness of GANs in scenario generation.

4.6.3 Day-ahead Scheduling

The results of the DA scheduling are illustrated and discussed in this subsection. The aggregator payments and system generation cost under different uncertainty levels. It can be observed that with the increase of the uncertainty level, the payments and cost increase in the pessimistic model and decrease in the optimistic model.

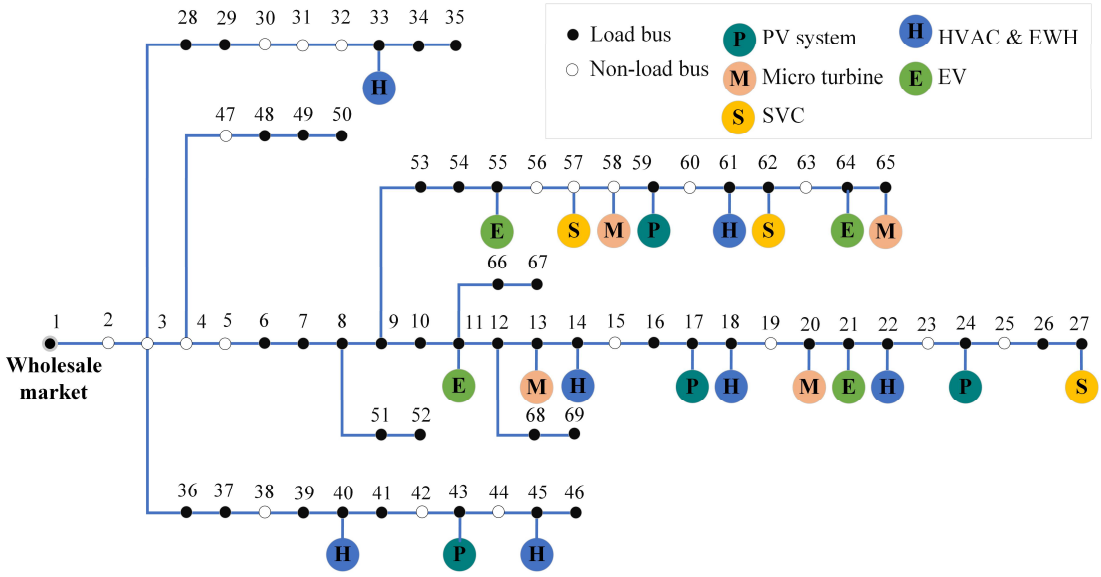
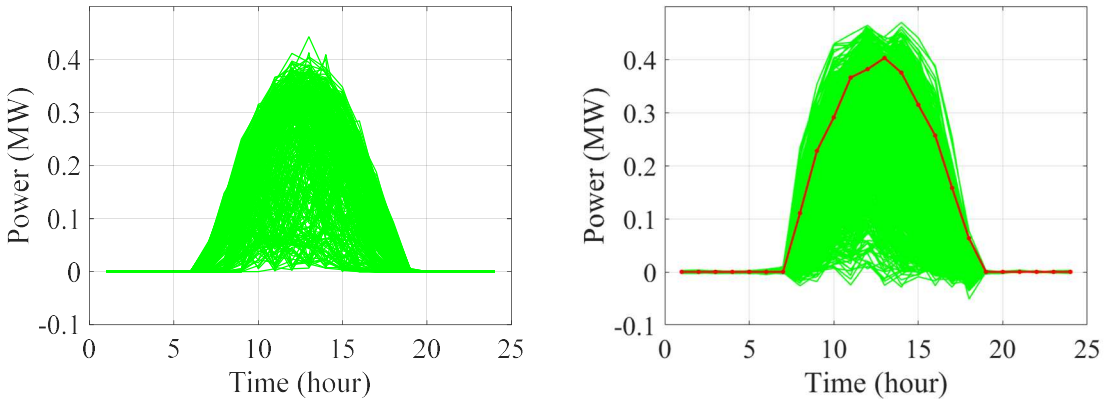


Figure 4.2. The modified IEEE 69-bus system.

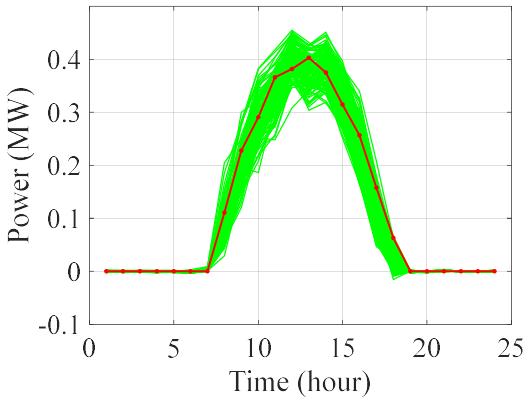
Table 4.3. Parameters of the modified IEEE 69-bus system.

Class	Parameter	Typical Value
MT	Location	Bus #13, 20, 58, 65
	Bidding price	$ 70/MWh
	Capacity	0.5 MW
	α_i	0.95
SVC	Location	Bus #27, 57, 62
	Bidding price	$ 0/MVarh
	Capacity	0.5 MVar
PV	Location	Bus #17, 24, 43, 59
	Bidding price	$ 15/MWh
	Capacity	0.5 MW
	α_i	0.95
System constraints	V^{min}	0.95 p.u.
	V^{max}	1.05 p.u.
	V_{sub}	1.05 p.u.
	Peak fixed load	5.323 MW + j3.773 MVar
HVAC & EWH aggregator	Location	Bus #14, 18, 22, 33, 40, 45, 61
	Number of houses	200, 200, 200, 200, 200, 200, 200
	SOC limit	[0.15, 0.85]
	Ramp up/down rate	0.1
	Water mass m (kg)	144, 162, 180, 198, 216, 162, 180
	Heat loss H_r ($\times 10^{-2}$ kW)	5.6, 6.3, 7, 7.7, 8.4, 6.3, 7
	HVAC synchronization limit	[0.1, 0.7]
	EWH synchronization limit	[0, 0.7]
EV aggregator	Location	Bus #11, 21, 55, 64
	Number of EVs	300, 300, 300, 300
	Number of chargers	25, 25, 25, 25
	SOC limit	[0.2, 0.8]

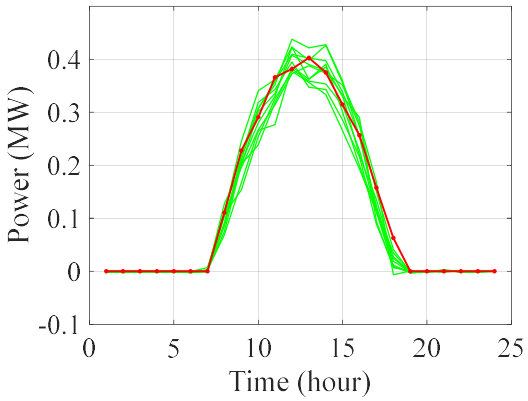


(a) Historical set

(b) GANs generated set



(c) Candidate set



(d) Reduced set

Figure 4.3. PV power scenario sets.

This is because a bigger uncertainty level will worsen the worst operating condition for the pessimistic model while extending the feasible region for the optimistic model. Note that when the uncertainty scaler is too large, like $\alpha^h \geq 0.05$, the pessimistic problem becomes infeasible, which indicates that the uncertainty level can affect the feasibility of the worst case. The simulation results are shown in Table 4.4.

The reason that α^h is less than α^w and α^e is that the indoor temperature is set to a tight range (e.g., [18, 22]℃), thus a smaller α^h is proper. Also, a bigger α^h will easily make the indoor temperature exceeds the setting range due to the accumulative effect of the uncertainty which will further cause the problem infeasible.

The expected DLMP profile of the pessimistic model in Case 1 is illustrated in Figure 4.4. Here, the expected DLMP is defined as the weighted sum of the DLMP of all scenarios. At each time step, the DLMP varies spatially. This is because the marginal power loss price is a component of DLMP as stated in (4.36). Due to the radial topology, if there is no DG power injection, the DLMP increases when the node is farther away from node 1 because of a higher power loss factor at that node. The DLMP and its components of one branch (branch 1-2-3-4-47-48-49-50) at t = 19:00 are shown in Table 4.5. Since no voltage constraints are violated, thus the voltage support price is \$0.

At the same node, DLMP is lower during off-peak hours and higher during peak hours. This is because the wholesale market price is the main component of the DLMP, and thus DLMP has a similar pattern to the wholesale market price. With these characteristics, DLMP can be used to incentivize power consumption for flexible loads.

The system load profiles of the pessimistic model under different uncertainty levels are analyzed. In addition, the load profile of no flexible residential load is also depicted. Here, "no flexible load" means that residential loads do not response to the DLMP and are regarded as fixed loads. It can be observed that if compared with the Case "No flex", Case 1~ Case 10 have the load shifting effect, and Case 1 shifts the most load. The load shifting becomes weak as the uncertainty level increases.

The system load profiles of the optimistic model are depicted. It can be found that all cases achieve the load shifting, and Case 10 is the best. Also, the electricity consumption decreases with the increase of uncertainty level.

Table 4.4. Aggregator payments and system generation cost under different uncertainty levels.

Case	Uncertainty level				Load aggregator payment ($)		System generation cost ($)	
	α^h	α^w	α^e	α^{temp}	Optimistic	Pessimistic	Optimistic	Pessimistic
1	0	0	0	0	999.00	999.00	3349.63	3349.63
2	0.001	0.01	0.01	0.005	985.08	1013.54	3335.71	3364.17
3	0.002	0.02	0.02	0.010	971.41	1028.25	3322.04	3378.88
4	0.003	0.03	0.03	0.015	958.18	1043.09	3308.81	3393.72
5	0.004	0.04	0.04	0.020	945.22	1058.08	3295.85	3408.71
6	0.005	0.05	0.05	0.025	932.62	1073.45	3283.25	3424.08
7	0.006	0.06	0.06	0.030	921.09	1088.94	3271.72	3439.57
8	0.007	0.07	0.07	0.035	910.65	1104.49	3261.29	3455.12
9	0.008	0.08	0.08	0.040	900.39	1120.38	3251.03	3471.01
10	0.009	0.09	0.09	0.045	890.35	1136.04	3240.98	3486.67
No flex	0	0	0	0	1529.71	1529.71	3850.27	3850.27

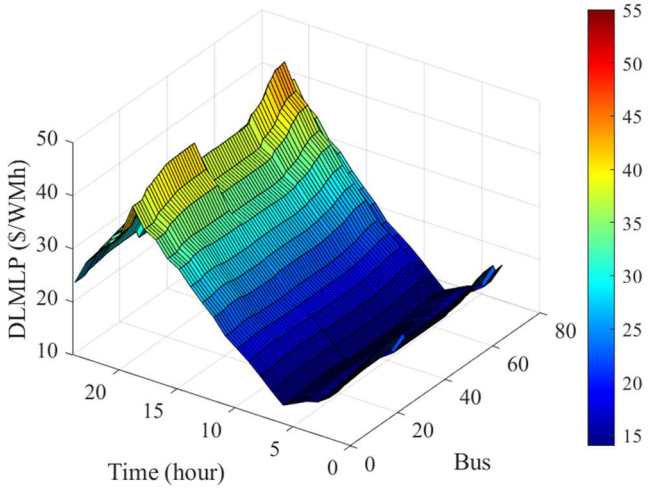


Figure 4.4. Expected DLMP.

Table 4.5. DLMP and its components of one branch at t = 19:00.

Node	DLMP ($)	Energy ($)	Loss ($)	Voltage support ($)
1	41.240	41.24	0	0
2	41.242	41.24	0.002	0
3	41.244	41.24	0.004	0
4	41.249	41.24	0.009	0
47	41.251	41.24	0.011	0
48	41.298	41.24	0.058	0
49	41.447	41.24	0.207	0
50	41.468	41.24	0.228	0

Figure 4.5 shows the system load profiles of the pessimistic model under different uncertainty levels. Figure 4.6 dipicts the system load profiles of the optimistic model. From Figure 4.5 and Figure 4.6, it can be concluded that bigger uncertainty level induces conservative results for the pessimistic model while radical results for the optimistic model.

4.6.4 Real-time Scheduling

In this subsection, the optimistic results and the pessimistic results obtained by DA schedule and the results obtained by RT schedule are analyzed and discussed.

The flexible load profiles of the DA and RT schedules are shown in Figure 4.7. For the pessimistic DA model, it can be found that during 5:00-13:00, the RT load curve is a bit higher than that of DA, while lower during 14:00-24:00. For the optimistic DA model, during 1:00-9:00, the RT load curve is somewhat overlapped with that of DA, while higher during 10:00-24:00. Overall, the optimistic DA schedule has the best load shifting effect, then the RT schedule and the pessimistic DA schedule. Such results are intuitive because the optimistic model represents the best ideal case, the pessimistic model represents the worst ideal case, and RT achieves a balance by modifying the two extreme cases by knowing more realistic operating information.

The individual indoor temperatures in one HVAC aggregator in DA and RT are shown in Figure 4.8 (a)(b)(c). The individual water temperatures in one EWH aggregator are shown in Figure 4.8 (d)(e)(f).

From Figure 4.8 (c), the HVAC indoor temperatures are just above the lower temperature set point during time intervals 40 ~ 80, and below the upper temperature set point during time intervals 115 ~ 144. This is exactly the precooling of HVACs and the DLMP plays an important role in forming these patterns. Incentivized by the temporal characteristic of the DLMP and the thermal storage characteristic of buildings, HVACs are turned on more frequently to cool down the building when the DLMP is low and are turned on less frequently to maintain the indoor temperature within the setting boundary when the DLMP is high. Water has a similar thermal storage characteristic due to its high specific heat capacity. Thus, water temperature shows similar patterns to the buildings' temperature. As shown in Figure 4.8 (f), EWHs preheat water first and then maintain the water temperature within the setting range.

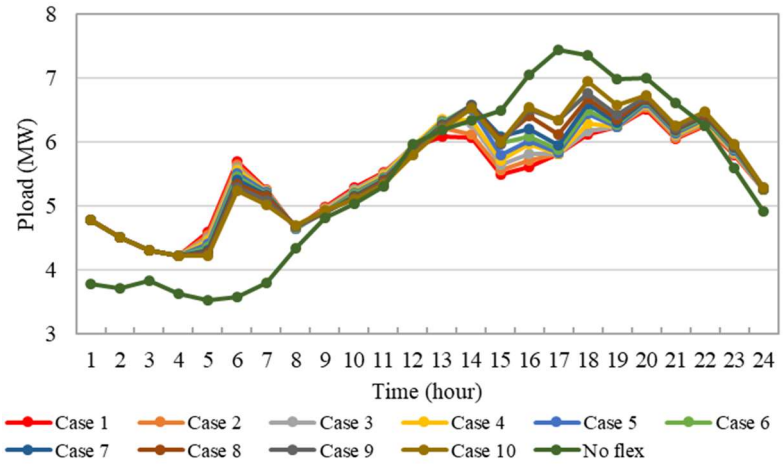


Figure 4.5. System load profiles under different uncertainty levels for the pessimistic model.

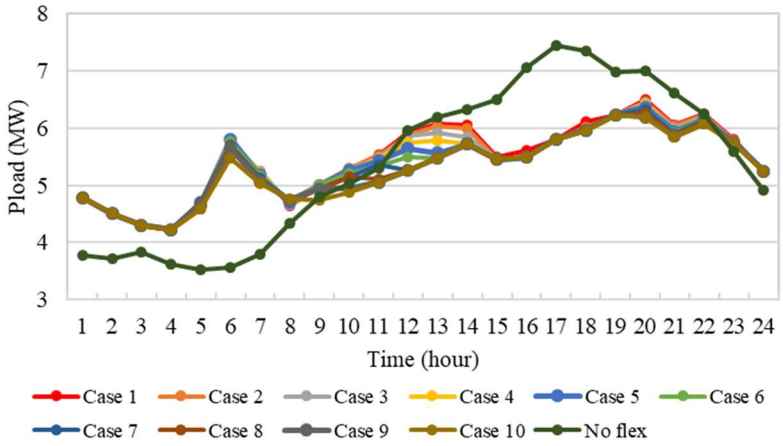


Figure 4.6. System load profiles under different uncertainty levels for the optimistic model.

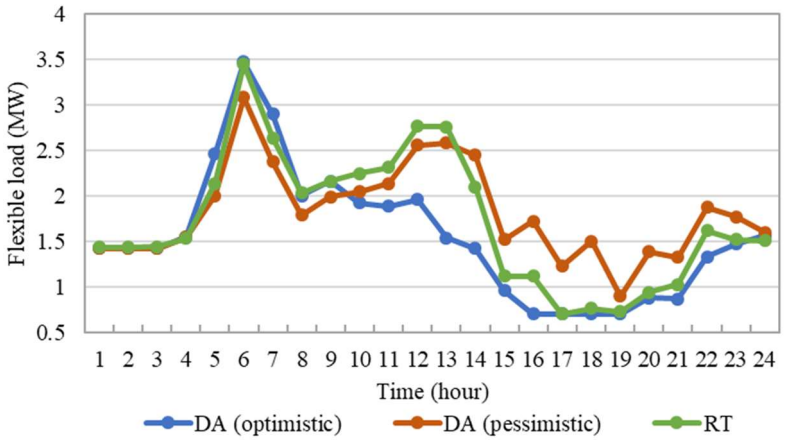


Figure 4.7. Load profiles of total flexible load in day-ahead and real-time schedules.

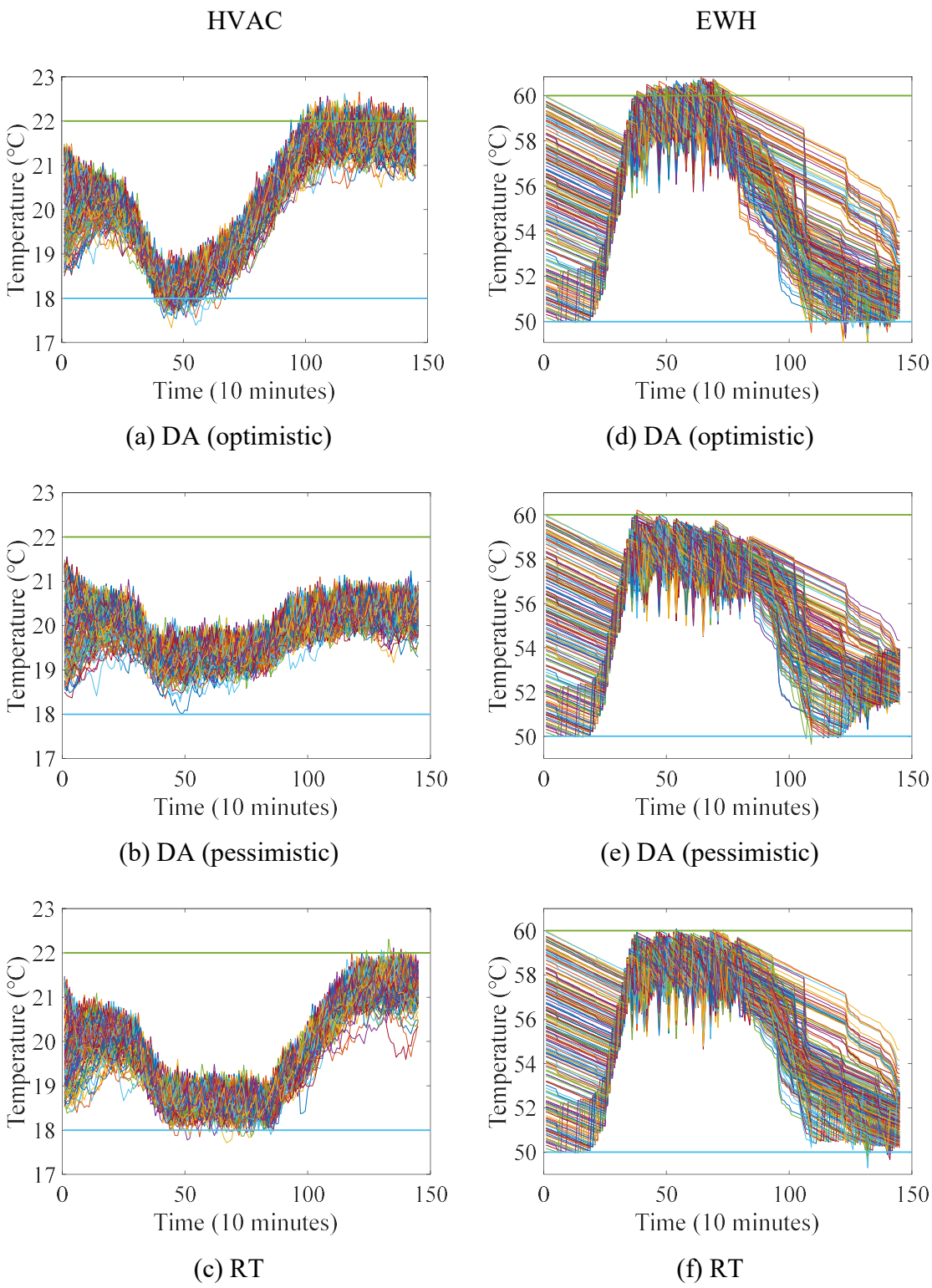


Figure 4.8. Indoor temperature profiles of HVACs and water temperatures of EWHs for 150 intervals of 10 minutes/interval.

In addition, it can be observed that obviously, the individual indoor temperatures in the optimistic DA model usually exceed the setting temperature boundary, while the temperatures in the pessimistic model are mainly distributed in the middle of the temperature boundary, indicating the HVAC flexibility is either overused or underutilized. The temperatures in RT are well maintained inside or around the boundary, which means the precooling of HVACs is properly utilized. From Figure 4.8 (d)(e)(f), water temperatures in RT are also better maintained in the setting boundary than that of DA.

These findings indicate that the day ahead scheduling is too radical or too conservative. The deployment of RHO by updating the operating information can significantly mitigate radical or conservative DA scheduling.

4.7 Conclusions

In this chapter, a three-layer market structure is established to quantitatively identify the flexibility potentials of residential buildings. In the day-ahead schedule, uncertainties from all layers are considered, which are the random power consumption behaviors, weather temperature forecasts, and PV power outputs. Then, a hybrid interval-stochastic programming is proposed, in which the Gaussian noise, interval forecast and GANs are utilized to model uncertainties respectively. In real-time, RHO is applied to continuously modify the day-ahead schedule according to the latest released information. Case studies have the following conclusions:

- The trilevel structure can well utilize the residential demand flexibility to benefit individual users and satisfy their power needs, as well as reducing the distribution system total operational cost.
- The proposed hybrid interval-stochastic programming can effectively handle the uncertain bilevel problem and maintain the problem tractability. It can also provide optimistic and pessimistic results for decision-makers.
- By integrating the latest system operating and forecast information, the RHO scheme can mitigate the radicalness and conservativeness of the day-ahead schedule.

Chapter 5 Profit-Oriented BESS Siting and Sizing in Deregulated Distribution Systems

Within the deregulation process of distribution systems, the distribution locational marginal price (DLMP) provides effective market signals for future unit investment. In this context, this chapter proposes a two-stage stochastic bilevel programming (TS-SBP) model for investors to best allocate battery energy storage systems (BESSs). The first stage obtains the optimal siting and sizing of BESSs on a limited budget. The second stage, a bilevel BESS arbitrage model, maximizes the arbitrage revenue in the upper level and clears the distribution market in the lower level. Karush-Kuhn-Tucker (KKT) optimality conditions, strong duality theory, and the big-M method are utilized to transform the TS-SBP model into a tractable two-stage stochastic mixed-integer linear programming (TS-SMILP) model. A novel statistics-based scenario extraction algorithm is proposed to generate a series of typical operating scenarios. Then, scale reduction strategies for BESS candidate buses and inactive voltage constraints are proposed to reduce the scale of the TS-SMILP model. Finally, case studies on the IEEE 33-bus and 123-bus systems validate the effectiveness of the DLMP in incentivizing BESS planning and the efficiency of the two proposed scale reduction strategies.

5.1 Introduction

Traditionally, a power system has a unidirectional structure where electricity is generated by generators and then delivered via transmission and distribution lines to consumers, who are at the end of the supply chain. However, in recent decades, the electricity industry has been witnessing the emergence of distributed energy resources (DERs) in distribution systems [2]. The proliferation of DERs transforms the unidirectional system into a bidirectional system, making the distribution system both more flexible and more active, and more complex. To take advantage of these new opportunities and to keep pace with deregulation in power distribution systems, the concept of a distribution market has been proposed and widely studied [8][36].

The distribution locational marginal price (DLMP), the extension of locational marginal price (LMP) to distribution networks, has been proposed to either guide the consumption of flexible loads, or act as the bidding price of DERs when participating in the distribution market. In [97][99], the DLMP varies throughout the course of a day and is utilized to optimize the charging schedule for electric vehicles (EVs) and household demand response to alleviate congestion issues. In [26], the DLMP is regarded as both the microgrid (MG) bidding price and the clearing price of the distribution system operator (DSO). A bilevel model is built and a strategic bidding strategy is proposed to maximize microgrid profits. A similar bi-level model is proposed in [81] to achieve optimal EV aggregator scheduling.

The above studies mainly focus on short-term operations. However, DLMP also releases continuous and effective market signals to practitioners, which can incentivize future DERs investment. Among all types of DERs, the battery energy storage system (BESS) plays a significant role due to its flexible charging/discharging characteristic and its increasing penetration level. Between 2011 and 2020, the Federal Energy Regulatory Commission Orders No. 755 [194], 841 [195] and 2222 [29] have gradually removed the barriers to BESS participation in the energy and ancillary market. In the industry field, various related trading products, such as CAISO's flexible ramping product [196] and PJM's Regulation D [197], have promoted the deployment of BESSs. The BESS cost also continues to decrease as manufacturing technology advances. All these advantages are driving the acceleration of BESS installation, which is likely to continue into the foreseeable future [30]. In this context, the optimal allocation of BESSs has already been extensively studied.

Traditionally, in normal operating conditions, the optimal allocation of BESSs or distributed generators (DGs) aimed to minimize the investment cost and the long-term cumulative operating cost of distribution systems or to satisfy the system operating conditions (e.g., meeting the load growth, improving voltage profile and reducing power losses), usually from the viewpoint of the DSO or a utility [141]-[144], [198]. In [198], a stochastic mixed-integer linear programming (MILP) model was formulated to optimally site and size BESSs to minimize both the system operating cost and the BESS investment cost. The optimal placement and sizing of energy storage systems (ESSs) to minimize total energy losses was studied in [141]. A single-level mixed-integer second-order cone

programming (MISOCP) model was established in [142] to determine the optimal siting and sizing for BESSs. Reference [143] determined the optimal BESS allocation to maximize net revenue. This problem in an imbalanced system was further studied in [144]. Reference [199] aimed to characterize the economic effect of the ESS geometrically and investigate the optimal energy-power ratio for the ESS.

These studies were performed in a regulated distribution system. However, in the deregulated distribution systems, the planning objective and investment goal will be different from the regulated case because of the profitability of private DER owners. Considering the characteristics of electricity price in competitive distribution systems, such as the spatial and temporal difference of the DLMP, private DER owners have the motivation to install DERs at optimal locations with optimal sizes to maximize profits if possible.

A few studies have been developed in this background. The authors in [200] proposed a bi-level wind-storage expansion model to maximize investor profits in the transmission level market, in which only the capacity was optimized. In [149], a three-stage model for network reinforcement and DER planning was proposed. The objective was to maximize asset owners' profit by optimizing the location and construction time of new lines or DERs. DLMP in the third stage was utilized as the market signal to modify the planning in the first two stages. In [145], MGs were assumed to trade with the DSO. MG locations were based on the weighted sum of loss sensitivity factors and voltage sensitivity factors. The installation time and DER type were determined by solving a bilevel model with DSO in the upper level and MG in the lower level. Reference [146] determined the optimal sizes for renewable generators and ES in a deregulated market with given candidate sites. An adaptive robust model for investment planning of DERs was proposed in [147], in which the 8760-hour operating conditions in each planning year were clustered to a tractable count. In [148], with the fixed size of wind turbines (WTs), an exhaustive search method was proposed to find the most convenient WT allocations and the priority of installations.

In the above studies, electricity price and earned profit have been proposed and deployed to motivate system investment. These studies did provide some insights for planning in a distribution market environment. However, there are still important issues that have not

been well addressed in the literature. 1) The important daily day-ahead market clearing is seldom considered, as shown in [145][147] in which the operating conditions are reduced or clustered to a low resolution, not to consecutive 24 hours. 2) These proposed methods may not be suitable for BESS planning since the daily operating constraints for BESS cannot be included, such as the constraint (5.10) in Section 5.2.2. 3) In [145]-[148], as an indicator of the physical operating condition, DLMP is not fully modeled or utilized, its potential in incentivizing system planning can be further explored.

To fill these gaps, this chapter focuses on the optimal siting and sizing of BESSs for private investors. This planning is formulated as a two-stage stochastic bilevel programming (TS-SBP) problem. The first stage determines the locations, sizes, and number of BESSs within a limited budget. The second stage maximizes investors' arbitrage profits in the long-term operation, which is modeled as a bi-level problem with the investors in the upper level and the DSO in the lower level. The contributions are summarized as follows:

- The DLMP is applied as the price signal to incentivize the BESS planning in a deregulated distribution system. The proposed planning approach maximizes investors' profit and improves system operating conditions, which is aligned with the incentive compatibility that benefits both the BESS owners and the distribution system.
- A TS-SBP arbitrage model is established, in which the planning stage and the operating stage are combined as a two-stage problem, and the operating stage is formulated as a bi-level problem. The objective is to minimize the maintenance cost and maximize the arbitrage revenue.
- From the 1-year historical LMP and system load dataset, a *k*-means based scenario extraction algorithm is proposed to extract the most representative patterns of consecutive 24 hours LMP and system load profiles and their corresponding discrete joint probabilities. The extraction accuracy is validated and this innovation enables the day-ahead market clearing.
- Based on the unique characteristics (e.g., the limited number of BESS to be installed and the huge number of inactive constraints) of this problem, two scale-

reduction strategies, BESS candidate buses reduction and inactive voltage constraints reduction, are proposed to reduce the computational complexity for this large-scale optimization problem. The simulation results demonstrate the accuracy of these strategies.

It should be noted that this work addresses profit-oriented BESS planning, which is appropriate for areas where resilience is not a considerable concern. However, in areas with resilience as a significant concern such as coastal regions prone to extreme weather like hurricanes, the problem may follow a fundamentally different model with resilience as a major factor, which can be a future work to investigate.

The rest of the chapter is organized as follows. Section 5.2 describes the TS-SBP model. Section 5.3 proposes the scenario extraction algorithm. Section 5.4 presents the solution methods and two scale-reduction strategies. Case studies are presented in Section 5.5. Section 5.6 concludes the paper.

5.2 Problem Formulation

The mathematical formulation of the TS-SBP model is presented in this section. The overall framework is shown in Figure 5.1.

5.2.1 The First Stage Problem: Optimal Siting & Sizing

The first stage aims to optimize the site and size of BESS units, which means private investors intend to determine the best locations and best sizes to maximize their revenue.

$$\max \quad -\sum_{i\in\Omega_{BS}}\left(c^{Mf}P_i^{rated}+c^{Mv}E_i^{rated}\right)+E\left[f\left(\boldsymbol{x},s\right)\right] \tag{5.1}$$

$$s.t.$$

$$\sum_{i\in\Omega_{BS}}\delta_i \le N_{BS}^{\max} \tag{5.2}$$

$$\sum_{i\in\Omega_{BS}}k^pP_i^{rated}+k^eE_i^{rated}\le C^{Bgt} \tag{5.3}$$

$$P^{\min}\delta_i \le P_i^{rated} \le P^{\max}\delta_i \tag{5.4}$$

$$E^{\min}\delta_i \le E_i^{rated} \le E^{\max}\delta_i \tag{5.5}$$

$$E_i^{rated}=4\cdot P_i^{rated} \tag{5.6}$$

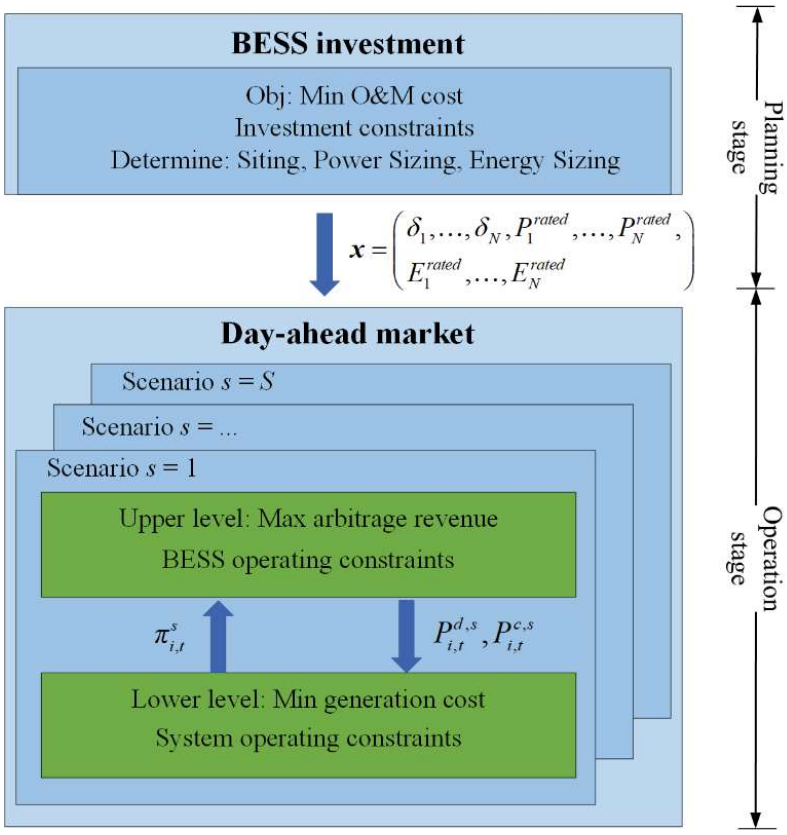


Figure 5.1. The framework of the TS-SBP model.

$$E\left[f\left(\boldsymbol{x},s\right)\right]=365\cdot\sum_{s\in S}p\left(s\right)f\left(\boldsymbol{x},s\right) \tag{5.7}$$

where (5.1) minimizes the operation and maintenance (O&M) costs and maximizes the arbitrage revenue of the BESS over a year.

The decision variables include the BESS locations, rated power, and rated energy: $\boldsymbol{x}=\left(\delta_1,\ldots,\delta_N,P_1^{rated},\ldots,P_N^{rated},E_1^{rated},\ldots,E_N^{rated}\right)$, the first two items in (5.1) are the expression of the O&M costs; (5.2) restricts the number of BESSs to be installed; (5.3) is the investment budget limit [201], where the installation cost of a BESS is approximated as a linear function of P_i^{rated} and E_i^{rated} [202][203]; (5.4) and (5.5) are BESS size constraints; (5.6) is the fixed energy-power ratio which is for simplification and is aligned with the arbitrage operating requirement [202]; and in (5.7), $f\left(\boldsymbol{x},s\right)$ is the optimal value of scenario *s* in the second stage problem.

5.2.2 The Second Stage Problem: BESS Operation in a Deregulated Distribution Market

In this stage, BESSs participate in the distribution-level electricity market to maximize their arbitrage revenue. This problem has the following assumptions:

- A day-ahead electricity market is established in the distribution level. DERs provide bids and offers to the DSO, which clears the market and broadcasts the DLMP to all participants.
- BESSs are modeled as price takers that only submit load/generation quantities and the DSO decides the DLMP.

Based on these assumptions, the BESS owner and the DSO have different interests. At the same time, BESSs' charging/discharging power and system DLMP are coupled variables. Thus, a bilevel model is an appropriate representation of the coupled relationship. Note that (5.8)-(5.24) represent the scenario *s*. For simplicity, the expressions $\forall t\in\Omega_T$ and $s\in S$ behind each equation are neglected.

1) The upper level: The BESS sells energy during high DLMP hours and buys during low DLMP hours. Its objective is to maximize arbitrage revenue.

$$
\begin{aligned}
f\left(\boldsymbol{x},s\right) &= \max \sum_{t\in\Omega_T}\sum_{i\in\Omega_{BS}} \pi_{i,t}^{s}\cdot P_{i,t}^{BESS,s} \\
&= \max \sum_{t\in\Omega_T}\sum_{i\in\Omega_{BS}} \pi_{i,t}^{s}\cdot\left(\sqrt{\eta_i}P_{i,t}^{d,s} - P_{i,t}^{c,s}\Big/\sqrt{\eta_i}\right)
\end{aligned} \tag{5.8}
$$

$$
s.t.
$$

$$
E_{i,t+1}^{s} = E_{i,t}^{s} + P_{i,t}^{c,s} - P_{i,t}^{d,s} \tag{5.9}
$$

$$
E_{i,t=0}^{s} = E_{i,t=T}^{s} \tag{5.10}
$$

$$
SOC_i^{\min}\cdot E_i^{rated} \le E_{i,t+1}^{s} \le SOC_i^{\max}\cdot E_i^{rated} \tag{5.11}
$$

$$
0 \le P_{i,t}^{c,s} \le P_i^{rated},\ 0 \le P_{i,t}^{d,s} \le P_i^{rated} \tag{5.12}
$$

where in (5.8), round-trip efficiency η_i is used instead of using charging and discharging efficiencies [204]; (5.9) calculates the stored energy in the BESS with 1 hour as the time interval; (5.10) ensures that the daily charged and discharged energy is equal; (5.11) is the state of charge (SOC) constraint; (5.12) are the charging and discharging power limits.

2) The lower level: The DSO clears the market intending to minimize total generation costs as well as maintain physical operating constraints.

$$
\min h\left(\boldsymbol{z},\boldsymbol{y},s\right) = \sum_{t\in\Omega_T}\left(\sigma_{sub,t}^{p,s}P_{sub,t}^{G,s} + \sigma_{sub,t}^{q,s}\widehat{Q}_{sub,t}^{G,s} + \sum_{i\in\Omega_G}\left(\sigma_{i,t}^{p,s}P_{i,t}^{G,s} + \sigma_{i,t}^{q,s}\widehat{Q}_{i,t}^{G,s}\right)\right) \tag{5.13}
$$

$$
s.t.
$$

$$
P_{sub,t}^{G,s} + \sum_{i\in\Omega_G}P_{i,t}^{G,s} + \sum_{i\in\Omega_{BS}}P_{i,t}^{BESS,s} = \sum_{i\in\Omega_N}P_{i,t}^{D,s} + P_t^{L,s} : \lambda_t^{p,s} \tag{5.14}
$$

$$
Q_{sub,t}^{G,s} + \sum_{i\in\Omega_G}Q_{i,t}^{G,s} = \sum_{i\in\Omega_N}Q_{i,t}^{D,s} + Q_t^{L,s} : \lambda_t^{q,s} \tag{5.15}
$$

$$
V_{j,t}^{s} = V_{sub,t}^{s} + \sum_{i\in\Omega_N}Z_{j,i}^{p}\left(P_{i,t}^{G,s} + P_{i,t}^{BESS,s} - P_{i,t}^{D,s}\right) + \sum_{i\in\Omega_N}Z_{j,i}^{q}\left(Q_{i,t}^{G,s} - Q_{i,t}^{D,s}\right) \tag{5.16}
$$

$$
V^{\min} \le V_{j,t}^{s} \le V^{\max} : \omega_{j,t}^{v\min,s}, \omega_{j,t}^{v\max,s}, \forall j \in \Omega_N \tag{5.17}
$$

$$
P_i^{G,\min} \le P_{i,t}^{G,s} \le P_i^{G,\max} : \omega_{i,t}^{p\min,s}, \omega_{i,t}^{p\max,s}, \forall i \in \Omega_{MT} \tag{5.18}
$$

$$
0 \le Q_{i,t}^{G,s} \le P_{i,t}^{G,s}\tan(\arccos\alpha_i) : \omega_{i,t}^{q\min,s}, \omega_{i,t}^{q\max,s}, \forall i \in \Omega_{MT} \tag{5.19}
$$

$$
Q_i^{G,\min} \le Q_{i,t}^{G,s} \le Q_i^{G,\max} : \omega_{i,t}^{q\min,s}, \omega_{i,t}^{q\max,s}, \forall i \in \Omega_{SVC} \tag{5.20}
$$

$$-Q_{i,t}^{G,s} \le \widehat{Q}_{i,t}^{G,s}, Q_{i,t}^{G,s} \le \widehat{Q}_{i,t}^{G,s} : \kappa_{i,t}^{-,s}, \kappa_{i,t}^{+,s}, \forall i \in \Omega_G \tag{5.21}$$

$$\pi_{i,t}^{s} = \lambda_t^{p,s} + \lambda_t^{p,s} \cdot \frac{\partial P_t^{loss,s}}{\partial P_{i,t}^{D,s}} + \lambda_t^{q,s} \cdot \frac{\partial Q_t^{loss,s}}{\partial P_{i,t}^{D,s}} + \sum_{j \in \Omega_N} \left(\omega_{j,t}^{v\min,s} - \omega_{j,t}^{v\max,s} \right) Z_{j,i}^{p} \tag{5.22}$$

where (5.14) and (5.15) are active and reactive equality power constraints with the substation regarded as a large capacity generator; (5.16) is the linearized voltage expression derived from [36][205]; (5.17) is the voltage limit; (5.18)-(5.19) are the active and reactive power limits of microturbines (MTs); (5.20) is the reactive power limit of static var compensators (SVCs); in (5.21), $\widehat{Q}_{i,t}^{G,s} = \left| Q_{i,t}^{G,s} \right|$ since it is assumed that both absorbing and generating reactive power can induce cost [8]; and (5.22) is the DLMP expression derived from the Lagrangian function of this level. The power losses are linearized according to Taylor's series [36]:

$$P_t^{L,s} \approx P_t^{L,s^*} + \sum_{i \in \Omega_N} \frac{\partial P_t^{L,s}}{\partial P_{i,t}^{G,s}} \left(\Delta P_{i,t}^{G,s} - \Delta P_{i,t}^{D,s} \right) + \sum_{i \in \Omega_N} \frac{\partial P_t^{L,s}}{\partial Q_{i,t}^{G,s}} \left(\Delta Q_{i,t}^{G,s} - \Delta Q_{i,t}^{D,s} \right) \tag{5.23}$$

$$Q_t^{L,s} \approx Q_t^{L,s^*} + \sum_{i \in \Omega_N} \frac{\partial Q_t^{L,s}}{\partial P_{i,t}^{G,s}} \left(\Delta P_{i,t}^{G,s} - \Delta P_{i,t}^{D,s} \right) + \sum_{i \in \Omega_N} \frac{\partial Q_t^{L,s}}{\partial Q_{i,t}^{G,s}} \left(\Delta Q_{i,t}^{G,s} - \Delta Q_{i,t}^{D,s} \right) \tag{5.24}$$

where $\Delta P_{i,t}^{G,s} = P_{i,t}^{G,s} - P_{i,t}^{G,s^*}$ represents the power difference between two close operating points, and $\Delta Q_{i,t}^{G,s}$, $\Delta P_{i,t}^{D,s}$ and $\Delta Q_{i,t}^{D,s}$ have similar expressions.

In (5.22), it can be found that the DLMP consists of three components: marginal energy price, marginal power loss price, and voltage support price. Marginal energy price is determined by the bidding price of the marginal unit. Marginal power losses price is to reflect the power loss associated with delivering power. Since the power loss percentage in a distribution system is usually high (relative to transmission systems), it is not negligible and should be priced. Similarly, voltage is an important operating criterion and should be included. Voltage support price represents the cost of maintaining voltage within the acceptable boundary, it is calculated using the shadow price and will be zero if there is no binding voltage constraint. The detailed analysis and discussion of the three DLMP components and their impacts on flexible loads can be found in [100].

5.2.3 Compact Notation

To make the whole model concise and clear, a compact notation is used to elaborate the proposed TS-SBP model [206]. The first stage is:

$$\max \quad -\boldsymbol{c}^T \boldsymbol{x} + 365 \cdot \sum_{s \in S} p(s) f(\boldsymbol{x}, s) \tag{5.25}$$

$$s.t. \quad \boldsymbol{A}\boldsymbol{x} \le \boldsymbol{b} \tag{5.26}$$

where $\boldsymbol{x} \in \mathbb{Z}_+^{p_1} \times \mathbb{R}_+^{n_1 - p_1}$ represents the binary and continuous decision variables; (5.26) is the matrix representation of constraints (5.2)-(5.7) with $\boldsymbol{A} \in \mathbb{R}_+^{m_1 \times n_1}$, $\boldsymbol{b} \in \mathbb{R}_+^{m_1}$; p_1 is the number of candidate buses; n_1 is the number of total decision variables; and m_1 is the number of constraints.

The second stage is given by:

$$f(\boldsymbol{x}, s) = \max \ \boldsymbol{\pi}^T \boldsymbol{y} \tag{5.27}$$

$$s.t. \quad \boldsymbol{W}(s)\boldsymbol{y} \le \boldsymbol{r}(s) - \boldsymbol{T}(s)\boldsymbol{x} \tag{5.28}$$

$$\boldsymbol{\pi} \in \arg\min h(\boldsymbol{z}, \boldsymbol{y}, s) \tag{5.29}$$

$$s.t. \quad \boldsymbol{G}(s)\boldsymbol{z} \le \boldsymbol{e}(s) - \boldsymbol{K}(s)\boldsymbol{y} \tag{5.30}$$

where $\boldsymbol{y} \in \mathbb{R}_+^{n_2}$, $\boldsymbol{\pi} \in \mathbb{R}_+^{n_2}$, $\boldsymbol{W} \in \mathbb{R}_+^{m_2 \times n_2}$, $\boldsymbol{r} \in \mathbb{R}_+^{m_2}$, $\boldsymbol{T} \in \mathbb{R}_+^{m_2 \times n_1}$, $\boldsymbol{z} \in \mathbb{R}_+^{n_3}$, $\boldsymbol{G} \in \mathbb{R}_+^{m_3 \times n_3}$, $\boldsymbol{e} \in \mathbb{R}_+^{m_3}$, $\boldsymbol{K} \in \mathbb{R}_+^{m_3 \times n_2}$.

5.3 Scenario Extraction and Variable Nodal Loads

In the TS-SBP formulation, the DLMP plays an important role in this planning problem. In the meantime, the DLMP is significantly influenced by the wholesale market LMP and the distribution system load. However, because the LMP and load vary every hour and every day, applying all historical data will significantly increase the computational burden, making this problem intractable. Thus, a natural alternative is to extract a series of representative operating scenarios from the historical dataset, which are defined as possible LMP profile and system load profile combinations in this study.

5.3.1 Scenario Extraction

The statistics-based scenario extraction includes three steps: historical LMP and load clustering, scenario generation, and scenario reduction. The detailed procedures are shown in Table 5.1.

In this table, $\Omega_{LMP,i}=\{d_k,\ldots,d_n\}$ and $\Omega_{load,i}=\{d_l,\ldots,d_m\}$ refer to the LMP cluster i and the system load cluster i, respectively; d_k is the k^{th} day in a year.

And $n(\cdot)$ represents the number of elements in a set; $\boldsymbol{\pi}_{LMP}(i,j)$ and $\boldsymbol{D}_{load}(i,j)$ are the LMP and system load profiles in day j in cluster i, respectively, which represent the LMP and load for 24 hours; $\boldsymbol{\pi}_{LMP}(i,j)$ and $\boldsymbol{D}_{load}(i,j)$ are the centroids of the LMP and system load cluster i, respectively; $p(s)$ is the discrete joint probability.

Note that each centroid is regarded as an LMP pattern or a load profile pattern that is most likely to appear in one year. $p(s)$ is the probability that one LMP pattern and one load pattern happen on the same day in one year. Each LMP and load pattern combination is regarded as a scenario.

5.3.2 Variability in Nodal Loads

In the preceding subsection, the system load profile refers to the total load profile of all nodes in a distribution system. However, the load at each node is usually hard to forecast with high variability. Thus, for simplicity, it is assumed that all nodal loads have the same normalized active and reactive load profiles with the system load in each scenario [206][207]. Additionally, a random multiplier is applied to each nodal load to simulate the randomness of the load.

$$P_{i,t}^{D,s}=\tau_{i,t}^{s}\cdot M_{i,t}^{P}\cdot P_{t}^{D,s} \tag{5.31}$$

$$Q_{i,t}^{D,s}=\tau_{i,t}^{s}\cdot M_{i,t}^{Q}\cdot Q_{t}^{D,s} \tag{5.32}$$

where $\tau_{i,t}^{s}$ refers to a multiplier that follows a Gaussian distribution, $\tau_{i,t}^{s}\sim N(1,0.04^2)$; $M_{i,t}^{P}$ and $M_{i,t}^{Q}$ are the normalized active and reactive load; $P_{t}^{D,s}$ and $Q_{t}^{D,s}$ are the active and reactive system loads of scenario s.

Table 5.1. Detailed procedure of scenario extraction and reduction algorithm.

Algorithm 1: Scenario Extraction and Reduction	
Input	Historical hourly LMP and system load profiles in a year
Output	Typical LMP and system load scenarios associated with discrete joint probabilities
1	***K*-means clustering:**
2	Utilize the elbow method to obtain the optimal number of LMP clusters and system load clusters, respectively.
3	Partition the daily LMP and system load profiles into k_{LMP} and k_{load} clusters.
4	For each cluster, calculate its centroid: $$\boldsymbol{\pi}_{LMP}(i) = 1/n(\Omega_{LMP,i}) \cdot \sum_{j \in \Omega_{LMP,j}} \boldsymbol{\pi}_{LMP}(i,j)$$ $$\boldsymbol{D}_{load}(i) = 1/n(\Omega_{load,i}) \cdot \sum_{j \in \Omega_{load,j}} \boldsymbol{D}_{load}(i,j)$$
5	**Scenario generation:**
6	For LMP cluster *i* and system load cluster *j*, calculate the discrete joint probability: $$p(s) = p_{LMP,load}(i,j) = n(\Omega_{LMP,i} \cap \Omega_{load,j})/365$$
7	In total, $k_{LMP} \cdot k_{load}$ scenarios and corresponding probabilities are generated.
8	**Scenario reduction:**
9	Remove scenarios with probabilities below a threshold.
10	Normalize the discrete joint probabilities of the remaining scenarios (let their summation be 1).

5.4 Solution Methods

The previous Section 5.2 and Section 5.3 build the proposed model for siting and sizing BESSs. The mathematical solution is discussed in this section.

The solution to the proposed TS-SBP model includes two steps. In the first step, the bilevel problem of the second stage is converted to a single-level problem via Karush-Kuhn Tucker (KKT) optimality conditions. After that, the TS-SBP model becomes a two-stage stochastic MILP (TS-SMILP) problem. In the second step, based on the unique characteristics of this TS-SMILP problem, two relaxation methods are proposed to make this problem tractable.

5.4.1 Solving the Bilevel Problem

1) MPEC formulation: Due to the linear property of the lower level, its optimal solution can be obtained by solving the KKT optimality conditions. Thus, the bilevel problem is converted to a single-level problem by adding the KKT conditions to the constraints of the upper level. Then the single-level problem is a mathematical program with equilibrium constraints (MPEC).

$$\max\ (5.8) \tag{5.33}$$

$$s.t.\ \textit{Constraints}\ (5.9)\text{-}(5.12),\ (5.14)\text{-}(5.16),\ (5.22)\text{-}(5.24),\ (5.31)\text{-}(5.32) \tag{5.34}$$

$$\begin{aligned}&\sigma_{i,t}^{p,s}-\lambda_t^{p,s}\left(1-\frac{\partial P_t^{L,s}}{\partial P_{i,t}^{G,s}}\right)-\sum_{j\in\Omega_N}\left(\omega_{j,t}^{v\min,s}-\omega_{j,t}^{v\max,s}\right)Z_{j,i}^{p}\\&+\lambda_t^{q,s}\frac{\partial Q_t^{L,s}}{\partial P_{i,t}^{G,s}}-\omega_{i,t}^{p\min,s}+\omega_{i,t}^{p\max,s}=0,\quad \forall i\in\Omega_G\end{aligned} \tag{5.35}$$

$$\sigma_{i,t}^{q,s}-\kappa_{i,t}^{-,s}-\kappa_{i,t}^{+,s}=0,\quad \forall i\in\Omega_G \tag{5.36}$$

$$\begin{aligned}&\lambda_t^{p,s}\frac{\partial P_t^{L,s}}{\partial Q_{i,t}^{G,s}}-\lambda_t^{q}\left(1-\frac{\partial Q_t^{L,s}}{\partial Q_{i,t}^{G,s}}\right)-\sum_{j\in\Omega_N}\left(\omega_{j,t}^{v\min,s}-\omega_{j,t}^{v\max,s}\right)Z_{j,i}^{q}\\&-\omega_{i,t}^{q\min,s}+\omega_{i,t}^{q\max,s}-\kappa_{i,t}^{-,s}+\kappa_{i,t}^{+,s}=0,\quad \forall i\in\Omega_G\end{aligned} \tag{5.37}$$

$$0\le\omega_{j,t}^{v\min,s}\perp\left(V_{j,t}^{s}-V^{\min}\right)\ge 0,\quad \forall j\in\Omega_N \tag{5.38}$$

$$0\le\omega_{j,t}^{v\max,s}\perp\left(V^{\max}-V_{j,t}^{s}\right)\ge 0,\quad \forall j\in\Omega_N \tag{5.39}$$

$$0\le\omega_{i,t}^{p\min,s}\perp\left(P_{i,t}^{G,s}-P_i^{G,\min}\right)\ge 0,\quad \forall i\in\Omega_G \tag{5.40}$$

$$0 \le \omega_{i,t}^{p\max,s} \perp \left(P_i^{G,\max} - P_{i,t}^{G,s}\right) \ge 0, \quad \forall i \in \Omega_G \tag{5.41}$$

$$0 \le \omega_{i,t}^{q\min,s} \perp \left(Q_{i,t}^{G,s} - Q_i^{G,\min}\right) \ge 0, \quad \forall i \in \Omega_G \tag{5.42}$$

$$0 \le \omega_{i,t}^{q\max,s} \perp \left(Q_i^{G,\max} - Q_{i,t}^{G,s}\right) \ge 0, \quad \forall i \in \Omega_G \tag{5.43}$$

$$0 \le \kappa_{i,t}^{-,s} \perp \left(\widehat{Q}_{i,t}^{G,s} + Q_{i,t}^{G,s}\right) \ge 0, \quad \forall i \in \Omega_G \tag{5.44}$$

$$0 \le \kappa_{i,t}^{+,s} \perp \left(\widehat{Q}_{i,t}^{G,s} - Q_{i,t}^{G,s}\right) \ge 0, \quad \forall i \in \Omega_G \tag{5.45}$$

where (5.35)-(5.37) are stationary conditions, and (5.38)-(5.45) are complementary slackness conditions.

2) MILP formulation: The MPEC is a nonlinear problem with the bilinear terms in (5.33) and the nonlinear complementary slackness conditions. Thus, strong duality theory and the big-M method have been used to reformulate the MPEC problem as a MILP problem that is tractable [100][101].

$$\begin{aligned}
\sum_{t\in\Omega_T}\sum_{i\in\Omega_{BS}} \pi_{i,t}^{s} \cdot P_{i,t}^{BESS,s} &= \sum_{t\in\Omega_T}\sum_{i\in\Omega_{BS}} \left(\begin{array}{l} \lambda_t^{p,s} + \lambda_t^{p,s} \dfrac{\partial P_t^{L,s}}{\partial P_{i,t}^{D,s}} + \lambda_t^{q} \dfrac{\partial Q_t^{L,s}}{\partial P_{i,t}^{D,s}} \\ + \sum\limits_{j\in\Omega_N} (\omega_{j,t}^{v\min,s} - \omega_{j,t}^{v\max,s}) Z_{j,i}^{p} \end{array} \right) P_{i,t}^{BESS,s} \\
&= \left\{ \begin{array}{l}
\sum\limits_{t\in\Omega_T} \lambda_t^{p,s} \left(\sum\limits_{i\in\Omega_N} \left(1 + \dfrac{\partial P_t^{L,s}}{\partial P_{i,t}^{D,s}}\right) P_{i,t}^{D,s} + \sum\limits_{i\in\Omega_N} \dfrac{\partial P_t^{L,s}}{\partial Q_{i,t}^{D,s}} Q_{i,t}^{D,s} + P_t^{L0,s} \right) \\
+ \sum\limits_{t\in\Omega_T} \lambda_t^{q,s} \left(\sum\limits_{i\in\Omega_N} \left(1 + \dfrac{\partial Q_t^{L,s}}{\partial Q_{i,t}^{D,s}}\right) Q_{i,t}^{D,s} + \sum\limits_{i\in\Omega_N} \dfrac{\partial Q_t^{L,s}}{\partial P_{i,t}^{D,s}} P_{i,t}^{D,s} + Q_t^{L0,s} \right) \\
+ \sum\limits_{t\in\Omega_T}\sum\limits_{j\in\Omega_N} \omega_{j,t}^{v\min,s} \left(V^{\min} - V_{sub,t}^{s} + \sum\limits_{i\in\Omega_N} Z_{j,i}^{p} P_{i,t}^{D,s} + \sum\limits_{i\in\Omega_N} Z_{j,i}^{q} Q_{i,t}^{D,s} \right) \\
- \sum\limits_{t\in\Omega_T}\sum\limits_{j\in\Omega_N} \omega_{j,t}^{v\max,s} \left(V^{\max} - V_{sub,t}^{s} + \sum\limits_{i\in\Omega_N} Z_{j,i}^{p} P_{i,t}^{D,s} + \sum\limits_{i\in\Omega_N} Z_{j,i}^{q} Q_{i,t}^{D,s} \right) \\
+ \sum\limits_{t\in\Omega_T}\sum\limits_{i\in\Omega_G} \left(\omega_{i,t}^{p\min,s} P_i^{G,\min} - \omega_{i,t}^{p\max,s} P_i^{G,\max} \right) \\
+ \sum\limits_{t\in\Omega_T}\sum\limits_{i\in\Omega_G} \left(\omega_{i,t}^{q\min,s} Q_{i,t}^{G,\min} - \omega_{i,t}^{q\max,s} Q_{i,t}^{G,\max} \right)
\end{array} \right\} \\
&\quad - \sum_{t\in\Omega_T} \left(\sigma_{sub,t}^{p,s} P_{sub,t}^{G,s} + \sigma_{sub,t}^{q,s} \widehat{Q}_{sub,t}^{G,s} + \sum_{i\in\Omega_G} \left(\sigma_{i,t}^{p,s} P_{i,t}^{G,s} + \sigma_{i,t}^{q,s} \widehat{Q}_{i,t}^{G,s} \right) \right)
\end{aligned} \tag{5.46}$$

The objective function (5.33) is reformulated as (5.46). Each constraint in (5.38)-(5.45) is reformulated as:

$$0 \le \omega_{i,t} \le M_{i,t} v_{i,t}, 0 \le g_{i,t}(x) \le M_{i,t}(1 - v_{i,t}) \tag{5.47}$$

So far, the completed MILP problem can be presented as follows:

$$\max (5.46) \tag{5.48}$$

$$s.t.\ \textit{Constraints}\ (5.34) - (5.37), (5.47) \tag{5.49}$$

5.4.2 Solving the Two-stage Problem

With the reformulation of the second stage in the preceding subsection, the TS-SBP problem becomes a TS-SMILP problem which is a large-scale optimization problem that requires huge computational resources. To reduce the computational burden, the problem scale can be reduced via two aspects according to the specific characteristics of the original problem.

1) Candidate BESS buses reduction: The candidate BESS buses are binary variables that are associated with a series of constraints. However, only a limited number of buses are realistic candidate sites due to geographical and physical limits in industrial practices. Thus, these candidate buses can be reduced to a limited set of probable buses instead of all buses.

2) *Inactive voltage constraints reduction*: Continuous and binary variables, especially voltage-related ones in the second stage, account for most of the decision variables and constraints throughout the entire problem. However, most voltage constraints are inactive, and they can be omitted to reduce the number of complementary slackness conditions.

The complete solution procedure including detailed candidate buses and inactive voltage constraints reduction is described in Table 5.2.

It should be noted that **Step 3** is more like data pre-processing since candidate buses may be influenced by the investor's preference as well as the actual operating conditions which are hard to handle quantitatively. Here, **Step 3** obtains the most probable installation buses but does not ensure the equivalence with the original problem.

Table 5.2. Overall solution procedure.

Algorithm 2: Overall Solution Procedure

1. Decomposition: Since there is a finite set of scenarios, (5.25) can be reformulated as:

$$\max \quad 365 \cdot \sum_{s \in S} p(s)\left(-\boldsymbol{c}^T \boldsymbol{x}_s + \boldsymbol{\pi}_s{}^T \boldsymbol{y}_s\right)$$

Decompose it into S subproblems.

2. Initialization: For each $s \in S$, compute:

$$\left(\boldsymbol{x}_s, \boldsymbol{y}_s\right) \in \arg\max -\boldsymbol{c}^T \boldsymbol{x}_s + \boldsymbol{\pi}_s{}^T \boldsymbol{y}_s$$

3. Candidate buses reduction: Obtain the aggregated binary variable: $\hat{\boldsymbol{\delta}} = \sum_{s \in S} p_s(s)\boldsymbol{\delta}_s$, where $\hat{\boldsymbol{\delta}} = \left\{\hat{\delta}_1, \ldots, \hat{\delta}_{\Omega_N}\right\}$; remove $\hat{\delta}_i$ with low values; the rest are the most probable buses.

4. Voltage constraints reduction: Check $\boldsymbol{V}_s = \left\{V_1, \ldots, V_{\Omega_N}\right\}$, $s \in S$, identify buses at which voltage constraints are never violated; then, remove constraints at these buses.

5. Solving: With reduced candidate buses and voltage constraints, compute: $\left(\boldsymbol{x}, \boldsymbol{y}_s\right) \in \arg\max -\boldsymbol{c}^T \boldsymbol{x} + 365 \cdot \sum_{s \in S} p(s) \boldsymbol{\pi}_s{}^T \boldsymbol{y}_s$.

6. Voltage constraints update: Check whether the removed voltage constraints are violated or not. If yes, add the violated ones and go back to **Step 5**; otherwise, the algorithm terminates.

5.5 Case Studies

The proposed model is tested on the modified IEEE 33-bus and 123-bus distribution systems. Simulations are performed on a personal laptop with an Intel Core i7-8650U CPU and 16GB RAM. The codes are carried out in MATLAB R2020a, YALMIP and GUROBI 9.0.0.

5.5.1 IEEE 33-Bus Distribution System

1) System description: The modified IEEE 33-bus system is illustrated in Figure 5.2. Two MTs are located at buses 18 and 33, respectively, and two SVCs are located at buses 16 and 30, respectively. The parameters of DGs, the distribution system, BESS investment and operating constraints are listed in Table 5.3.

2) Scenario extraction: The daily day-ahead LMP and load profiles in one year have been obtained from PJM [170], and the time range is 1/1/2020-12/31/2020. After *k*-means clustering, the optimal cluster numbers obtained via the elbow method are $k_{LMP} = 7$ and $k_{load} = 6$, respectively. The normalized LMP patterns, load patterns, and their discrete joint probabilities are shown in Figure 5.3. It can be seen that some probabilities are 0 which means the corresponding LMP pattern and load pattern have never appeared on the same day. Thus, among the 42 scenarios, we can remove the scenarios with probabilities less than 0.01. Then, 21 scenarios are kept.

To validate the effect of the scenario extraction, the best way is to compare the optimal sites and sizes that are obtained by solving the proposed TS-SBP model with all 365 scenarios (1-year LMP and load data) and that with extracted scenarios, respectively. However, the first one requires huge computation resources, it is intractable in our current laboratory environment. Thus, an alternative method is proposed to achieve the validation: given the optimal sites and sizes obtained by extracted scenarios, compare the annual net profit of all scenarios and that of extracted scenarios. Due to the variability consideration of nodal loads shown in (5.31)(5.32), the simulation is run multiple times.

The curves of the average annual net profit are illustrated in Figure 5.4. It can be found that the two curves become flat and closer with the increase of simulation times.

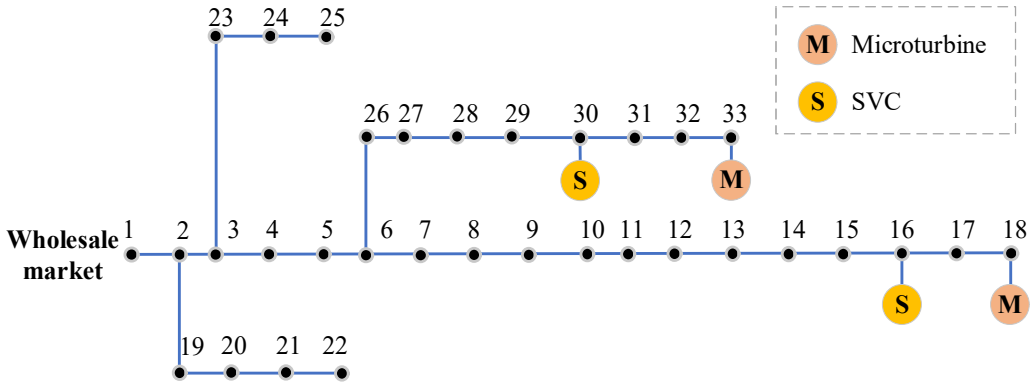
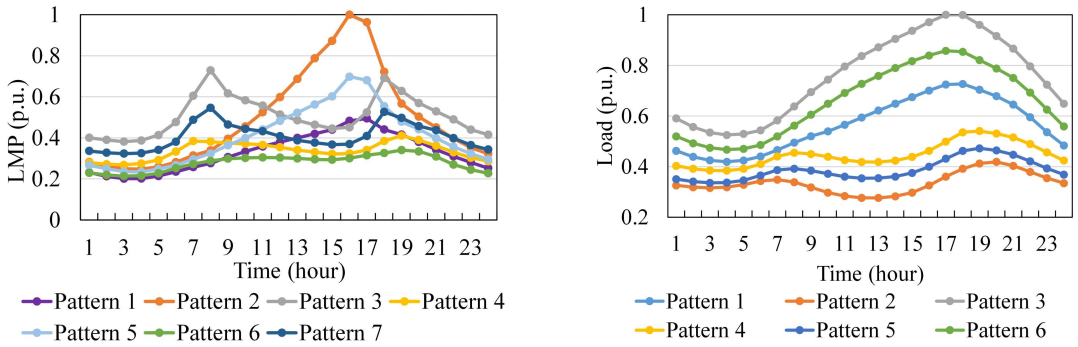


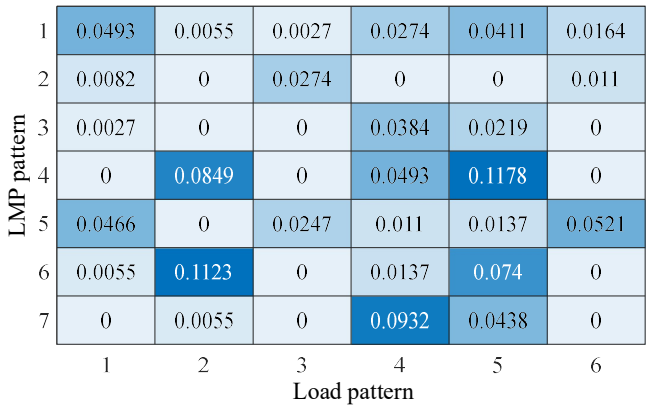
Figure 5.2. Modified IEEE 33-bus system.

Table 5.3. Parameters of the modified IEEE 33-bus system.

Class	Parameter	Typical Value
MT	Location	Bus #18, 33
	Bidding price	$ 70/MWh
	Capacity	0.5 MW
	α_i	0.95
SVC	Location	Bus #16, 30
	Bidding price	$ 0/MVarh
	Capacity	0.5 MVar
System constraints	V^{min}	0.95 p.u.
	V^{max}	1.05 p.u.
	V_{sub}	1.0 p.u.
	Peak load	6.316 MW + j3.026 MVar
Investment constraints	N_{BS}^{max}	5
	C^{Bgt}	$ 1×10^6
	P^{min} / P^{max}	0.1 MW / 0.4 MW
	E^{min} / E^{max}	0.4 MWh / 1.2 MWh
BESS operating constraints	SOC_i^{min} / SOC_i^{max}	0.2 / 0.8
	η_i	0.81



(a) LMP patterns (b) Load patterns



(c) Probability

Figure 5.3. LMP patterns, load patterns, and their discrete joint probabilities.

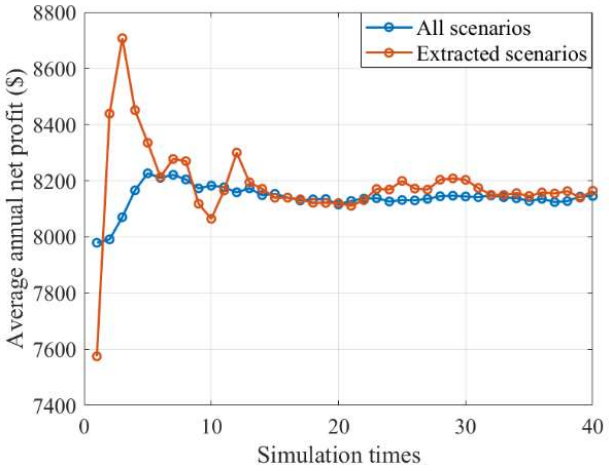


Figure 5.4. Average annual net profit of all scenarios and that of extracted scenarios.

3) BESS siting and sizing results: After Algorithm 2 has been performed, 11 buses are selected as the most probable BESS candidate buses, Ω_{BS} = {10-12, 14-18, 31-33}, the voltage constraints at 12 buses are kept, Ω_V = {9-15, 17-18, 31-33}.

To verify the effectiveness of the proposed scale reduction methods, five cases with different reduced items are formulated in Table 5.4. and Table 5.5 presents the siting and sizing results.

From Table 5.5, it can be found that Cases 1-5 have the same BESS siting and sizing results. The annual net profit of Case 1 is slightly different which is reasonable because more scenarios are considered. Cases 2-5 have close annual net profits, but significantly different computational times. In these cases, both candidate bus reduction and inactive voltage constraint reduction can improve computational efficiency. Their combination makes for the best-observed performance.

Comparison of intermediate results among Cases 2-5 is presented since they have the same scenarios. Here, Case 2 is set as the benchmark, Cases 3-5 are compared with Case 2. Then, the number of constraints and variables, the accumulated difference of voltage, DLMP, DG power output, and BESS power output are provided in Table 5.6, respectively. The accumulated voltage difference is calculated using the following equation:

$$\Delta V = \sum_{s\in S}\sum_{t\in\Omega_T}\sum_{j\in\Omega_N}\frac{\left|V_{j,t}^{s,rel}-V_{j,t}^{s,ben}\right|}{V^{ben,\max}} \tag{5.50}$$

where $V_{j,t}^{s,rel}$ and $V_{j,t}^{s,ben}$ are the voltage of scenario s at bus j and time t for the relaxed case and benchmark case respectively, $V^{ben,\max}$ is the maximum value. The DLMP difference ($\Delta DLMP$), DG power output difference (ΔP^{DG}), and BESS power output difference (ΔP^{BESS}) are calculated in a similar formula. Note that the accumulated difference is the summation of individual differences of all scenarios at all time slots and all buses.

From Table 5.6, it can be found that the application of relaxations can reduce the number of constraints and decision variables. In addition, all the accumulated differences of variables are of small value. All of these validate the effectiveness of the proposed scale reduction methods.

Table 5.4. Different cases.

Cases	Reduced Items		
	Scenarios	Voltage constraints	Candidate buses
Case 1	×	×	×
Case 2	√	×	×
Case 3	√	×	√
Case 4	√	√	×
Case 5	√	√	√

*×: not reduced, √: reduced.

Table 5.5. Results of different cases.

Cases	BESS bus (#)	P^{rated}/E^{rated} (kW/ kWh)	Annual net profit ($)	Time (s)
Case 1	11, 15, 18, 31, 33	100/400, 149/597, 103/414, 107/426, 100/400	9302.22	7936
Case 2	11, 15, 18, 31, 33	100/400, 149/597, 103/414, 107/426, 100/400	9129.37	3442
Case 3	11, 15, 18, 31, 33	100/400, 149/597, 103/414, 107/426, 100/400	9129.38	1338
Case 4	11, 15, 18, 31, 33	100/400, 149/597, 103/414, 107/426, 100/400	9129.38	2390
Case 5	11, 15, 18, 31, 33	100/400, 149/597, 103/414, 107/426, 100/400	9129.38	1077

Table 5.6. Comparison of intermediate results.

Cases	Constraint	Variable	ΔV	$\Delta DLMP$	ΔP^{DG}	ΔP^{BESS}
Case 2	410801	227907	--	--	--	--
Case 3	321063	183489	0.0162	0.0938	0.0317	0.4189
Case 4	326129	185571	0.0162	0.0938	0.0317	0.4189
Case 5	236391	141153	0.0162	0.0938	0.0317	0.4189

The expected DLMP is defined as the weighted sum of the DLMPs of all scenarios. It is illustrated in Figure 5.5. The optimal BESS locations are buses #11, 15, 18, 31, and 33. These locations are intuitively reasonable because the daily DLMP gap (the difference between the highest DLMP and the lowest DLMP) is high in these buses, as shown in Figure 5.5. Therefore, BESS owners make more profits. It can be concluded that the DLMP provides effective market signals for the BESS investment. On the other hand, the higher DLMP reflects the scarcity of generation resources and stressed operating conditions. Thus, from the perspective of the DSO, installing BESSs in these locations can increase the local power supply, and benefit the stressed distribution system with a positive effect on the DSO. This is aligned with the incentive compatibility mechanism. System improvement is discussed in the next subsection.

4) Load profile and voltage improvement: Among the reduced scenarios, we select scenario 13 which has the highest system load level. In the second stage, system load profiles over one day before and after BESS installation are shown in Figure 5.6. It can be found that with the integration of BESSs, peak load at t = 13:00-19:00 is shifted to off-peak hours t = 2:00-6:00. The operation stress in the heavy load condition is relieved.

The nodal voltage profiles in this scenario after BESS installation are shown in Figure 5.7. It can be observed that the voltage profiles over one day are well maintained in the voltage boundaries.

5) Effect of DER penetration level: With the integration of various DERs, the number of existing DERs can also affect the optimal allocation of BESSs. In this subsection, four cases are formulated to study the effects of different DER penetration levels. Here, photovoltaics (PVs) are selected as a new DER with a bidding price of $15/MWh and a capacity of 0.5 MW. The locations of DERs are listed in Table 5.7. The simulation results can be found in Table 5.8.

From Table 5.8, it can be seen that with the increase of DER penetration level, the optimal BESS allocation is changed and the annual net profit is reduced. The main reason is as follows: compared to MTs and the wholesale LMP, PVs usually have the lowest bidding price, thus they easily win the bidding. With the large-scale integration of PVs, the DLMP profile changes and the overall system DLMP is reduced.

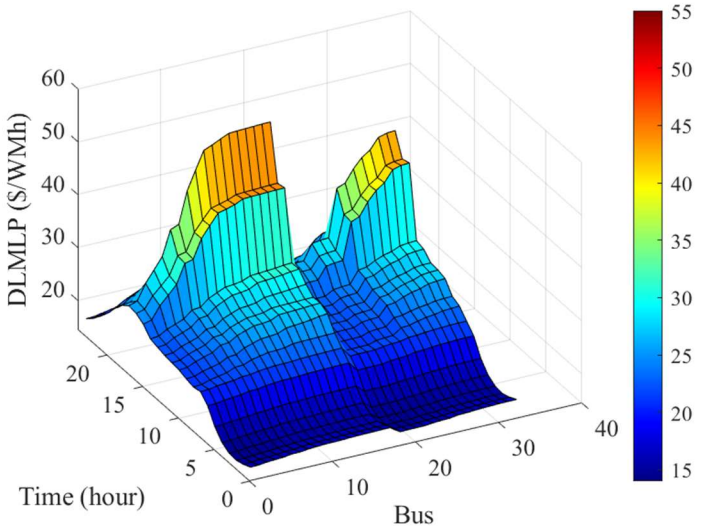


Figure 5.5. Expected DLMP of Case 5.

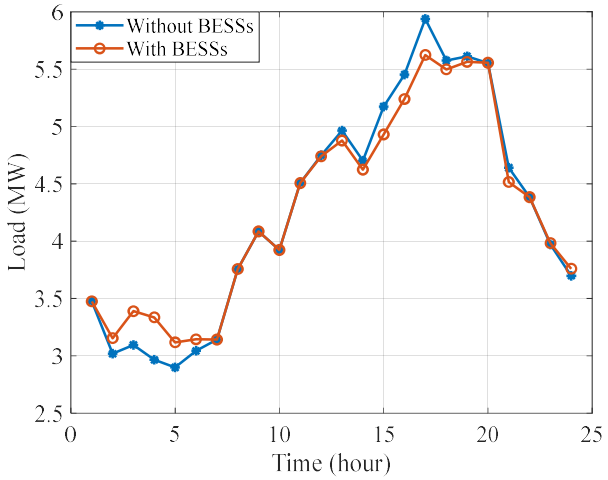


Figure 5.6. System load profiles with and without BESSs.

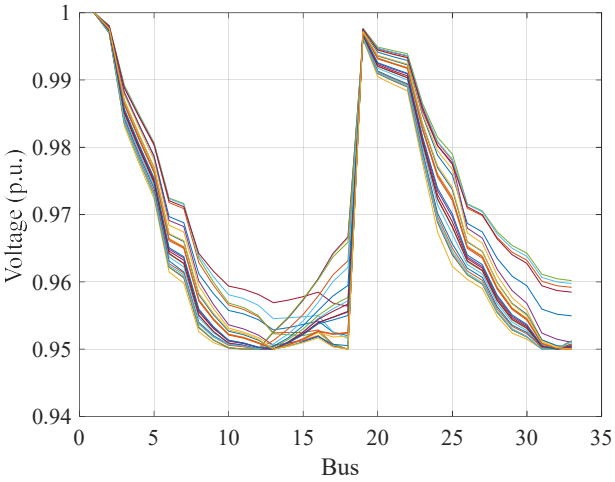


Figure 5.7. Nodal voltage profiles with BESSs.

Table 5.7. Different DER penetration levels.

Cases	DERs	Number	Bus (#)
Case 1	SVC	2	16, 30
	MT	2	18, 33
	PV	0	None
Case 2	SVC	2	16, 30
	MT	2	18, 33
	PV	2	12, 28
Case 3	SVC	2	16, 30
	MT	3	8, 18, 33
	PV	3	12, 14, 28
Case 4	SVC	3	10, 16, 30
	MT	4	8, 18, 26, 33
	PV	5	12, 14, 17, 31, 32

Table 5.8. Simulation results.

Cases	BESS bus (#)	P^{rated} / E^{rated} (kW/ kWh)	Annual net profit ($)	Time (s)
Case 1	11, 15, 18, 31, 33	100/400, 149/597, 103/414, 107/426, 100/400	9129.37	1077
Case 2	15, 18, 32, 33	100/400, 149/597, 100/400, 210/840	5858.96	492
Case 3	16, 18, 32, 33	101/405, 141/563, 100/400, 217/869	5705.55	580
Case 4	16, 18, 32, 33	100/400, 129/514, 100/400, 231/923	5184.61	1692

Since the optimal allocation of BESSs is closely related to the DLMP, the allocation and profit are changed as well. A more comprehensive analysis of profit reduction can be found in [100].

PVs are studied here because they are one of the most common DGs that can be installed in the distribution system. A PV can be replaced by other DGs and the simulation results will be different, but the in-depth reasoning should be similar. Also note, BESS mitigation of the volatility of PVs is not the focus of this chapter.

6) Comparison with other models: It is beneficial to compare the proposed model with other models. Here, two more models are formulated. In Model 2, it is assumed that all BESSs have the same and fixed sizes, only sites are to be determined. In Model 3, the candidate bus set is Ω_{BS} = {11-18, 33}, which is obtained by the method proposed in [145], and other conditions are kept the same with the proposed model. The simulation results are shown in Table 5.9. The BESS locations of Model 2 are close to that of the proposed model, but the annual net profit is suboptimal. In Model 3, the candidate bus set determination and optimal siting and sizing are separated. And its profit is not the best. This indicates that a comprehensive algorithm (e.g., Algorithm 2) that combines these two items is truly effective and promising.

5.5.2 IEEE 123-Bus Distribution System

1) System description: The topology of the modified IEEE 123-bus system is shown in Figure 5.8 . Six MTs, five SVCs and six PVs are already installed in the system. Parameters of the system are listed in Table 5.10. System constraints, BESS investment, and operating constraints are the same as those in Table 5.3.

2) BESS siting and sizing results: The normalized LMP patterns, load patterns, and their discrete joint probabilities are the same as those in Figure 5.3. To reduce the computational burden, scenarios with probabilities less than 0.02 were removed. Then, 16 scenarios were kept.

After Algorithm 2 is performed, seven buses are selected as the candidate BESS buses, Ω_{BS} = {65, 66, 85, 94, 104, 112, 114}, while the voltage constraints at twenty buses are kept, Ω_{V} = {65, 66, 71, 75, 83-85, 87-96, 104, 113, 114}.

Table 5.9. Comparison with other models.

Models	BESS bus (#)	P^{rated}/E^{rated} (kW/ kWh)	Annual net profit ($)
Proposed model	11, 15, 18, 31, 33	100/400, 149/597, 103/414, 107/426, 100/400	9129.37
Model 2	11, 15, 17, 32, 33	112/448, 112/448, 112/448, 111/445, 112/448	8780.28
Model 3	11, 15, 16, 18, 33	100/400, 110/439, 100/400, 103/413, 146/585	8794.21

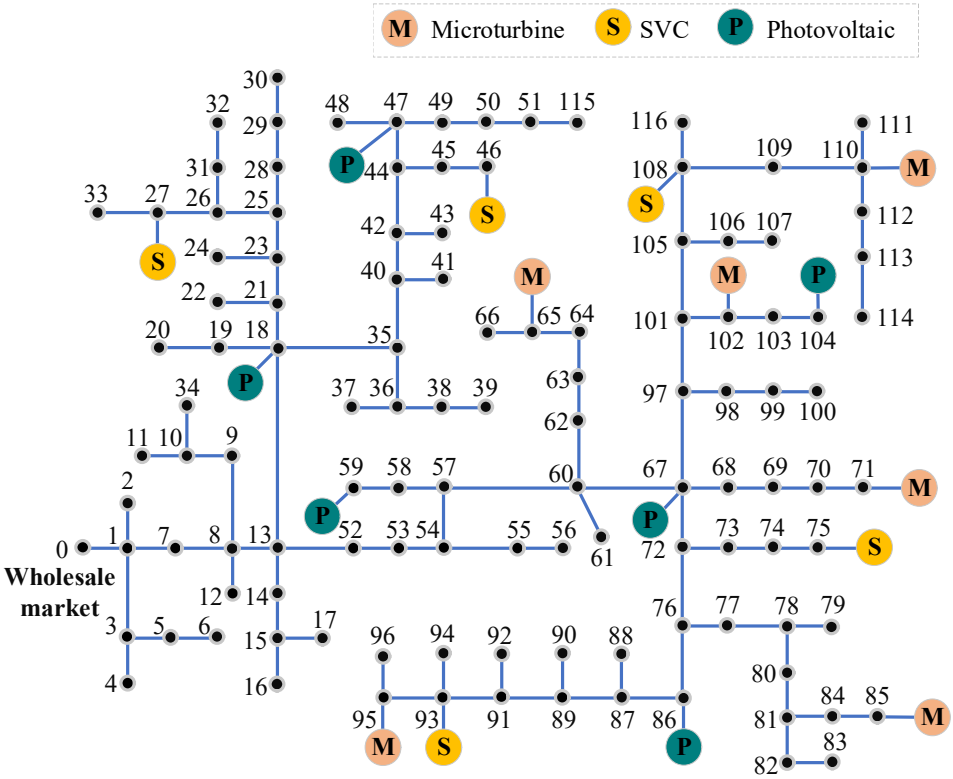


Figure 5.8. Modified IEEE 123-bus system.

Table 5.10. Parameters of the modified IEEE 123-bus system.

Class	Parameter	Typical Value
MT	Location	Bus #65, 71, 85, 95, 102, 110
	Bidding price	$ 70/MWh
	Capacity	0.5 MW
	α_i	0.95
SVC	Location	Bus #27, 46, 75, 93, 108
	Bidding price	$ 0/MVarh
	Capacity	0.5 MVar
PV	Location	Bus #18, 47, 59, 67, 86, 104
	Bidding price	$ 15/MWh
	Capacity	0.5 MW
	α_i	0.95
System parameters	Peak load	7.06 MW + j3.88 MVar

Table 5.11 and Table 5.12 present the simulation results of the five cases that are formulated in Table 5.4. Form Table 5.11, it can be found that the sites and sizes of Cases 2 & 4 and Cases 3 & 5 are slightly different. This validates the discussion at the end of Section IV that the reduction of candidate buses does not ensure equivalence with the original problem. However, these results are still very close, such as the similar annual net profit, similar sizes, and close locations of BESSs. Thus, the allocation results of Case 5 are acceptable for investors.

From Table 5.12, all the accumulated differences are still in a small value. Also, comparing the number of constraints and variables in Table 5.12 with that in Table 5.6, it can be seen that a bigger percentage of constraints and variables is reduced. It indicates these relaxation strategies have a better performance with the increase of system scale. The computational time is maintained at an acceptable level, which further demonstrates that the proposed relaxation strategies can achieve a tradeoff between accuracy and efficiency.

3) Load profile and voltage improvement: In this subsection, scenario 4 is selected. Figure 5.9 shows the load shifting effect, where the load at t = 16:00-18:00 is shifted to off-peak hours t = 3:00-4:00. The nodal voltage profiles with BESSs are shown in Figure 5.10, and the voltage profiles are well maintained.

4) Comparison with other models: The comparison with other models is presented in Table 5.13. In Model 3, the candidate bus set is Ω_{BS} = {66, 71, 75, 84, 85, 104, 111-114}. It can be found that Model 2 and the proposed model have the same optimal sites, but its profit is not the best. In Model 3, the number of optimal sites reduces to 3. This further shows that the joint optimization of sites and sizes is the best choice.

5.6 Conclusions

In this chapter, a profit-oriented BESS planning problem that sites and sizes BESSs is proposed in a deregulated distribution system with the integration of DLMP. This problem is formulated as a TS-SBP model, in which the first stage determines the optimal sites and sizes of BESSs, and the second stage maximizes investors' operating revenue. Typical operating scenarios are extracted from the historical dataset by statistical methods. Two scale-reduction strategies are proposed to relax the original problem. Numerical studies on two systems demonstrate the following conclusions:

Table 5.11. Results of different cases.

Cases	BESS bus (#)	P^{rated}/E^{rated} (kW/ kWh)	Annual net profit ($)	Time (s)
Case 1	N/A	N/A	N/A	N/A
Case 2	65, 66, 85, 113	100/400, 159/635, 200/802, 100/400	4604.90	9808
Case 3	65, 66, 85, 114	100/400, 160/642, 199/795, 100/400	4604.30	2790
Case 4	65, 66, 85, 113	100/400, 159/635, 200/802, 100/400	4604.90	2126
Case 5	65, 66, 85, 114	100/400, 160/642, 199/795, 100/400	4604.30	1272

Table 5.12. Comparison of intermediate results.

Cases	Constraint	Variable	ΔV	$\Delta DLMP$	ΔP^{DG}	ΔP^{BESS}
Case 2	100426	554079	--	--	--	--
Case 3	662277	384789	0.1175	0.0456	0.0615	1.2686
Case 4	709355	406623	9.3e-9	9.4e-10	2.3e-8	9.3e-9
Case 5	367365	237333	0.1175	0.0456	0.0615	1.2686

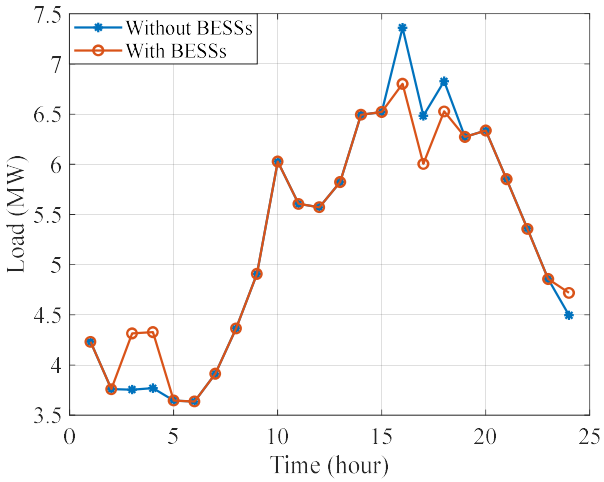


Figure 5.9. System load profiles with and without BESSs.

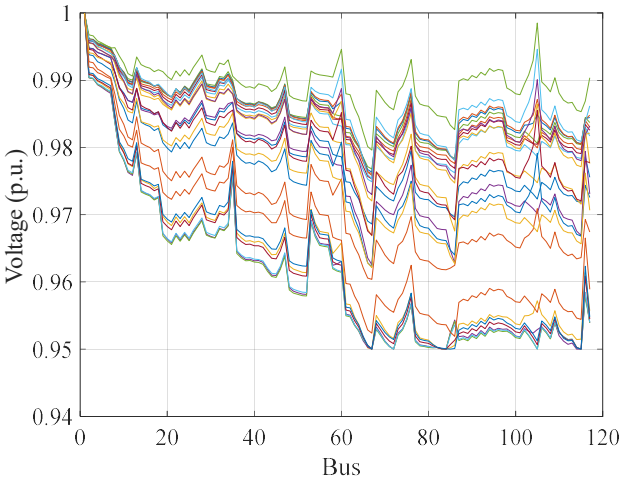


Figure 5.10. Nodal voltage profiles with BESSs.

Table 5.13. Comparison with other models.

Models	BESS bus (#)	P^{rated}/E^{rated} (kW/ kWh)	Annual net profit ($)
Proposed model	65, 66, 85, 114	100/400, 160/642, 199/795, 100/400	4604.30
Model 2	65, 66, 85, 114	140/560, 140/560, 140/560, 139/557	4589.28
Model 3	66, 85, 113	256/1023, 203/814, 100/400	4601.14

- The DLMP can act as an effective price signal to incentivize BESS planning. This is a special attribute of the deregulated system that is quite different from traditional ones.
- The proposed two scale-reduction strategies are verified to both significantly improve the computational efficiency and maintain the result accuracy.
- Optimal siting and sizing are shown to be beneficial for both BESS investors and the DSO, such that it is aligned with the incentive compatibility in market operation.

In this chapter, although only the energy market is studied, BESSs can also participate in the ancillary service market to mitigate the uncertainty of renewable generators or regulate the system frequency, which may be explored in future works. Additionally, the proposed model and solution methods can be easily extended to other DER planning problems. Future work may also be extended to resilience-oriented BESS planning for areas where resilience or extreme weather event is a major concern.

Chapter 6 A Hybrid Two-layer Pool-based and P2P Distribution Market Integrating Network Constraints and Transaction Autonomy

In a distribution system with a high penetration of distributed energy resources (DERs), it is important to ensure physical network constraints and satisfy prosumers' desire for a high degree of transaction autonomy. To address this, a hybrid two-layer distribution electricity market is proposed with a pool-based market at the upper layer considering the network constraints, and a community-based peer-to-peer (P2P) market at the lower layer ensuring trade autonomy. The pool-based market is centrally cleared, while the P2P market is cleared by a variant of the alternating direction multiplier method (ADMM) algorithm. Additionally, a novel quantity adjustment strategy is proposed to facilitate the equilibrium between peers and the distribution grid. The privacy of the grid and peers is preserved because only the distribution locational marginal price (DLMP) and energy quantity are exchanged between the two layers. Simulations on the IEEE 33-bus system validate the convergence performance of the ADMM algorithm and the quantity adjustment strategy. The lower layer P2P market can also react flexibly to the upper layer DLMP as either a net load or a net generation.

6.1 Introduction

The proliferation of distributed energy resources (DERs) is driving a transition from traditional passive distribution systems towards active and flexible ones. With this evolution, consumers seek a high degree of freedom to choose suppliers and producers aim for supply autonomy. To promote these needs and keep pace with the deregulation process, a market-based distribution system is believed to be a promising approach to optimally manage these DERs [212][213]. In this context, numerous academic studies and industrial pilot projects have been carried out. Based on these works, distribution-level markets can be classified into two categories: pool-based markets and peer-to-peer (P2P) markets.

The pool-based market resembles the wholesale electricity market which is centralized and hierarchical. The distribution system operator (DSO) collects bids and offers from all

participants, clears the market and broadcasts electricity prices such as the distribution locational marginal price (DLMP) to the system. The advantage of this market is that the physical operating conditions (e.g., power flow, voltage, imbalance) are easy to manage. In [52][8], the pool-based distribution market was established and DLMP was derived and analyzed. References [214][40] extended the single-phase electricity market to three phases and discussed the DERs operation in each phase. Studies in [150][215] explored the optimal operation of demand response and the optimal siting and sizing of battery energy storage systems within the pool-based market.

The P2P market is designed to be a less centralized, bottom-up and transparent market in which energy consumers, producers, and prosumers can trade autonomously [14]. In this market, each peer is able to negotiate, accept or reject a transaction based on their preferences and privacy considerations. The P2P market is a new and rapidly evolving area that has attracted many researchers, resulting in a vast number of publications. Currently, many P2P studies focus on two problems: (1) how to achieve load-generation balance between peers in a local system, and (2) how to integrate physical network constraints when applying the P2P market in a large system.

Regarding problem (1), various trading mechanisms, solution algorithms, and advanced technologies have been proposed. For trading mechanisms, different game theories have been applied to reach equilibrium, such as non-cooperative games for distributing surplus energy [216], Stackelberg games for modeling peer interactions [217], coalitional games [218] or Nash bargaining [71][219] for achieving fair benefit-sharing. In the auction theory-based mechanism, peers adjust their energy quantities and prices until they reach the load-generation balance [47][220]. Many decentralized/distributed algorithms have been designed to reach consensus between peers in an iterative way, such as the relaxed consensus + innovation (RCI) approach [221], the analytical target cascading (ATC) algorithm [222], and the privacy-preserving distributed optimization paradigm [223]. Additionally, blockchain technology provides a platform and tools to enable secure and transparent transactions for the P2P market [224].

In problem (2), network information is usually not available to public peers and its integration may increase the problem complexity and challenge the mechanisms and

algorithms mentioned above. Recent P2P studies have updated the market design by incorporating the network constraints into the negotiation loop [225][226]. In [227], the voltage sensitivity factor, power transfer sensitivity factor and power loss sensitivity factor were employed to assess the impact of P2P transactions on the network. In [41][228], the DSO charged peers for network usage, which could penalize P2P transactions that were unfavorable for the DSO. Reference [45] proposed a two-stage P2P market in which the DSO could disapprove certain trades to ensure system security. In [229], the DSO checked the feasibility of the P2P transactions and informed responsible peers to adjust their bids if network constraints were violated. The external network constraints were internalized by evaluating the impacts of P2P trades on the distribution system in [230].

The aforementioned works have extensively studied the two market structures, and they usually assume the P2P market and the distribution network are at the same level and that there is only one dominant market structure. However, since the future distribution level market is still an open topic, the pool-based and P2P markets are not necessarily mutually exclusive but can be coupled or co-exist within the same distribution system.

In this chapter, we propose a two-layer hybrid distribution market framework, which is illustrated in Figure 6.1. The upper layer pool-based market involves P2P community managers, large-capacity (relative to distribution systems) consumers and generators, while the lower layer community-level P2P market enables local consumers and producers to trade autonomously. The framework incorporates physical network constraints at the upper level and ensures transaction autonomy at the lower level. The exchange of information between the two levels is limited to the deficit/extra energy and economic signals. The contributions are summarized as follows:

- A two-layer market structure is proposed in the distribution system with both network security and transaction autonomy achieved.
- Privacy information of the network and peers is preserved. The network information is only accessed by the DSO at the upper layer, and utility and cost functions of peers are only known by themselves. Only DLMP and energy quantity are exchanged between the two layers.

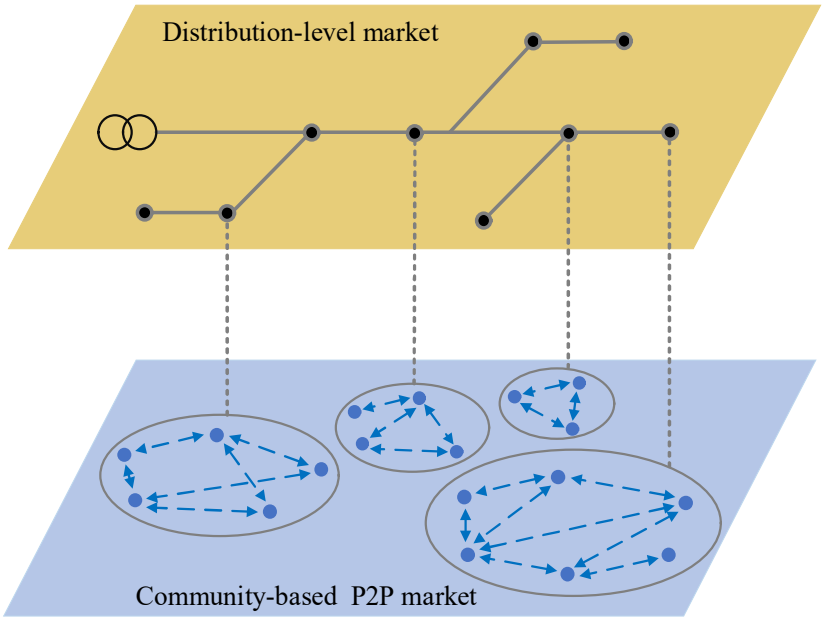


Figure 6.1. Framework of the two-layer market.

- In the community P2P market, a variant alternating direction multiplier method (ADMM) algorithm is adopted to achieve the negotiation process between peers. It is a decentralized method in which peers optimize their own problems independently and in parallel and transfer limited information.
- An energy quantity adjustment strategy is proposed to facilitate the equilibrium between peers and the distribution grid.

6.2 Network Topology Determinization

The high penetration of DERs has transformed the traditional unidirectional distribution system into a bidirectional one. In a bidirectional distribution system, a specific network topology is not necessarily the most economic and secure one at all times. Thus, in the proposed market, network reconfiguration is conducted before the day-ahead market to determine the switch on-off status and shunt capacitor status, with switching action cost considered in the model. This is analogous to the unit commitment which occurs before the market clearing in the wholesale market. Note that equations (6.1)-(6.24) are all time-dependent and the expression $\forall t \in \Omega_T$ behind each equation is neglected for simplicity.

6.2.1 Radial Network Constraints

In this study, the single commodity flow (SCF) [231] is adopted to model the radial distribution system. This method assumes a virtual lossless network that has the same topology and switch status as the target distribution system.

$$\sum_{i,j\in\Omega_L} s_{ij,t} = \left|\Omega_N\right| - 1, \quad \forall (i,j) \in \Omega_L \tag{6.1}$$

$$\sum_{k\in\delta(j)} F_{jk,t} - \sum_{i\in\pi(j)} F_{ij,t} = -1, \quad \forall j \in \Omega_N, j \neq sub \tag{6.2}$$

$$\sum_{k\in\delta(j)} F_{jk,t} = \left|\Omega_L\right|, \quad j = sub \tag{6.3}$$

$$-Ms_{ij,t} \leq F_{ij,t} \leq Ms_{ij,t}, \quad \forall (i,j) \in \Omega_L \tag{6.4}$$

where (6.1) ensures the number of closed lines is equal to the number of buses minus one; (6.2) restricts the load quantity at each non-substation node to one; (6.3) indicates that the power flow from the substation equals the number of lines; and (6.4) represents the line flow constraint using the big-M method.

6.2.2 Capacity Bank Operating Constraints

Capacity banks (CBs) are the main devices used for Volt/Var control. They adjust their reactive power output discretely by switching each capacitor.

$$Q_{i,t}^{CB} = \sum_{k \in \Omega_{CB,i}} u_{i,k,t} q_{i,k}^{cap}, \quad i \in \Omega_{CB} \tag{6.5}$$

$$\sum_{t \in \Omega_T} \left| u_{i,k,t} - u_{i,k,t-1} \right| \le N_i^{CB}, \quad i \in \Omega_{CB}, k \in \Omega_{CB,i} \tag{6.6}$$

Constraint (6.6) limits the number of times that capacitors can be switched on and off. This constraint can be reformulated as a series of linear functions by introducing an auxiliary variable $y_{i,k,t}^{cb}$.

$$\sum_{t \in \Omega_T} y_{i,k,t}^{cb} \le N_i^{CB}, \quad i \in \Omega_{CB}, k \in \Omega_{CB,i} \tag{6.7}$$

$$u_{i,k,t} - u_{i,k,t-1} \le y_{i,k,t}^{cb}, \quad i \in \Omega_{CB}, k \in \Omega_{CB,i} \tag{6.8}$$

$$u_{i,k,t-1} - u_{i,k,t} \le y_{i,k,t}^{cb}, \quad i \in \Omega_{CB}, k \in \Omega_{CB,i} \tag{6.9}$$

6.2.3 Switch Operating Constraints

Similarly, the number of switching times of distribution feeders or laterals can also be linearized as shown in (6.10)-(6.12).

$$\sum_{t \in \Omega_T} y_{ij,t}^{s} \le N_{ij}^{S}, \quad \forall (i,j) \in \Omega_L \tag{6.10}$$

$$s_{ij,t} - s_{ij,t-1} \le y_{ij,t}^{s}, \quad \forall (i,j) \in \Omega_L \tag{6.11}$$

$$s_{ij,t-1} - s_{ij,t} \le y_{ij,t}^{s}, \quad \forall (i,j) \in \Omega_L \tag{6.12}$$

6.2.4 DG Operating Constraints

Distributed generators (DGs), especially inverter-based DGs, can not only produce active power but also produce or absorb reactive power. To meet power factor requirements, the output power of DGs should fall within a certain range, typically [α_i lagging, α_i leading].

$$P_{i,t}^{G,\min} \le P_{i,t}^{G} \le P_{i,t}^{G,\max} \tag{6.13}$$

$$-P_{i,t}^{G} \tan(\arccos \alpha_i) \le Q_{i,t}^{G} \le P_{i,t}^{G} \tan(\arccos \alpha_i) \tag{6.14}$$

6.2.5 Network Configuration Formulation

P2P community managers first estimate the DLMP and submit their net load or net generation to the DSO, which then determines the network configuration. The objective is to minimize the total system cost, including generation cost, line switch action cost, and capacitor switch action cost. As network configuration mainly focuses on the status of line switches and bank switches, power losses are neglected and linearized DistFlow is utilized the simplify the model [232]. The problem is formulated as a MILP model which is tractable.

$$\min \sum_{t\in\Omega_T} \sigma^{p}_{sub,t} P^{G}_{sub,t} + \sum_{t\in\Omega_T}\sum_{i\in\Omega_G} \sigma^{p}_{i,t} P^{G}_{i,t} + C^{s} \sum_{t\in\Omega_T}\sum_{i,j\in\Omega_N} y^{s}_{ij,t} + C^{cb} \sum_{t\in\Omega_T}\sum_{i\in\Omega_{CB}}\sum_{k\in\Omega_{CB,i}} y^{cb}_{i,k,t} \quad (6.15)$$

s.t.

Constraints (6.1)-(6.14)

$$P^{G}_{j,t} - P^{D}_{j,t} = \sum_{k\in\delta(j)} P_{jk,t} - \sum_{i\in\pi(j)} P_{ij,t}, \quad \forall\ j\in\Omega_N \quad (6.16)$$

$$Q^{G}_{j,t} + Q^{CB}_{i,t} - Q^{D}_{j,t} = \sum_{k\in\delta(j)} Q_{jk,t} - \sum_{i\in\pi(j)} Q_{ij,t}, \quad \forall j\in\Omega_N \quad (6.17)$$

$$-M\left(1-s_{ij,t}\right) \le V_{i,t} - V_{j,t} - r_{ij}P_{ij,t} - x_{ij}Q_{ij,t} \le M\left(1-s_{ij,t}\right), \quad \forall\left(i,j\right)\in\Omega_L \quad (6.18)$$

$$V^{\min}_{j} \le V_j \le V^{\max}_{j}, \quad \forall j\in\Omega_N \quad (6.19)$$

$$-2S^{\max}_{ij} \le \sqrt{3}P_{ij,t} + Q_{ij,t} \le 2S^{\max}_{ij}, \quad \forall\left(i,j\right)\in\Omega_L \quad (6.20)$$

$$-S^{\max}_{ij} \le P_{ij,t} \le S^{\max}_{ij}, \quad \forall\left(i,j\right)\in\Omega_L \quad (6.21)$$

$$-2S^{\max}_{ij} \le \sqrt{3}P_{ij,t} - Q_{ij,t} \le 2S^{\max}_{ij}, \quad \forall\left(i,j\right)\in\Omega_L \quad (6.22)$$

$$-Ms_{ij,t} \le P_{ij,t} \le Ms_{ij,t}, \quad \forall\left(i,j\right)\in\Omega_L \quad (6.23)$$

$$-Ms_{ij,t} \le Q_{ij,t} \le Ms_{ij,t}, \quad \forall\left(i,j\right)\in\Omega_L \quad (6.24)$$

where (6.16)-(6.17) are the active and reactive power balance constraints; (6.18) calculates the voltage; (6.19) limits the voltage range; (6.20)-(6.22) linearize the quadratic thermal limit of distribution lines [207]; (6.23)-(6.24) ensure there is no power flow in line *i-j* if the switch is open.

6.3 Two-Layer Distribution Market Formulation

This section focuses on the two-layer market modeling. The upper layer is a centralized distribution level market. The lower layer is multiple community-based P2P markets that are located at different buses.

6.3.1 Distribution Level Market

The network configuration has determined the network topology and CBs' status at different time slots. Thus, the reactive power injection of CBs is known and can be regarded as a constant during the market clearing. Unlike the network configuration, power losses are considered in the market clearing process to obtain the accurate DLMP. The market clearing model is shown as follows.

$$\min \quad \sigma_{sub}^{p} P_{sub}^{G} + \sum_{i \in \Omega_G} \left(\sigma_i^p P_i^G \right) \tag{6.25}$$

$$s.t.$$

$$P_j^G - P_j^D = \sum_{k \in \delta(j)} P_{jk} - \sum_{i \in \pi(j)} (P_{ij} - r_{ij} l_{ij}), \quad \forall\ j \in \Omega_N \tag{6.26}$$

$$Q_j^G - Q_j^D = \sum_{k \in \delta(j)} Q_{jk} - \sum_{i \in \pi(j)} (Q_{ij} - x_{ij} l_{ij}), \quad \forall\ j \in \Omega_N \tag{6.27}$$

$$u_j = u_i - 2(r_{ij} P_{ij} + x_{ij} Q_{ij}) + (r_{ij}^2 + x_{ij}^2) l_{ij}, \quad \forall (i,j) \in \Omega_L \tag{6.28}$$

$$P_{ij}^2 + Q_{ij}^2 = l_{ij} u_i, \quad \forall (i,j) \in \Omega_L \tag{6.29}$$

$$P_{ij}^2 + Q_{ij}^2 = \left(S_{ij}^{\max} \right)^2, \quad \forall (i,j) \in \Omega_L \tag{6.30}$$

$$(V_j^{\min})^2 \le u_j \le (V_j^{\max})^2, \quad \forall\ j \in \Omega_N \tag{6.31}$$

$$u_j = V_j^2, \quad \forall\ j \in \Omega_N \tag{6.32}$$

$$l_{ij} = I_{ij}^2, \quad \forall (i,j) \in \Omega_L \tag{6.33}$$

It should be noted that (6.30) is a nonconvex constraint. The conic relaxation has been proposed to relax the quadratic equalities into inequalities as shown in (6.34).

$$P_{ij}^2 + Q_{ij}^2 \le l_{ij} u_i, \quad \forall (i,j) \in \Omega_L \tag{6.34}$$

Then (6.34) can be reformulated in a standard second-order cone form as (6.35).

$$\left\| \begin{matrix} 2P_{ij} \\ 2Q_{ij} \\ l_{ij}-u_i \end{matrix} \right\| \le l_{ij}+u_i, \quad \forall (i,j) \in \Omega_L \tag{6.35}$$

So far, the distribution level market clearing has been reformulated as a second-order cone programming (SOCP) problem. After solving the SOCP-based market, the DLMP can be recovered from the dual variables. The analytical expression of the DLMP can be found in [56].

6.3.2 Community-based P2P Market

In the P2P market, buyers and sellers can trade freely based on their preferences. The community manager is regarded as a profit-neutral agent between peers in the P2P market and the distribution grid. Thus, buyers can buy electricity through the community manager from the distribution grid at the DLMP, and the community manager acts as a seller. Sellers can sell electricity through the community manager to the distribution grid at feed-in tariff (FIT), and the community manager acts as a buyer. When trades in the P2P market are settled, the community manager aggregates the purchasing demand or selling willingness and submits them to the DSO.

For each P2P market, the mathematical formulation is shown below [45].

$$\min \quad \sum_{b\in\Omega_B} \left\{ -U_b(p_b) + c_b^E \right\} + \sum_{s\in\Omega_S} \left\{ C_s(p_s) - c_s^E \right\} \tag{6.36}$$

$$s.t.$$

$$c_b^E = \pi^{DLMP} \cdot (-p_{be}), \quad \forall b \in \Omega_B \tag{6.37}$$

$$c_s^E = \pi^{FIT} \cdot p_{se}, \quad \forall s \in \Omega_S \tag{6.38}$$

$$\pi^{FIT} = \alpha \pi^{DLMP} \tag{6.39}$$

$$p_b = -\sum_{s\in\Omega_S} p_{bs} - p_{be}, \quad \forall b \in \Omega_B \tag{6.40}$$

$$p_s = \sum_{b\in\Omega_B} p_{sb} + p_{se}, \quad \forall s \in \Omega_S \tag{6.41}$$

$$p_{bs} + p_{sb} = 0, \quad \forall b \in \Omega_B, \forall s \in \Omega_S \tag{6.42}$$

$$p_b^{\min} \le p_b \le p_b^{\max}, \quad \forall b \in \Omega_B \tag{6.43}$$

$$p_s^{\min} \le p_s \le p_s^{\max}, \quad \forall s \in \Omega_S \tag{6.44}$$

$$p_b \ge 0, p_{bs}, p_{be} \le 0, \quad \forall b \in \Omega_B, \forall s \in \Omega_S \tag{6.45}$$

$$p_s, p_{sb}, p_{se} \ge 0, \quad \forall b \in \Omega_B, \forall s \in \Omega_S \tag{6.46}$$

where objective function (6.36) maximizes the social welfare of the P2P market; U_b is the utility function of buyer *b* and C_s is the cost function of seller *s*; the power purchase payment of buyer *b* from the distribution level market is shown in (6.37), and the selling revenue of seller *s* to the distribution level market is shown in (6.38) [221]; (6.39) sets the FIT proportionate to the DLMP, and sets $0 < \alpha < 1$ to promote the transactions within the P2P market; (6.40) shows the purchasing load of a buyer from both sellers and the grid; similarly; (6.41) shows the selling quantity of a seller to both buyers and the grid; (6.42) forces the trade quantity between a seller and a buyer should be the same; (6.43)-(6.44) represent the power limit of buyers and sellers; (6.45)-(6.46) assume the buying power is negative while selling power is positive; in (6.47)-(6.48), the utility function U_b and the cost function C_s are modeled as quadratic functions.

$$U_b\left(p_b\right) = a_b p_b^2 + c_b p_b + d_b \tag{6.47}$$

$$C_s\left(p_s\right) = a_s p_s^2 + c_s p_s + d_s \tag{6.48}$$

6.4 Peer Matching Via ADMM

The ADMM is able to decompose the large-scale optimization problem into multiple sub-problems which can be solved in parallel and independently with limited information exchange. This algorithm does not rely on strong assumptions and can protect data privacy, making it widely applicable in various problems.

Reference [233] presented an exchange problem in which agents exchanged commodities within a network. The ADMM was shown to efficiently solve this problem. Constraint (6.42) follows a similar formulation as the exchange problem. Moreover, the P2P market formulation (6.36)-(6.48) has a highly decomposed structure. These characteristics make the ADMM an appropriate algorithm to achieve peer matching in a P2P market.

In the peer matching algorithm, each peer (buyer or seller) needs to update its own load or generation, then only exchange the quantity information with peers that have trade connections at the end of one iteration. After receiving the information from the other side, peers update their scaled dual variables and perform the next quantity update. This process continues until it satisfies the convergence criterion. The detailed peer matching process is presented below.

6.4.1 Buyer Update

In iteration *k*, each buyer $b \in \Omega_B$ updates its power purchasing quantities by optimizing its own problem as follows.

$$p_b^{k+1}, p_{be}^{k+1}, \boldsymbol{p}_{bs}^{k+1} = \arg\min_{p_b, p_{be}, \boldsymbol{p}_{bs}} \left\{ \begin{aligned} & -U_b\left(p_b\right) + c_b^E \\ & + \frac{\rho}{2}\left\| p_{be} - p_{be}^k + \overline{p}_{be}^k + u_{be}^k \right\|_2^2 \\ & + \frac{\rho}{2}\left\| \boldsymbol{p}_{bs} - \boldsymbol{p}_{bs}^k + \overline{\boldsymbol{p}}_{bs}^k + \boldsymbol{u}_{bs}^k \right\|_2^2 \end{aligned} \right\} \tag{6.49}$$

$$s.t. \ \text{constraints (6.37)(6.40)(6.43)(6.45)} \tag{6.50}$$

where $\boldsymbol{p}_{bs} = \left[p_{b1}, p_{b2}, \ldots, p_{b|\Omega_S|} \right]$.

6.4.2 Seller Update

In iteration *k*, each seller $s \in \Omega_S$ updates its power selling quantities by minimizing its cost as follows.

$$p_s^{k+1}, p_{se}^{k+1}, \boldsymbol{p}_{sb}^{k+1} := \arg\min_{p_s, p_{se}, \boldsymbol{p}_{sb}} \left\{ \begin{aligned} & C_s\left(p_s\right) - c_s^E \\ & + \frac{\rho}{2}\left\| p_{se} - p_{se}^k + \overline{p}_{se}^k + u_{se}^k \right\|_2^2 \\ & + \frac{\rho}{2}\left\| \boldsymbol{p}_{sb} - \boldsymbol{p}_{sb}^k + \overline{p}_{sb}^k + \boldsymbol{u}_{sb}^k \right\|_2^2 \end{aligned} \right\} \tag{6.51}$$

$$s.t. \ \text{constraints (6.38)(6.41)(6.44)(6.36)} \tag{6.52}$$

where $\boldsymbol{p}_{sb} = \left[p_{s1}, p_{s2}, \ldots, p_{s|\Omega_B|} \right]$.

6.4.3 Community Manager Update

As discussed before, the community manager has dual roles of either a buyer (buy electricity from generators) or a seller (sell electricity to consumers).

1) As a buyer, the community manager updates its problem as follows.

$$\boldsymbol{p}_{es}^{k+1} := \arg\min_{\boldsymbol{p}_{es}} \left(\frac{\rho}{2} \left\| \boldsymbol{p}_{es} - \boldsymbol{p}_{es}^{k} + \overline{\boldsymbol{p}}_{es}^{k} + \boldsymbol{u}_{es}^{k} \right\|_2^2 \right) \tag{6.53}$$

$$s.t. \qquad p_{es} \le 0 \tag{6.54}$$

where $\boldsymbol{p}_{es} = \left[p_{e1}, p_{e2}, \ldots, p_{e|\Omega_S|} \right]$.

Since vector $\boldsymbol{p}_{es}$ has the identity coefficient matrix $\boldsymbol{I}$, the optimal solution is thus the projection of $\left(\boldsymbol{p}_{es}^{k} - \overline{\boldsymbol{p}}_{es}^{k} - \boldsymbol{u}_{es}^{k} \right)$ onto the negative part of the column space of $\boldsymbol{I}$. It can be obtained analytically as:

$$\boldsymbol{p}_{es}^{k+1} = \min\left(\boldsymbol{0}, \boldsymbol{p}_{es}^{k} - \overline{\boldsymbol{p}}_{es}^{k} - \boldsymbol{u}_{es}^{k} \right) \tag{6.55}$$

2) As a seller, the community manager updates its problem as follows:

$$\boldsymbol{p}_{eb}^{k+1} := \arg\min_{\boldsymbol{p}_{eb}} \left(\frac{\rho}{2} \left\| \boldsymbol{p}_{eb} - \boldsymbol{p}_{eb}^{k} + \overline{\boldsymbol{p}}_{eb}^{k} + \boldsymbol{u}_{eb}^{k} \right\|_2^2 \right) \tag{6.56}$$

$$s.t. \qquad \boldsymbol{p}_{eb} \ge 0 \tag{6.57}$$

The analytical optimal solution is:

$$\boldsymbol{p}_{eb}^{k+1} = \max\left(\boldsymbol{0}, \boldsymbol{p}_{eb}^{k} - \overline{\boldsymbol{p}}_{eb}^{k} - \boldsymbol{u}_{eb}^{k} \right) \tag{6.58}$$

6.4.4 Scaled Dual Variable Update

All buyers, sellers and the community manager optimize their problems in parallel. After this, peers exchange the trading quantity with others and update the scaled dual variables as shown in (6.59)-(6.67).

$$\overline{p}_{bs}^{k+1} = \overline{p}_{sb}^{k+1} = \left(p_{bs}^{k+1} + p_{sb}^{k+1} \right) / 2, \quad \forall b \in \Omega_B, \forall s \in \Omega_S \tag{6.59}$$

$$\overline{p}_{be}^{k+1} = \overline{p}_{eb}^{k+1} = \left(p_{be}^{k+1} + p_{eb}^{k+1} \right) / 2, \quad \forall b \in \Omega_B \tag{6.60}$$

$$\overline{p}_{se}^{k+1} = \overline{p}_{es}^{k+1} = \left(p_{se}^{k+1} + p_{es}^{k+1} \right) / 2, \quad \forall s \in \Omega_S \tag{6.61}$$

$$u_{bs}^{k+1} = u_{bs}^{k} + \overline{p}_{bs}^{k+1}, \quad \forall b \in \Omega_B, \forall s \in \Omega_S \tag{6.62}$$

$$u_{sb}^{k+1} = u_{sb}^{k} + \overline{p}_{sb}^{k+1}, \quad \forall b \in \Omega_B, \forall s \in \Omega_S \tag{6.63}$$

$$u_{be}^{k+1} = u_{be}^{k} + \overline{p}_{be}^{k+1}, \quad \forall b \in \Omega_B \tag{6.64}$$

$$u_{eb}^{k+1} = u_{eb}^{k} + \overline{p}_{eb}^{k+1}, \quad \forall b \in \Omega_B \tag{6.65}$$

$$u_{se}^{k+1} = u_{se}^{k} + \overline{p}_{se}^{k+1}, \quad \forall s \in \Omega_S \tag{6.66}$$

$$u_{es}^{k+1} = u_{es}^{k} + \overline{p}_{es}^{k+1}, \quad \forall s \in \Omega_S \tag{6.67}$$

6.4.5 Preferences of Buyers and Sellers

It should be noted that each buyer is assumed to be able to select preferred sellers to negotiate according to the buyer's own preferences, such as clean energy, location, service, and credit history. Similarly, each seller can also select preferred buyers. Additionally, it is assumed that buyers and sellers in the P2P market are rational enough to make the optimal choices. The in-depth investigation of how to determine their preferences is not the focus of this study. This study only adopts the above assumptions.

6.5 Solution Framework

This section focuses on the overall solution framework, especially the proposed quantity adjustment strategy.

6.5.1 Overall Solution Procedure

Algorithm 1 outlines the complete solution procedure, which comprises four steps. First, the DSO determines the network topology and CB operating conditions before the market clearing. Second, in the distribution-level market, the DSO collects all the bids and offers from large-capacity DERs and P2P community managers, clears the market by solving the SOCP-based optimal power flow model, and broadcasts the DLMP to all market participants. Third, after receiving the DLMP, peers in the P2P market trade with preferred peers via the peer matching algorithm to reach a consensus. Although the transactions within peers are settled, the transactions between peers and the distribution grid are affected by the DLMP and FIT. Since the DLMP can guide consumers' choice to buy energy from the grid or not, and FIT can incentivize producers to sell energy to the grid or not, the peers' transaction quantities with the grid will change along with the changing DLMP until

equilibrium is reached. Lastly, to facilitate equilibrium between peers and the distribution grid, an additional quantity adjustment strategy is proposed.

6.5.2 Quantity Adjustment Strategy

At Step 2.1 in Algorithm 1, it is set $p_b \leftarrow p_b^{\max}$ and $p_s \leftarrow p_s^{\min}$ to obtain the highest DLMP and FIT. This is the worst case for buyers to buy energy from the grid and the best case for sellers to sell energy to the grid. Since it is set FIT < DLMP, the P2P market after peer matching can appear in three conditions from the perspective of the DSO.

- Net load: P2P market purchases power from the grid.
- Net generation: P2P market sells power to the grid.
- No power exchange: P2P market has no power exchange with the grid.

In the net load condition, if a buyer satisfies $p_b = p_b^{\max}$, it means the buyer's marginal profit, which is defined as the derivative of the utility function with respect to the load demand, is always higher than the DLMP and this buyer is able to buy energy from the grid. Meanwhile, other buyers may buy energy from the grid in the quantity adjustment process since the DLMP will change in the iteration and may be close to the buyer's marginal profit. In the net generation condition, if a seller satisfies $p_s = p_s^{\min}$, it means the seller's marginal cost is always lower than the FIT and this seller is not willing to sell energy to the grid, while other sellers may sell energy to the grid in the quantity adjustment process. In the no power exchange condition, the P2P market achieves the local load-generation balance on its own and does not have the intention to exchange power with the external grid. However, their intention may change as the DLMP and FIT change. As a result, the behaviors of buyers and sellers could be similar to net load and net generation conditions.

Based on the above analysis, it can be assumed that the consumer will reach equilibrium with the grid when its marginal profit equals the DLMP, and the producer will reach equilibrium with the grid when its marginal cost equals the FIT. In this way, the quantity adjustment strategy can be derived. The detailed procedure of the strategy is shown in Step 4 in Table 6.1, in which $\triangle \boldsymbol{\pi}^{DLMP} = \boldsymbol{\pi}^{DLMP,\upsilon+1} - \boldsymbol{\pi}^{DLMP,\upsilon}$, $\Delta \boldsymbol{p}_{bs} = \boldsymbol{p}_{bs}^{k+1} - \boldsymbol{p}_{bs}^{k}$, $\Delta \boldsymbol{p}_{sb} = \boldsymbol{p}_{sb}^{k+1} - \boldsymbol{p}_{sb}^{k}$.

Table 6.1. Overall solution procedure.

Algorithm 1: Overall Solution Procedure

1. Network configuration determination:

$$\left(s_{ij,t}, Q_{i,t}^{CB}\right) \leftarrow \text{solve (6.15)-(6.24)}$$

2. Distribution level market:

2.1. Initialization: $p_b \leftarrow p_b^{\max}$, $p_s \leftarrow p_s^{\min}$ for each P2P market.

2.2. Market clearing: $\boldsymbol{\pi}^{DLMP} \in \arg\min_{P_{sub}^G, P_i^G} \left\{ \sigma_{sub}^p P_{sub}^G + \sum_{i \in \Omega_G} \left(\sigma_i^p P_i^G \right) \right\}$

3. Peer matching in P2P market:

while $\left\|\Delta \boldsymbol{p}_{bs}\right\|_2 + \left\|\Delta \boldsymbol{p}_{sb}\right\|_2 \geq \varepsilon^{P2P}$ **do**

3.1. Buyer update:

$$\left(p_b^{k+1}, p_{be}^{k+1}, \boldsymbol{p}_{bs}^{k+1}\right) \leftarrow \text{ solve (6.49)(6.50) for } \forall b \in \Omega_B$$

3.2. Seller update:

$$\left(p_s^{k+1}, p_{se}^{k+1}, \boldsymbol{p}_{sb}^{k+1}\right) \leftarrow \text{ solve (6.51)(6.52) for } \forall s \in \Omega_S$$

3.3. Community manager update:

$$\boldsymbol{p}_{es}^{k+1} \leftarrow \min\left(\mathbf{0}, \boldsymbol{p}_{es}^k - \overline{\boldsymbol{p}}_{es}^k - \boldsymbol{u}_{es}^k\right)$$

$$\boldsymbol{p}_{eb}^{k+1} \leftarrow \max\left(\mathbf{0}, \boldsymbol{p}_{eb}^k - \overline{\boldsymbol{p}}_{eb}^k - \boldsymbol{u}_{eb}^k\right)$$

3.4. Scaled data update:

$$\begin{pmatrix} \overline{\boldsymbol{p}}_{bs}^{k+1}, \overline{\boldsymbol{p}}_{sb}^{k+1}, \overline{\boldsymbol{p}}_{be}^{k+1}, \overline{\boldsymbol{p}}_{eb}^{k+1}, \overline{\boldsymbol{p}}_{se}^{k+1}, \overline{\boldsymbol{p}}_{es}^{k+1} \\ \boldsymbol{u}_{bs}^{k+1}, \boldsymbol{u}_{sb}^{k+1}, \boldsymbol{u}_{be}^{k+1}, \boldsymbol{u}_{eb}^{k+1}, \boldsymbol{u}_{se}^{k+1}, \boldsymbol{u}_{es}^{k+1} \end{pmatrix} \leftarrow \text{solve (6.59)-(6.67) for } \forall b \in \Omega_B, \ \forall s \in \Omega_S$$

end while

4. Quantity adjustment:

while $\left\|\Delta \boldsymbol{\pi}^{DLMP}\right\|_2 \geq \varepsilon^{DLMP}$ **do**

4.1. Net load aggregation:

$$P^{D,\upsilon} \leftarrow \sum_{b \in \Omega_B} p_b^{\upsilon} - \sum_{s \in \Omega_S} p_s^{\upsilon}$$

Table 6.1 continued.

Algorithm 1: Overall Solution Procedure

4.2. Quantity update:

if $P^{D,\upsilon} > 0$ & $p_b^{\upsilon} < p_b^{\max}$ **then**

$$p_b^{\upsilon+1} \leftarrow \max\left\{p_b^{\min},\ \min\left\{p_b^{\upsilon} + \alpha_b\left(U_b'\left(p_b^{\upsilon}\right) - \pi^{DLMP,\upsilon}\right),\ p_b^{\max}\right\}\right\}$$

else if $P^{D,\upsilon} < 0$ & $p_s^{\upsilon} > p_s^{\min}$ **then**

$$p_s^{\upsilon+1} \leftarrow \max\left\{p_s^{\min},\ \min\left\{p_s^{\upsilon} + \alpha_s\left(\pi^{FIT,\upsilon} - C_s'\left(p_s^{\upsilon}\right)\right),\ p_s^{\max}\right\}\right\}$$

else if $P^{D,\upsilon} = 0$ & $\sum p_s^{\upsilon} = \sum p_s^{\max}$ **then**

$$p_b^{\upsilon+1} \leftarrow \max\left\{p_b^{\min},\ \min\left\{p_b^{\upsilon} + \alpha_b\left(U_b'\left(p_b^{\upsilon}\right) - \pi^{DLMP,\upsilon}\right),\ p_b^{\max}\right\}\right\}$$

else if $P^{D,\upsilon} = 0$ & $\sum p_b^{\upsilon} = \sum p_b^{\max}$ **then**

$$p_s^{\upsilon+1} \leftarrow \max\left\{p_s^{\min},\ \min\left\{p_s^{\upsilon} + \alpha_s\left(\pi^{FIT,\upsilon} - C_s'\left(p_s^{\upsilon}\right)\right),\ p_s^{\max}\right\}\right\}$$

4.3. DLMP update:

$$\boldsymbol{\pi}^{DLMP,\upsilon+1} \in \underset{P_{sub}^G, P_i^G}{\arg\min}\left\{\sigma_{sub}^p P_{sub}^G + \sum_{i\in\Omega_G}\left(\sigma_i^p P_i^G\right)\right\}$$

end while

6.6 Case Studies

The proposed market and solution method have been tested on a modified IEEE 33-bus distribution system. Simulations were performed on a personal laptop with an Intel Core i7-1165G7 CPU and 16GB RAM. The codes were carried out in Python 3.9 and GUROBI 9.5.0.

6.6.1 Simulation Setup

The original network topology is shown in Figure 6.2, in which five P2P markets are established, two 300 kW Photovoltaics (PVs), two 500 kW Microturbines (MTs), and three 5x50 kVar capacitor banks are installed. The day-ahead LMP of the wholesale market, forecasted power output of PV and scaled system load profile are obtained from PJM [234].

The switch on/off cost and capacitor bank on/off cost are assumed to be \$0.5 per time and \$1 per time, respectively [235][236]. The active power bidding prices of PVs and MTs are set at \$5/MWh and \$50/MWh, respectively. In (6.39), α is set to 0.6. The stopping criteria are set to $\varepsilon^{P2P} = 0.001$, $\varepsilon^{DLMP} = 0.0001$. Each P2P market includes multiple load aggregators (LAs) as buyers and generation aggregators (GAs) as sellers. The basic P2P market information is shown in Table 6.2 and the detailed peer information can be found in Appendix D.

6.6.2 Network Topology

Network determination is performed to obtain the network topology and capacitor bank operating status throughout the day. The results are shown in Table 6.3 and Table 6.4 respectively. Table 6.3 indicates that there are three network topologies in total, with changes occurring at t = 15:00 and t = 18:00 respectively. From Table 6.4, the total reactive power is 200 kVar before t = 8:00, whereas more capacitor banks are turned on after t = 9:00 causing the total reactive power to rise to 700 kVar. Additionally, it can also be observed that the total switch action time is 4 and the total capacitor bank action time is 13, both of which are within the device action time limits. The primary reason for these changes is the increase of system load over time, which induces power flow congestion and the low voltage issue. Thus, network reconfiguration and reactive power injection are activated to change the path and quantity of the power flow to maintain the voltage level.

Table 6.2. P2P markets.

Bus (#)	7	14	17	29	31
Number of LAs	4	3	5	3	2
Number of GAs	3	3	3	4	4

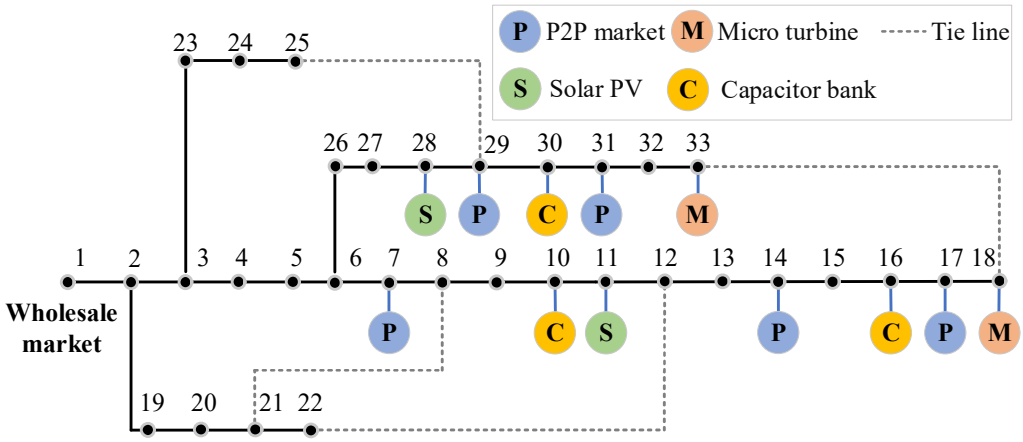


Figure 6.2. Network topology of the modified IEEE 33-bus system.

Table 6.3. Network topology.

Time period	Tie line (start bus (#) - end bus (#))
00:00 - 14:00	8-21, 12-22, 18-33, 25-29
15:00 - 17:00	10-11, 8-21, 18-33, 25-29
18:00 - 23:00	11-12, 8-21, 18-33, 25-29

Table 6.4. Capacitor bank operating status.

Bus (#)	Time period	Reactive power output (kVar)
10	00:00 - 8:00	0
	9:00 - 23:00	250
16	00:00 - 23:00	150
30	00:00 - 7:00	50
	8:00 - 23:00	250

6.6.3 Consensus of P2P Market Participants

After the network topology and capacitor bank status are determined, the market clearing process can be conducted between the distribution level market and P2P markets. The market clearing results are analyzed in this subsection and Subsection D. Taking the system at t = 14:00 as an example, this subsection focuses on the single P2P market analysis.

After running the peer matching algorithm, the transactions among the peers of the P2P market can be settled. Figure 6.3 illustrates the consensus of these peers in the P2P market that is located at bus 31. In this figure, "Pb1-s1" refers to the purchasing power of buyer 1 from seller 1. The negative value is used to maintain consistency with the definition of p_{bs} in (6.45).

Buyers and sellers can trade freely in the P2P market, with each buyer able to trade with every seller, and verse versa. The peers reach a consensus after multiple iterations of information sharing. Since buyers aim to maximize their profits, and therefore prefer purchasing power from the most affordable power sellers. For that reason, no buyers purchase electricity from seller 4 who has the highest electricity price. Moreover, each buyer only needs to share information with preferred sellers and each seller only shares information with preferred buyers. No data is shared between buyers or between sellers, preserving the privacy of peers.

In summary, this simulation validates the effectiveness of the proposed algorithm in achieving peer matching and protecting the privacy of peers.

6.6.4 Convergence Between the Two-layer Markets

Since the FIT is set to be lower than the DLMP, peers will prefer to trade within the P2P market before deciding to buy deficit power from the grid or sell extra power to the grid. According to (6.47)-(6.48), the buyer's marginal profit (BMP) and the seller's marginal price (SMP) determine the transactions between the buyers and sellers in the P2P market. By adjusting the parameters of peers in the P2P market and the distribution level market, the P2P markets are able to cover all three operating conditions: net load, net generation, and no power exchange.

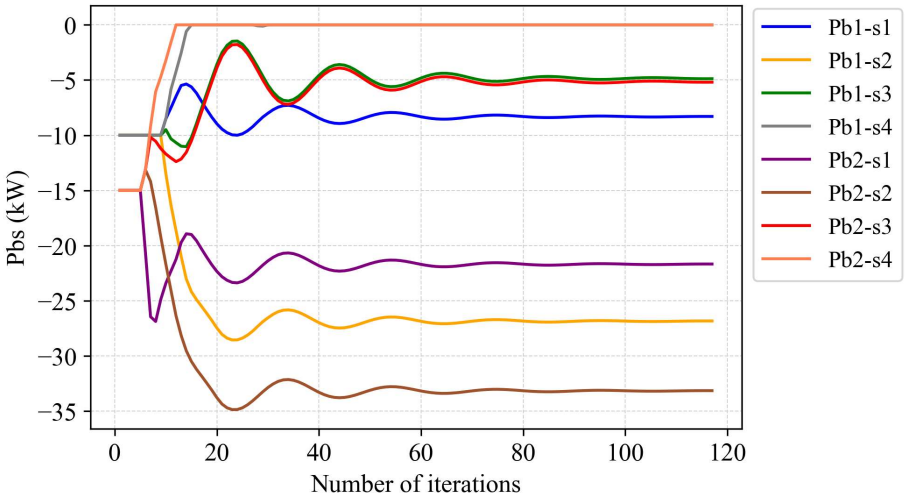


Figure 6.3. Consensus of a P2P market.

The convergence curve of the two-layer market is shown in Figure 6.4 and the converged net loads of P2P markets are presented in Table 6.5. It can be seen that the P2P markets at bus 7 and bus 17 act as loads, the P2P markets at bus 14 and bus 29 act as generators, and the P2P market at bus 31 has no power exchange with the grid. The net power of P2P markets at bus 7, bus 17 and bus 29 converges after several iterations of quantity adjustment, demonstrating the effectiveness of the proposed algorithm.

Although both P2P markets at bus 7 and bus 17 act as loads, their interaction with the grid is slightly different. At bus 7, the prices are set as BMP > DLMP > SMP, and the maximum load is higher than the maximum generation. Thus, consumers purchase the maximum generation from generators and buy the deficit load from the grid. At bus 17, the BMP is set slightly higher but close to the DLMP, and thus the consumer and the grid achieve equilibrium when BMP = DLMP during the quantity adjustment iteration. This explains why bus 7 converges faster than bus 17.

For the P2P market at bus 14, the prices are set as DLMP > BMP > FIT > SMP, and the maximum generation is higher than the maximum load. Therefore, the local generators can satisfy the local load demands and sell extra generation to the grid. At bus 29, the SMP is set a bit lower but close to the FIT, achieving an equilibrium between generator and grid when SMP = FIT during the quantity adjustment iteration.

At bus 31, the prices are set as DLMP > BMP > SMP > FIT, and the maximum generation is larger than the maximum load. The P2P market can achieve local power balance, and generators are not motivated to sell extra generation to the grid.

Based on the above analysis, there are multiple different convergence results of the P2P markets. Whether the P2P markets import power or export power depends on DLMP, FIT, BMP, SMP, extra load, and excess generation. The all-possible results can be found in [237] and the above analysis can be easily extended to explain these conditions.

6.6.5 Net Load of P2P Markets in One Day

This subsection focuses on the in-depth analysis of the net load of P2P markets throughout one day. In this subsection, the relationship between the net load and DLMP at different time internals are analyzed.

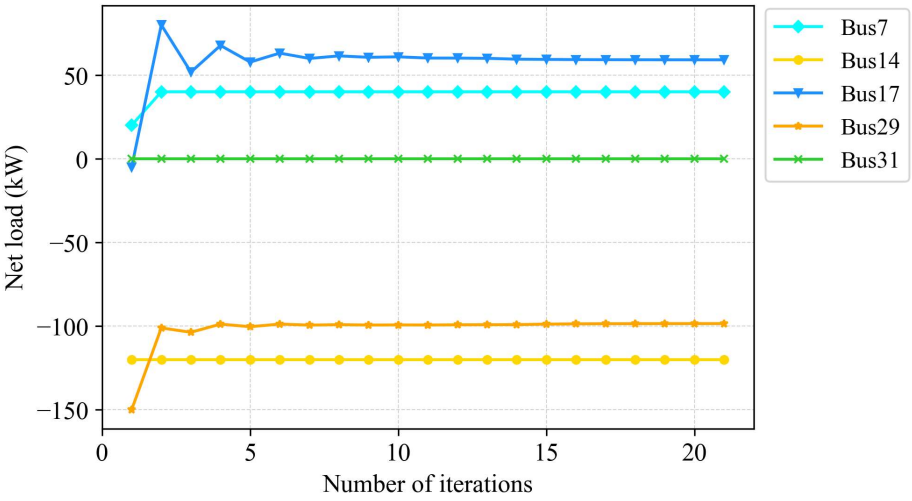


Figure 6.4. Convergence of the quantity adjustment.

Table 6.5. Net loads of P2P markets.

Bus (#)	7	14	17	29	31
Net load (kW)	40	-120	59.06	-98.67	0

Figure 6.5 presents the net load of five P2P markets over the course of a day, and Figure 6.6 shows the DLMP at five corresponding buses. In Figure 6.6, DLMPs for each bus display a similar pattern and are consistently close in value, with the differences being due to power losses. In Figure 6.5, the DLMP is shown to have a significant impact on the net load, with the P2P market serving as a load during times of low DLMP and a generator during times of high DLMP. This suggests that consumers in the P2P market prefer purchasing power from the grid over local generators when the DLMP is lower than the SMP, while generators are more likely to sell power to the grid when the FIT is high.

These results demonstrate that the DLMP can work as an incentive signal for peers to react flexibly and rationally in the two-layer market. This flexibility, in turn, enables peak load shaving, valley load filling, and emergency power supply for the distribution system, which can mitigate system operation stress during peak hours and improve system resilience under emergency conditions. Overall, the adoption of P2P markets in conjunction with the DLMP can provide significant benefits for peers locally, as well as improve the overall flexibility and resilience of the distribution system.

6.7 Conclusions

This section proposes a hybrid two-layer distribution market that enables trade autonomy in local communities while ensuring distribution system security. At the upper level, a pool-based market integrates physical operating constraints, while at the lower level, multiple less-centralized P2P markets support free transactions among DERs in communities. Numerical studies conducted on the IEEE 33-bus system demonstrate the following conclusions:

- Analogous to unit commitment in the wholesale market, the network topology is integrated in the market and determined before the market clearing.
- The ADMM algorithm enables parallel optimization of peers in the P2P market, and the proposed quantity adjustment strategy is effective in reaching equilibrium for P2P markets and the grid.
- The proposed two-layer market can protect the privacy of both the network and P2P peers and maintain the flexibility of the distribution system.

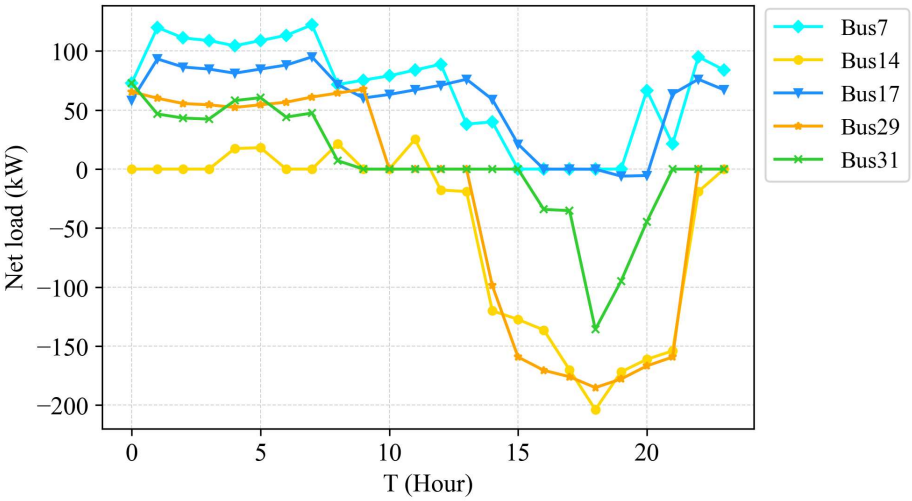


Figure 6.5. Net load of P2P markets throughout one day.

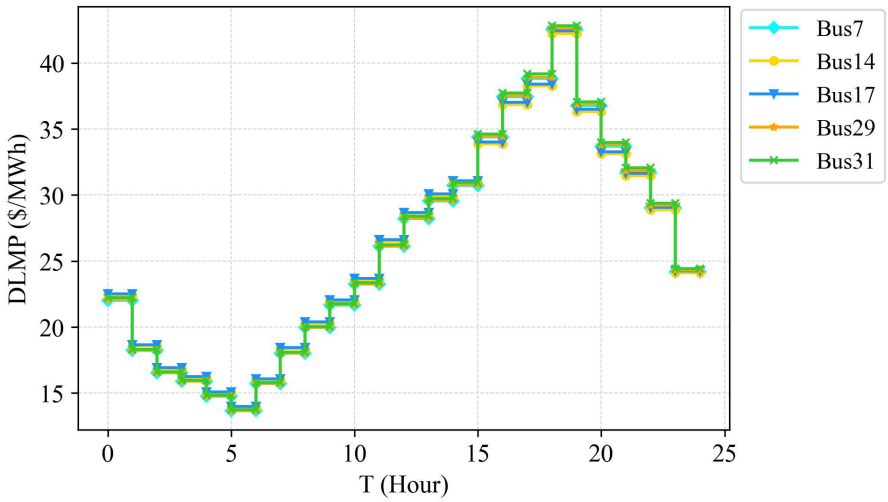


Figure 6.6. DLMP at five buses.

Chapter 7 Conclusions and Future Works

7.1 Summary of Current Progress

The distribution power grid is moving towards a more active and flexible system with the increasing penetration of DREs. In the industrial and academic fields, establishing local and distribution-level electricity markets provides an effective solution to managing large amounts of small-scale DERs. At the same time, pricing mechanisms, such as DLMP, play an important role in the operation of planning of distribution systems in a market environment. Within this context, a series of in-depth studies relating to the DLMP applications in the distribution-level markets are conducted in this dissertation.

Chapter 3 proposes utilizing DLMP as price signals to guide the electricity consumption for residential loads to reduce residents' electricity bills. A tri-level scheduling model is established, and load aggregation algorithm and load dispatch algorithms are designed, respectively. The simulation results show that the proposed model can benefit both the distribution system and residents. The in-depth analysis of DLMP components and payment components reveals three reasons leading to the benefit from flexible HVAC and EV loads: load shifts, DLMP step changes, and power losses.

Chapter 4 is the extension of the study in Chapter 3. In Chapter 4, both day-ahead schedule and real-time schedule are included and uncertainties from multiple sources are considered. In the day-ahead schedule, uncertainties of residents' electricity consumption behaviors, weather temperature forecasts, and PV power outputs are modeled. Then, a hybrid interval-stochastic programming is proposed to convert the uncertain problem into a tractable one. The above modeling is integrated into an RHO scheme which can continuously improve the schedule by utilizing the latest operating and forecast information. The simulation results show that the RHO scheme can mitigate the radicalness and conservativeness of the day-ahead schedule.

Chapter 5 presents a profit-oriented BESS planning problem with the DLMP acting as a price signal. This problem is formulated as a TS-SBP model. The first stage determines the optimal sites and sizes of BESSs, and the second stage maximizes investors' revenue under various operating scenarios. Moreover, two relaxation strategies are proposed to

reduce the large-scale optimization problem into a tractable one. The simulation results show that the optimal sites and sizes are beneficial for both BESS investors and the DSO, this is aligned with the incentive compatibility in the market. The two relaxation strategies are also verified to be effective in reducing the computational time and maintaining the result accuracy.

Chapter 6 presents a hybrid two-layer distribution market with a centralized distribution-level market in the upper layer and a decentralized community-based P2P market in the lower layer. The physical network constraints are considered, and data privacy of peers is preserved since only the DLMP and energy quantity are exchanged between the two layers. The simulation results show that variant of the ADMM algorithm can achieve the trading concesus among peers and the proposed quantity adjustment strategy and promote the convergence between two layers.

7.2 Future Directions

Based on research in the previous sections, the following topics and directions related to DLMP are believed to be worth investigating by the academic and industrial communities in the future.

7.2.1 Coordination Between Transmission-level Market and Distribution-level Market

With the increasing penetration of DERs, the role of traditional distribution networks as load-serving entities in wholesale electricity markets now evolves towards ADNs, which can proactively participate in wholesale markets. The proliferation of DERs enhances the interactions between distribution and transmission-level markets and needs coordination between the two markets to facilitate market clearing and pricing. In addition, the FERC Order 2222 [29] allows DERs and DER aggregators to participate in the wholesale market directly. Thus, it is worthwhile to explore and investigate effective pricing mechanisms, new market products, and participation models that could enable DERs to maximize their value and services to both distribution and transmission systems in a coordinated manner.

7.2.2 Integration with P2P Energy Trading

P2P energy trading is emerging in the distribution system as the number of prosumers and DERs grows. P2P trading may happen among prosumers in a local community/microgrid or among aggregators in the distribution system. P2P has many advantages as stated in Table 1.1, but it may not work as a standalone solution because the trading agents are myopic to network conditions and thus P2P trading may violate system security constraints. Also, not all customers may participate in P2P trading. Therefore, the mutual impact between P2P trading and the distribution market and DLMP needs to be fundamentally examined and understood. For example, when the network constraints are binding, in what priority should the participants in P2P trading or non-P2P DERs/prosumers be dispatched? How much of the system regulation cost should the participants in P2P trading bear? The DLMP could be designed to accommodate or align with P2P trading in distribution systems that retain the properties of P2P trading, such as preserving privacy and trading preferences, and meanwhile ensure system operational security and price fairness to all customers.

7.2.3 Profit-oriented Investment

As discussed in Section V.C, pricing mechanisms can be effective market signals for infrastructure or DER investment. Due to cost-reflective and spatiotemporal characteristics, the DLMP can provide continuous and explicit incentives for system planners, stakeholders, and investors who intend to install DGs, MGs, or ESSs, or otherwise upgrade system infrastructure. The traditional planning problem in a regulated distribution system is transitioned to a profit-oriented one to make more profits and recover the investment costs. Pioneering works [145]-[150] have tried to use price signals to incentivize system planning which still needs further study in a more competitive environment. Especially with the employment of DLMPs as incentive signals and the emerging various trading forms in modern distribution systems, broad and in-depth studies of profit-oriented DER planning and investment are necessary and attractive.

7.2.4 Pricing Uncertainty

With more DERs integrated into the distribution network, it is essential to consider the uncertainty in the distribution market. The current deterministic optimization-based model might not be able to handle the high dimensional uncertainties of DERs in the future grid. Also, most works focus on addressing uncertainties to ensure system security but increase the operating cost. All participants generally share this additional cost, which is not truly fair. Based on the rule "who causes the problem is the one who should be responsible," uncertainty sources should undertake this part of the cost. In [35][38][50], uncertainty has been priced or internalized into the DLMP or LMP. These pioneering works provide helpful insights for pricing uncertainty. Thus, the definition of uncertainty prices and how to utilize uncertainty prices to quantify the impacts of DER uncertainty on the local voltage violations, line overloading, and DER service deliverability are topics deserving further study.

7.3 Possible Barriers and Challenges of Implementing DLMP

Despite the advantages mentioned above and the promising future of the distribution-level market and DLMP, there are still several important potential barriers and challenges to implementing the DLMP in practice.

7.3.1 Aggregation Technology

Within a high DER penetration system, the DSO does not have the same level of visibility, control, and situational awareness of DERs on its system as the ISO does with transmission-connected generators. Thus, it is necessary to develop new communication and control technologies that can aggregate a huge number of small DERs into a large virtual aggregator to participate in distribution markets or provide grid services. Furthermore, infrastructure is indispensable for a fully competitive distribution market. Therefore, before such technologies and infrastructure are mature and can be widely applied, it may be a little early to extensively implement the distribution market and the DLMP.

7.3.2 Variability and Acceptance of DLMP

The DLMP is influenced by the substation LMP, nodal load demands, and power output of DGs [100]. These factors vary widely with time, thus, the DLMP also varies significantly within a day, days, weeks, months, seasons, etc., making a general daily DLMP pattern hard to obtain. In addition, the distribution system operates in a standard network configuration in normal conditions, but it reconfigures the network in emergency events, such as heavy loads and power outages. Network reconfiguration may further change the DLMP pattern. These characteristics complicate the electricity price both temporally and spatially. Compared to the flat electricity rate and TOU that are fixed over a long time, the DLMP may be more complicated for power consumers to navigate. Thus, the price mechanisms should be carefully designed to consider the actual reactions of the consumers, and a LA should play an essential role in bridging the DSO and consumers. Studies in consumer psychology may be conducted, and a survey on the acceptance of the DLMP may be performed [157].

7.3.3 Investigation of Policy to Ensure Fairness and Efficiency of Distribution Markets

Due to the typical radial structure of distribution networks, the power consumption in the upstream will significantly influence that in the downstream. For instance, if consumers close to the substation (i.e., upstream) consume a large amount of energy, the amount of energy that distant consumers can obtain is limited due to line capacity and voltage limits. Meanwhile, distant consumers need to pay more if the operating limits bind. A few studies have proposed mechanisms to mitigate such an issue. In [35], hedging rights were utilized to mitigate the undesirable effects of increased DLMP to aggregators. In [158], Jain's fairness index was applied in the DLMP mechanism to achieve fair cost allocation. However, these methods do not fully resolve the fairness issue. It is still an important topic which needs further investigation.

7.3.4 Market Power in Distribution Markets

Currently, most studies in existing literature have been carried out with the assumption of a perfectly competitive market. The distribution-level market could be imperfect in the

real world because the number of large-scale participants is possibly limited. Further, different from the wholesale market, the unique characteristics of the distribution market, such as voltage and imbalance, can impact the DLMP considerably. These factors enable participants to exercise market power for better profit, such as increasing the clearing price. Thus, regulatory authorities need to propose measures to prevent or mitigate the abuse of market power. So far, these issues are rarely studied at the distribution level. Therefore, the market power-related topics, such as market power assessment, market power exercise, and mitigation measures, must be investigated to achieve an efficient distribution level market.

References

[1] K. Horowitz *et al*., "An overview of distributed energy resource (DER) interconnection: current practices and emerging solutions," National Renewable Energy Laboratory, Denver, CO, USA, Tech. Rep. NREL/TP-6A20-72102, April 2019.

[2] J. J. Cook, K. Ardani, E. O'Shaughnessy, B. Smith, and R. Margolis, "Expanding PV value: lessons learned from utility-led distributed energy resource aggregation in the United States," National Renewable Energy Laboratory, Golden, CO, USA, Tech. Rep. NREL/TP-6A20-71984, Nov. 2018.

[3] R. R. Mohassel *et al*., "A survey on advanced metering infrastructure," *Int. J. Elect. Power Energy Syst.*, vol. 63, pp. 473-484, 2014.

[4] Q. Shi *et al*., "Estimating the profile of incentive-based demand response (IBDR) by integrating technical models and social-behavioral factors," *IEEE Trans. Smart Grid*, vol. 11, no. 1, pp. 171-183, Jan. 2020.

[5] J. Hao, D. W. Gao, and J. J. Zhang, "Reinforcement learning for building energy optimization through controlling of central HVAC system," *IEEE Open Access Journal of Power and Energy*, vol. 7, pp. 320-328, 2020.

[6] X. Kou *et al*., "Model-based and data-driven HVAC control strategies for residential demand response," *IEEE Open Access Journal of Power and Energy*, vol. 8, pp. 186-197, 2021.

[7] K. E. Lonergan and G. Sansavini, "Business structure of electricity distribution system operator and effect on solar photovoltaic uptake: An empirical case study for Switzerland," *Energy Policy*, vol. 160, pp. 112683, 2022.

[8] L. Bai, J. Wang, F. Li, *et al*., "Distribution locational marginal pricing (DLMP) for congestion management and voltage support," *IEEE Trans. Power Syst.*, vol. 33, no. 4, pp. 4061-4073, July 2018.

[9] S. Yousefi, M. P. Moghaddam, and V. J. Majd, "Optimal real time pricing in an agent-based retail market using a comprehensive demand response model," *Energy*, vol. 36, no. 9, pp. 5716-5727, 2011.

[10] P. O. Rosell *et al*., "Optimization problem for meeting distribution system operator requests in local flexibility markets with distributed energy resources," *Appl. Energy*, vol. 210, pp. 881-895, 2018.

[11] X. Jin, Q. Wu, and H. Jia, "Local flexibility markets: Literature review on concepts, models and clearing methods," *Appl. Energy*, vol. 261, pp. 1-35, 2020.

[12] C. A. Correa-Florez, A. Michiorri, and G. Kariniotakis, "Optimal participation of residential aggregators in energy and local flexibility markets," *IEEE Trans. Smart Grid*, vol. 11, no. 2, pp. 1644-1656, Mar. 2020.

[13] P. Goncalves Da Silva, D. Ilić, and S. Karnouskos, "The impact of smart grid prosumer grouping on forecasting accuracy and its benefits for local electricity market trading," *IEEE Trans. Smart Grid*, vol. 5, no. 1, pp. 402-410, Jan. 2014.

[14] Y. Parag and B. K. Sovacool, "Electricity market design for the prosumer era," *Nature energy*, vol. 1, no. 4, pp. 1-6, April 2016.

[15] F. Lezama, J. Soares, P. Hernandez-Leal, M. Kaisers, T. Pinto, and Z. Vale, "Local energy markets: Paving the path toward fully transactive energy systems," *IEEE Trans. Power Syst*., vol. 34, no. 5, pp. 4081-4088, Sept. 2019.

[16] S. Chen and C. C. Liu, "From demand response to transactive energy: state of the art," *J. Modern Power Syst. Clean Energy*, vol. 5, no. 1, pp. 10-19, Jan. 2017.

[17] National Grid and UK Power Networks, "Transmission and distribution interface 2.0 (TDI) - bid document to Ofgem," RIIO Network Innovation Competition (NIC), London, UK, Tech. Rep. NGET_UKPN_TDI2.0/V.01, 2018. [Online]. Available: https://www.ofgem.gov.uk/ofgem-publications/107804.

[18] SmartNet, "TSO-DSO coordination for acquiring ancillary services from distribution grids-The SmartNet project final results", 2019. [Online]. Available: http://smartnet-project.eu/wp-content/uploads/2019/05/SmartNet-Booktlet.pdf.

[19] Centrica, "Cornwall local energy market", 2018. [Online]. Available: https://www.centrica.com/innovation/cornwall-local-energy-market.

[20] Piclo Flex. Accessed: Mar. 10, 2022. [Online]. Available: https://picloflex.com/.

[21] NODES. Accessed: Mar. 10, 2022. [Online]. Available: https://nodesmarket.com/.

[22] C. Heinrich, C. Ziras, A. L. Syrri, and H. W. Bindner, "EcoGrid 2.0: A large-scale field trial of a local flexibility market," *Appl. Energy*, vol. 261, pp. 114399, 2020.

[23] European Union. (2021, April 1). EMPOWER. [Online]. Available: https://cordis.europa.eu/project/id/646476.

[24] E. Mengelkamp, J. Gärttner, K. Rock, S. Kessler, L. Orsini, C. Weinhardt, "Designing microgrid energy markets: A case study: The Brooklyn microgrid", *Appl. Energy*, vol. 210, pp. 870-880, 2018.

[25] P2P-SmarTest. Accessed: Mar. 10, 2022. [Online]. Available: https://www.p2psmartest-h2020.eu/deliverables.

[26] Y. Wu, M. Barati, and G. J. Lim, "A pool strategy of microgrid in power distribution electricity market," *IEEE Trans. Power Syst.*, vol. 35, no. 1, pp. 3-12. Jan. 2019.

[27] J. C. D. Prado and W. Qiao, "A stochastic bilevel model for an electricity retailer in a liberalized distributed renewable energy market," *IEEE Trans. Sustain. Energy*, vol. 11, no. 4, pp. 2803-2812, Oct. 2020.

[28] W. Zhong, S. Xie, K. Xie, Q. Yang, and L. Xie, "Cooperative P2P energy trading in active distribution networks: An MILP-based Nash bargaining solution," *IEEE Trans. Smart Grid*, vol. 12, no. 2, pp. 1264-1276, Mar. 2021.

[29] Federal Energy Regulatory Commission (FERC), Order No. 2222, "A new day for distributed energy resources," Sept. 17, 2020. [Online]. Available: https://www.ferc.gov/media/ferc-order-no-2222-fact-sheet.

[30] "Battery storage in the United States: an update on market trends," U.S. Energy Information Administration, Washington, DC, USA, July 2020.

[31] S. J. Kazempour, A. J. Conejo, and C. Ruiz, "Strategic bidding for a large consumer," *IEEE Trans. on Power Syst*., vol. 30, no. 2, pp. 848-856, July 2014.

[32] D. S. Kirschen and G. Strbac, "Introduction," in *Fundamentals of Power System Economics*, 2nd ed., Jersey City, John Wiley & Sons, 2018.

[33] X. Kou, F. Li *et al*., "A scalable and distributed algorithm for managing residential demand response programs using alternating direction method of multipliers (ADMM)," *IEEE Trans. Smart Grid*, vol. 11, no. 6, pp. 4871- 4882, June 2020.

[34] P. Cramton, "Electricity market design," *Oxford Review of Economic Policy*, vol.33, no.4, pp. 589-612, 2017.

[35] S. Hanif, P. Creutzburg, H. B. Gooi, and T. Hamacher, "Pricing mechanism for flexible loads using distribution grid hedging rights," *IEEE Trans. Power Syst*., vol. 34, no. 5, pp. 4048-4059, Sept. 2019.

[36] H. Yuan, F. Li *et al*., "Novel linearized power flow and linearized OPF models for active distribution networks with application in distribution LMP," *IEEE Trans. Smart Grid*, vol. 9, no. 1, pp. 438-448, Jan. 2018.

[37] R. Mieth and Y. Dvorkin, "Distribution electricity pricing under uncertainty," *IEEE Trans. Power Syst*, vol. 35, no. 3, pp. 2325-2338, May 2020.

[38] L. Wang, Z. Zhu, C. Jiang, and Z. Li, "Bi-level robust optimization for distribution system with multiple microgrids considering uncertainty distribution locational marginal price," *IEEE Trans. Smart Grid*, vol. 12, no. 2, pp. 1104-1117, Mar. 2021.

[39] J. Wei *et al*., "DLMP using three-phase current injection OPF with renewables and demand response," *IET Renew. Power Gener.*, vol. 13, no.7, pp. 1160-1167, May 2019.

[40] B. Wang, N. Tang, R. Bo, and F. Li, "Three-phase DLMP model based on linearized power flow for distribution with application to DER benefit studies," *Int. J. Electr. Power Energy Syst.*, vol. 130, pp. 106884, 2021.

[41] J. Kim and Y. Dvorkin, "A P2P-dominant distribution system architecture," *IEEE Trans. Power Syst.*, vol. 35, no. 4, pp. 2716-2725, July 2020.

[42] T. Sousa, T. Soares, P. Pinson, F. Moret, T. Baroche, and E. Sorin, "Peer-to-peer and community-based markets: A comprehensive review." *Renew. Sustain. Energy Rev*, vol. 104, pp. 367-378, 2019.

[43] W. Tushar, T. K. Saha, C. Yuen, D. Smith, and H. V. Poor, "Peer-to-peer trading in electricity networks: An overview," *IEEE Trans. Smart Grid*, vol. 11, no. 4, pp. 3185-3200, July 2020.

[44] W. Tushar, C. Yuen, T. K. Saha, T. Morstyn, A. C. Chapman, M. J. E. Alam, S. Hanif, and H. V. Poor, "Peer-to-peer energy systems for connected communities: A

review of recent advances and emerging challenges," *Appl. Energy*, vol. 282, pp. 116131, 2021.

[45] Y. Liu, L. Wu, and J. Li, "A two-stage peer-to-peer energy trading model for distribution systems with participation of utility," *CSEE J. Power Energy Syst*., vol. 7, no. 5, pp. 893-902, Sept. 2021.

[46] K. Zhang, S. Troitzsch, S. Hanif, and T. Hamacher, "Coordinated market design for peer-to-peer energy trade and ancillary services in distribution grids," *IEEE Trans. Smart Grid*, vol. 11, no. 4, pp. 2929-2941, July 2020.

[47] H. Haggi and W. Sun, "Multi-round double auction-enabled peer-to-peer energy exchange in active distribution networks," *IEEE Trans. Smart Grid*, vol. 12, no. 5, pp. 4403-4414, Sept. 2021.

[48] E. Münsing, J. Mather, and S. Moura, "Blockchains for decentralized optimization of energy resources in microgrid networks," *Proc. IEEE Conf. Control Technol*. Appl., Kohala Coast, Hawaii, USA, 2017, pp. 2164–2171.

[49] M. Shahidehpour, M. Yan, P. Shikhar, S. Bahramirad, and A. Paaso "Blockchain for Peer-to-Peer transactive energy trading in networked microgrids: Providing an effective and decentralized strategy." *IEEE Electrif. Mag.*, vol. 8, no.4, pp. 80-90, Dec. 2020.

[50] I. J. Perez-Arriaga, J. D. Jenkins, and C. Batlle, "A regulatory framework for an evolving electricity sector: Highlights of the MIT utility of the future study," *Econ. Energy Environ. Policy*, vol. 6, no. 1, 2017, pp. 71-92.

[51] F. Li and R. Bo, "DCOPF-based LMP simulation: algorithm, comparison with ACOPF, and sensitivity." *IEEE Trans. Power Syst*., vol. 22, no. 4, pp. 1475-1485, Oct. 2007.

[52] P. M. Sotkiewicz and J. M. Vignolo, "Nodal pricing for distribution networks: Efficient pricing for efficiency enhancing DG," *IEEE Trans. Power Syst*., vol. 21, no. 2, pp. 1013-1014, May 2006.

[53] G. T. Heydt, B. H. Chowdhury, *et al*., "Pricing and control in the next power distribution system," *IEEE Trans. Smart Grid*, vol. 3, no. 2, pp. 907–914, Jun. 2012.

[54] Y. K. Renani, M. Ehsan, and M. Shahidehpour, "Optimal transactive market operations with distribution system operators," *IEEE Trans. Smart Grid*, vol. 9, no. 6, pp. 6692-6701, Nov. 2018.

[55] W. Wei *et al*., "Estimating DLMP confidence intervals in distribution networks with AC power flow model and uncertain renewable generation," *IET Gener. Transm. Distrib*., vol. 14, no. 8, pp. 1467-1475, Mar. 2020.

[56] A. Papavasiliou, "Analysis of distribution locational marginal prices," *IEEE Trans. Smart Grid*, vol. 9, no. 5, pp: 4872-4882, Sep. 2017.

[57] H. Ye, Y. Ge, M. Shahidehpour, and Z. Li, "Uncertainty marginal price, transmission reserve, and day-ahead market clearing with robust unit commitment," *IEEE Trans. Power Syst*., vol. 32, no. 3, pp. 1782-1795, May 2017.

[58] L. Exizidis, J. Kazempour, A. Papakonstantinou, P. Pinson, Z. De Grève, and F. Vallée, "Incentive-compatibility in a two-stage stochastic electricity market with high wind power penetration," *IEEE Trans. Power Syst*., vol. 34, no. 4, pp. 2846-2858, July 2019.

[59] H. Zhong, L. Xie, and Q. Xia, "Coupon incentive-based demand response: Theory and case study," *IEEE Trans. Power Syst*., vol. 28, no. 2, pp. 1266-1276, May 2013.

[60] A. D. Giorgio and L. Pimpinella, "An event driven smart home controller enabling consumer economic saving and automated demand side management," *Appl. Energy*, vol. 96, pp. 92-103, 2012.

[61] K. Herter and S. Wayland, "Residential response to critical-peak pricing of electricity: California evidence," *Energy*, vol. 35, pp. 1561-1567, 2010.

[62] J. Vuelvas and F. Ruiz, "Rational consumer decisions in a peak time rebate program," *Electric Power Systems Research*, vol. 143, pp. 533-543, 2017.

[63] S. Bhattacharya, K. Kar and J. H. Chow, "Optimal precooling of thermostatic loads under time-varying electricity prices," *Proc. IEEE American Control Conference (ACC)*, Seattle, WA, USA, 2017, pp. 1407-1412.

[64] Y. J. Kim, "Optimal price based demand response of HVAC systems in multizone office buildings considering thermal preferences of individual occupants buildings," *IEEE Trans. Ind. Informat.*, vol. 14, no. 11, pp. 5060-5073, Nov. 2018.

[65] W. Zhong, K. Xie, Y. Liu, S. Xie, and L. Xie, "Nash mechanisms for market design based on distribution locational marginal prices," *IEEE Trans. Power Syst.*, early access, 2022.

[66] W. Tushar, T. K. Saha, C. Yuen, P. Liddell, R. Bean, and H. V. Poor, "Peer-to-peer energy trading with sustainable user participation: A game theoretic approach," *IEEE Access*, vol. 6, pp. 62932-62943, Oct. 2018.

[67] W. Tushar, T. K. Saha, C. Yuen, T. Morstyn, and M. D. McCulloch, "A motivational game-theoretic approach for peer-to-peer energy trading in the smart grid," *Appl. Energy*, vol. 243, pp. 10-20, June 2019.

[68] C. Long, C. Z. J. Wu, L. Thomas, M. Cheng, and N. Jenkins, "Peer-to-peer energy trading in a community microgrid," *in Proc. IEEE Power Energy Soc. Gen. Meeting*, Chicago, IL, USA, Jul. 2017, pp. 2-6.

[69] Y. Zhou, J. Wu, and C. Long, "Evaluation of peer-to-peer energy sharing mechanisms based on a multiagent simulation framework," *Appl. Energy*, vol. 222, pp. 993-1022, July 2018.

[70] J. Li, Y. Ye, D. Papadaskalopoulos, and G. Strbac, "Computationally efficient pricing and benefit distribution mechanisms for incentivizing stable peer-to-peer energy trading," *IEEE Internet Things J.*, vol. 8, no. 2, pp. 734-749, Jan. 2021.

[71] H. Wang and J. Huang, "Incentivizing energy trading for interconnected microgrids," *IEEE Trans. Smart Grid*, vol. 9, no. 4, pp. 2647-2657, Jun. 2018.

[72] I. Alsaleh and L. Fan, "Distribution locational marginal pricing (DLMP) for multiphase systems," *2018 North American Power Symposium (NAPS), IEEE*, 2018, Fargo, ND, USA, pp. 1-6.

[73] L. Edmonds *et al*., "Three-phase distribution locational marginal pricing to manage unbalanced variable renewable energy," *IEEE Power Energy Soc. Gen. Meeting*, IEEE, 2020, pp. 1-5.

[74] F. Xin *et al*., "Introducing uncertainty components in locational marginal prices for pricing wind power and load uncertainties," *IEEE Trans. Power Syst.*, vol. 34, no. 3, pp. 2013-2024, Jan. 2019.

[75] P. Andrianesis and M Caramanis, "Distribution network marginal costs: enhanced AC OPF including transformer degradation," *IEEE Trans. Smart Grid*, vol. 11, no. 5, pp. 3910-3920, Sept. 2020.

[76] T. Yang, Y. Guo, L. Deng, H. Sun, and W. Wu, "A linear branch flow model for radial distribution networks and its application to reactive power optimization and network reconfiguration," *IEEE Trans. Smart Grid*, vol. 12, no. 3, pp. 2027-2036, May 2021.

[77] M. E. Baran and F. F. Wu, "Network reconfiguration in distribution systems for loss reduction and load balancing," *IEEE Trans. Power Del*., vol. 4, no. 2, pp. 1401-1407, Apr. 1989.

[78] C. Zhang, Y. Xu, Z. Dong, and J. Ravishankar, "Three-stage robust inverter-based voltage/var control for distribution networks with high-level PV," *IEEE Trans. Smart Grid*, vol. 10, no. 1, pp. 782-793, Jan. 2019.

[79] L. Gan and S. H. Low, "Convex relaxations and linear approximation for optimal power flow in multiphase radial networks," *2014 Power Systems Computation Conference*, Wroclaw, Poland, 2014, pp. 1-9.

[80] Y. Du, F. Li, *et al*., "A cooperative game approach for coordinating multi-microgrid operation within distribution systems," *Appl. Energy*, vol. 222, pp. 383-395, 2018.

[81] B. S. K. Patnam and N. M. Pindoriya, "DLMP calculation and congestion minimization with EV aggregator loading in a distribution network using bilevel program," *IEEE Systems Journal*, vol. 15, no. 2, pp. 1835-1846, June 2021.

[82] J. Zhang, M. Cui, B. Li, H. Fang, and Y. He, "Fast solving method based on linearized equations of branch power flow for coordinated charging of EVs (EVCC)," *IEEE Trans. Veh. Technol*., vol. 68, no. 5, pp. 4404–4418, May 2019.

[83] B. Park, Y. Chen, F. Li *et al*., "Optimal demand response incorporating distribution LMP with PV generation uncertainty," *IEEE Trans. Power Syst*., vol. 37, no. 2, pp. 982-995, Mar. 2022.

[84] Y. Liu, N. Zhang, Y. Wang, J. Yang, and C. Kang, "Data-driven power flow linearization: A regression approach," *IEEE Trans. Smart Grid*, vol. 10, no. 3, pp. 2569-2580, May 2019.

[85] B. Liu *et al*., "Enhanced deep neural networks with transfer learning for distribution LMP considering load and PV uncertainties". *Int. J. Electr. Power Energy Syst*., vol. 147, pp. 108780, 2023.

[86] Y. Wang, N. Zhang, H. Li, J. Yang, and C. Kang, "Linear three-phase power flow for unbalanced active distribution networks with PV nodes," *CSEE J. Power Energy Syst*., vol. 3, no. 3, pp. 321-324, Sep. 2017.

[87] X. Bai, H. Wei, K. Fujisawa, and Y. Wang, "Semidefinite programming for optimal power flow problems," *Int. J. Elect. Power Energy Syst*., vol. 30, pp. 383-392, 2008.

[88] J. Lavaei and S. H. Low, "Zero duality gap in optimal power flow problem," *IEEE Trans. Power Syst*., vol. 27, no. 1, pp. 92-107, Feb. 2012.

[89] C. Zhao, E. Dall'Anese, and S. H. Low, "Convex relaxation of OPF in multiphase radial networks with delta connection," *Proc. of Bulk Power Systems Dynamics and Control Symposium*, Charleston, SC, USA, 2017, pp. 0885-8950.

[90] Y. Liu, J. Li, and L. Wu, "Distribution system restructuring: Distribution LMP via unbalanced ACOPF," *IEEE Trans. Smart Grid*, vol. 9, no. 5, pp. 4038-4048, Sept. 2018.

[91] R. A. Jabr, "Radial distribution load flow using conic programming," *IEEE Trans. Power Syst.*, vol. 21, no. 3, pp. 1458-1459, Aug. 2006.

[92] M. Farivar and S. H. Low, "Branch flow model: Relaxations and convexification–Part I," *IEEE Trans. Power Syst*., vol. 28, no. 3, pp. 2554–2572, Aug. 2013.

[93] W. Wei, J. Wang, N. Li, and S. Mei, "Optimal power flow of radial networks and its variations: A sequential convex optimization approach," *IEEE Trans. Smart Grid*, vol. 8, no. 6, pp. 2974-2987, Nov. 2017.

[94] S. H. Low, "Convex relaxation of optimal power flow–Part I: Formulations and equivalence," *IEEE Trans. Control Netw. Syst*., vol. 1, no. 1, pp. 15–27, Mar. 2014.

[95] S. H. Low, "Convex relaxation of optimal power flow–Part II: Exactness," *IEEE Trans. Control Netw. Syst.*, vol. 1, no. 2, pp. 177–189, June 2014.

[96] S. Nematshahi and H. R. Mashhadi, "Distribution network reconfiguration with the application of DLMP using genetic algorithm," *Proc. IEEE Electr. Power Energy Conf. (EPEC)*, Saskatoon, Saskatchewan, Canada, 2017, pp. 1-5.

[97] R. Li, Q. Wu, and S. S. Oren, "Distribution locational marginal pricing for optimal electric vehicle charging management," *IEEE Trans. Power Syst.*, vol. 29, no. 1, pp. 203-211, Jan. 2014.

[98] S. Huang, Q. Wu, S. S. Oren, R. Li, and Z. Liu, "Distribution locational marginal pricing through quadratic programming for congestion management in distribution networks," *IEEE Trans. Power Syst.*, vol. 30, no. 4, pp. 2170-2178, Jul. 2015.

[99] W. Liu, *et al*., "Day-ahead congestion management in distribution systems through household demand response and distribution congestion prices," *IEEE Trans. Smart Grid*, vol. 5, no. 6, pp. 2739–2747, Jul. 2014.

[100] X. Wang, F. Li, *et al*., "Tri-level scheduling model considering residential demand flexibility of aggregated HVACs and EVs under distribution LMP (DLMP)," *IEEE Trans. Smart Grid*, vol. 12, no. 5, pp. 3990-4002, Sept. 2021.

[101] M. Caramanis, E. Ntakou, W. Hogan, A. Chakrabortty, and J. Schoene, "Co-optimization of power and reserves in dynamic T&D power markets with nondispatchable renewable generation and distributed energy resources," *Proc. IEEE*, vol. 104, no. 4, pp. 807–836, Apr. 2016.

[102] Z. Yuan, M. R. Hesamzadeh, and D. R. Biggar, "Distribution locational marginal pricing by convexified ACOPF and hierarchical dispatch," *IEEE Trans. Smart Grid.*, vol. 9, no. 4, pp. 3133-3142, July 2018.

[103] P. Jacquot, "DLMP-based coordination procedure for decentralized demand response under distribution network constraints," arXiv preprint arXiv:2004.06004, 2020.

[104] Z. Yang, H. Zhong, A. Bose, T. Zheng, Q. Xia, and C. Kang, "A linearized OPF model with reactive power and voltage magnitude: A pathway to improve the MW-only DC OPF," *IEEE Trans. Power Syst.*, vol. 33, no. 2, pp. 1734-1745, Mar. 2018.

[105] Y. Wang, S. Wang, and L. Wu, "Distributed optimization approaches for emerging power systems operation: A review," *Electric Power Systems Research*, vo. 144, pp. 127-135, 2017.

[106] S. Hanif, K. Zhang, C. M. Hackl, M. Barati, H. B. Gooi, and T. Hamacher, "Decomposition and equilibrium achieving distribution locational marginal prices

using trust-region method," *IEEE Trans. Smart Grid.*, vol. 10, no. 3, pp. 3269-3281, May 2019.

[107] S. Suganya, S. C. Raja, and P. Venkatesh, "Simultaneous coordination of distinct plug-in hybrid electric vehicle charging stations: A modified particle swarm optimization approach," *Energy*, vol. 138, pp. 92-102, 2017.

[108] D. K. Molzahn *et al*., "A survey of distributed optimization and control algorithms for electric power systems," *IEEE Trans. Smart Grid*, vol. 8, no. 6, pp. 2941-2962, Nov. 2017.

[109] S. Boyd, N. Parikh, E. Chu, B. Peleato, and J. Ecksteinm, "Distributed optimization and statistical learning via the alternating direction method of multipliers," *Found. Trends Mach. Learn*., vol. 3, no. 1, pp. 1-122, 2011.

[110] X. Kou, F. Li *et al*., "A comprehensive scheduling framework using SP-ADMM for residential demand response with weather and consumer uncertainties," *IEEE Trans. Power Syst.,* vol. 36, no. 4, pp. 3004-3016, July 2021.

[111] Y. Wang, L. Wu, and S. Wang, "A fully-decentralized consensus-based ADMM approach for DC-OPF with demand response," *IEEE Trans. Smart Grid*, vol. 8, no. 6, pp. 2637-2647, Mar. 2016

[112] Z. Tan, P. Yang, and A. Nehorai, "An optimal and distributed demand response strategy with electric vehicles in the smart grid," *IEEE Trans. Smart Grid*, vol. 5, no. 2, pp. 861-869, Mar. 2014.

[113] D. H. Nguyen, S. Azuma, and T. Sugie, "Novel control approaches for demand response with real-time pricing using parallel and distributed consensus-based ADMM," *IEEE Trans. Ind. Electron.*, vol. 66, no. 10, pp. 7935-7945, Dec. 2018.

[114] F. Shen, Q. Wu, X. Jin, B. Zhou, C. Li, and Y. Xu, "ADMM-based market clearing and optimal flexibility bidding of distribution-level flexibility market for day-ahead congestion management of distribution networks," *Int. J. Electr. Power Energy Syst.*, vol.123, pp.1-14, 2020.

[115] Y. He, Q. Chen, J. Yang, Y. Cai, and X. Wang, "A multi-block ADMM based approach for distribution market clearing with distribution locational marginal price," *Int. J. Electr. Power Energy Syst.*, vol. 128, pp. 106635, 2021.

[116] K. Zhang, S. Hanif, C. M. Hackl, and T. Hamacher, "A framework for multi-regional real-time pricing in distribution grids," *IEEE Trans. Smart Grid*, vol. 10, no. 6, pp. 6826-6838, Nov. 2019.

[117] H. M. Kim *et al*., "Target cascading in optimal system design," *J. Mech. Des*. Vol. 125, no. 3, pp. 474-480, Sept. 2003.

[118] A. Kargarian *et al*, "Toward distributed/decentralized DC optimal power flow implementation in future electric power systems," *IEEE Trans. on Smart Grid*, vol. 9, no. 4, pp.2574-2594. Oct. 2016.

[119] M. Xie *et al*., "Autonomous optimized economic dispatch of active distribution system with multi-microgrids," *Energy*, vol. 153, pp. 479-489, 2018.

[120] P. Du *et al*., "A bi-level linearized dispatching model of active distribution network with multi-stakeholder participation based on analytical target cascading," *IEEE Access*, vol. 7, pp. 154844-154858, Oct. 2019.

[121] A. Mohammadi and A. Kargarian, "Accelerated and robust analytical target cascading for distributed optimal power flow," *IEEE Trans. Ind. Informat*., vol. 16, no. 12, pp. 7521-7531, Feb. 2020.

[122] J. Zhang, L. Che, X. Wan, and M. Shahidehpour, "Distributed hierarchical coordination of networked charging stations based on peer-to-peer trading and EV charging flexibility quantification," *IEEE Trans. Power Syst*., early access, 2021.

[123] M. Kraning, E. Chu, J. Lavaei, and S. Boyd, "Dynamic network energy management via proximal message passing," *Found. Trends Optim*., vol. 1, no. 2, pp. 70-122, 2013.

[124] E. Ntakou and M. Caramanis, "Distribution network electricity market clearing: Parallelized PMP algorithms with minimal coordination," *Proc. IEEE 53rd Annu. Conf. Decis. Control (CDC)*, Los Angeles, CA, USA, 2014, pp. 1687-1694.

[125] E. Ntakou and M. Caramanis, "Enhanced convergence rate of inequality constraint shadow prices in PMP algorithm cleared distribution power markets," *Proc. Amer. Control Conf.*, Boston, MA, USA, 2016, pp.1433-1439.

[126] S. Chakrabarti and R. Baldick, "Look-ahead SCOPF (LASCOPF) for tracking demand variation via auxiliary proximal message passing (APMP) algorithm," *Int. J. Electr. Power Energy Syst.*, vol. 116, pp. 105533, 2020.

[127] G. Cohen, "Auxiliary problem principle and decomposition of optimization problems," J. *Optim. Theory Appl*., vol. 32, no. 3, pp. 277–305, Nov. 1980.

[128] A. Ahmadi-Khatir, A. J. Conejo, and R. Cherkaoui, "Multi-area unit scheduling and reserve allocation under wind power uncertainty," IEEE Trans. Power Syst., vol. 29, no. 4, pp. 1701–1710, Jul. 2014.

[129] M. Alkhraijah, M. Alowaifeer, S. Grijalva, and D. K. Molzahn, "Distributed multi-period DCOPF via an auxiliary principle problem algorithm," *IEEE Tex. Power Energy Conf*., College Station, TX, USA, 2021, pp. 1-6.

[130] A. R. Di Fazio, C. Risi, M. Russo, and M. De Santis, "Distributed voltage optimization based on the auxiliary problem principle in active distribution systems," *55th Int. Univ. Power Eng. Conf., Torino*, Italy, 2020, pp. 1-6.

[131] C. Eid, P. Codani, Y. Perez, J. Reneses, and R. Hakvoort, "Managing electric flexibility from distributed energy resources: A review of incentives for market design," *Renew. Sustain. Energy Rev*., vol. 64, pp. 237-247, 2016.

[132] T. Zhao and Z. Ding, "Cooperative optimal control of battery energy storage system under wind uncertainties in a microgrid," *IEEE Trans. Power Syst.*, vol. 33, no. 2, pp. 2292-2300, Mar. 2018.

[133] P. Siano and D. Sarno, "Assessing the benefits of residential demand response in a real time distribution energy market," *Appl. Energy*, vol. 161, pp. 533-551, 2016.

[134] H. Mohsenian-Rad, "Optimal demand bidding for time-shiftable loads," *IEEE Trans. Power Syst*., vol. 30, no. 2, pp. 939-951, Mar. 2015.

[135] S. Rahman, A. Haque, and Z. Jing, "Modeling and performance evaluation of grid-interactive efficient buildings (GEB) in a microgrid environment," *IEEE Open Access Journal of Power and Energy*, vol. 8, pp. 423-432, 2021.

[136] M. Song, W. Sun, Y. Wang, M. Shahidehpour, Z. Li, and C. Gao, "Hierarchical scheduling of aggregated TCL flexibility for transactive energy in power systems," *IEEE Trans. Smart Grid*, vol. 11, no. 3, pp. 2452-2463, May 2020.

[137] Y. Du, F. Li, K. Kurte, J. Munk, and H. Zandi, "Demonstration of intelligent HVAC load management with deep reinforcement learning," *IEEE Power Energy Mag*., vol. 20, no. 3, pp. 42-53, May-June 2022.

[138] J. Wei, Y. Zhang, J. Wang, and L. Wu, "Distribution LMP-based demand management in industrial park via a bi-level programming approach," *IEEE Trans. Sustain. Energy*, vol. 12, no. 3, pp. 1695-1706, July 2021.

[139] Y. Du and F. Li, "A hierarchical real-time balancing market considering multi-microgrids with distributed sustainable resources," *IEEE Trans. Sustain. Energy*, vol. 11, no.1, pp, 72-83. Jan. 2018.

[140] Z. Wang *et al*., "Robust optimization based optimal DG placement in microgrids," *IEEE Trans. Smart Grid*, vol. 5, no. 5, pp. 2173-2182, Sept. 2014.

[141] Y. Tang and S. H. Low, "Optimal placement of energy storage in distribution networks," *IEEE Trans. Smart Grid*, vol. 8, no. 6, pp. 3094-3103, Nov. 2017.

[142] L. Bai, T. Jiang, F. Li, *et al*, "Distributed energy storage planning in soft open point based active distribution networks incorporating network reconfiguration and DG reactive power capability," *Appl. Energy*, vol. 210, pp. 1082-1091, 2018.

[143] Y. Zhang, A. Anvari-Moghaddam, S. Peyghami, T. Dragičević, Y. Li and F. Blaabjerg, "Optimal sizing of behind-the-meter battery storage for providing profit-oriented stackable services", *IEEE Trans. Smart Grid*, early access.

[144] X. Su, Z. Zhang, Y. Liu, Y. Fu, F. Shahnia, C. Zhang, and Z. Dong, "Sequential and comprehensive BESSs placement in unbalanced active distribution networks considering the impacts of BESS dual attributes on sensitivity," *IEEE Trans. Power Syst*., vol. 36, no. 4, pp. 3453-3464, July 2021.

[145] M. H. S. Boloukat and A. A. Foroud, "Multiperiod planning of distribution networks under competitive electricity market with penetration of several microgrids, part I: Modeling and solution methodology," *IEEE Trans. Ind. Informat*., vol. 14, no. 11, pp. 4884-4894, Nov. 2018.

[146] R. Atia and N. Yamada, "Distributed renewable generation and storage systems sizing in deregulated energy markets," *2015 International Conference on Renewable*

Energy Research and Applications (ICRERA), Palermo, Italy, Nov. 2015, pp. 258-262.

[147] E. Samani and F. Aminifar, "Tri-level robust investment planning of DERs in distribution networks with AC constraints," *IEEE Trans. Power Syst*., vol. 34, no. 5, pp. 3749-3757, Sept. 2019.

[148] P. Lamaina, D. Sarno, P. Siano, A. Zakariazadeh, and R. Romano, "A model for wind turbines placement within a distribution network acquisition market," *IEEE Trans. Ind. Informat*., vol. 11, no. 1, pp. 210-219, Feb. 2015.

[149] X. Xiao, F. Wang, M. Shahidehpour, Z. Li, and M. Yan, "Coordination of distribution network reinforcement and DER planning in competitive market," *IEEE Trans. Smart Grid*, vol. 12, no. 3, pp. 2261-2271, May 2021.

[150] X. Wang, F. Li, Q. Zhang, Q. Shi, and J. Wang, "Profit-oriented BESS siting and sizing in deregulated distribution systems," *IEEE Trans. Smart Grid*, vol. 14, no. 2, pp. 1528-1540, March 2023.

[151] E. A. Farsani, H. A. Abyaneh, M. Abedi, and S. H. Hosseinian, "A novel policy for LMP calculation in distribution networks based on loss and emission reduction allocation using nucleolus theory," *IEEE Trans. Smart Grid*, vol. 31, no. 1, pp. 143-152, Jan. 2016.

[152] S. Hanif, T. Massier, H. B. Gooi, T. Hamacher, and T. Reindl, "Cost optimal integration of flexible buildings in congested distribution grids," *IEEE Trans. Power Syst*., vol. 32, no. 3, pp. 2254-2266, May 2017.

[153] J. Hu, J. Wu, X. Ai, and N. Liu, "Coordinated energy management of prosumers in a distribution system considering network congestion," *IEEE Trans. Smart Grid*, vol. 12, no. 1, pp. 468-478, Jan. 2021.

[154] CAISO. (2021, Sept. 8). *Flex alert extended through tomorrow due to widespread heat in west*. [Online]. Available: https://www.flexalert.org/news.

[155] H. Chen, L. Fu, L. Bai, *et al*, "Distribution market-clearing and pricing considering coordination of DSOs and ISO: An EPEC approach", *IEEE Trans. Smart Grid*, vol. 12, no. 4, pp. 3150-3162, July 2021.

[156] Gridworks, "Coordination of transmission and distribution operations in a high distributed energy resource electric grid," CAISO, PG&E, SCE, SDG&E, Gridworks, Tech. Rep., Jun. 2017. Accessed: Oct. 11, 2021. [Online]. Available: https://gridworks.org/wp-content/uploads/ 2017/01/Gridworks_CoordinationTransmission. pdf

[157] Y. Shen, Y. Li, Q. Zhang, F. Li, and Z. Wang, "Consumer psychology based optimal portfolio design for demand response aggregators," *J. Mod. Power Syst. Clean Energy*, vol. 9, no. 2, pp. 431-439, Mar. 2021.

[158] A. K. Zarabie, S. Das, and M. N. Faqiry, "Fairness-regularized DLMP-based bilevel transactive energy mechanism in distribution systems," *IEEE Trans. Smart Grid*, vol. 10, no. 6, pp. 6029-6040, Jan. 2019.

[159] R. Mowris and E. Jones, "Peak demand and energy savings from properly sized and matched air conditioners," *ACEEE Summer Study on Energy Efficiency in Buildings*, Pacific Grove, CA, USA, 2008, pp. 196-208.

[160] A. Roth and J. Reyna, "Grid-interactive efficient buildings technical report series: Whole-building controls, sensors, modeling, and analytics," NREL, Denver, CO, USA, Tech. Rep. NREL/TP-5500-75478, DOE/GO-102019-5230, Dec. 2019.

[161] M. Ostadijafari, R. R. Jha, and A. Dubey, "Demand-side participation via economic bidding of responsive loads and local energy resources," *IEEE Open Access Journal of Power and Energy*, vol. 8, pp. 11-22, 2021.

[162] J. Fortuny-Amat and B. McCarl, "A representation and economic interpretation of a two-level programming problem," *J. Oper. Res. Soc*., vol. 32, no. 9, pp. 783-792, Sep. 1981.

[163] B. M. Sanandaji, T. L. Vincent, and K. Poolla, "Ramping rate flexibility of residential HVAC loads," *IEEE Trans. Sustain. Energy*, vol. 7, no. 2, pp. 865–874, Apr. 2016.

[164] J. Dong, M. Starke, B. Cui, J. Munk, E. Tsybina, C. Winstead; Y. Xue; M. Olama and T. Kuruganti, "Battery equivalent model for residential HVAC," *IEEE Power Energy Soc. Gen. Meeting*, IEEE, Aug. 2020.

[165] N. Lu and Y. Zhang, "Design considerations of a centralized load controller using thermostatically controlled appliances for continuous regulation reserves," *IEEE Trans. Smart Grid*, vol. 4, no. 2, pp. 914-921, June 2012.

[166] Z. Hu, M. Xiong, H. Shang, and A. Deng, "Anti-interference measurement methods of the coupled transmission-line capacitance parameters based on the harmonic components," *IEEE Trans. Power Deliv*., vol. 31, no. 6, pp. 2464-2472, Dec. 2016.

[167] L. Baringo and A. J. Conejo, "Strategic offering for a wind power producer," *IEEE Trans. Power Syst.*, vol. 28, no. 4, pp. 4645-4654, Nov. 2013.

[168] Z. Hu *et al*., "Bi-level robust dynamic economic emission dispatch considering wind power uncertainty", *Electric Power Systems Research*, vol. 135, pp. 35-47, 2016.

[169] P. R. Hartley, K. B. Medlock III, and O. Jankovska, "Electricity reform and retail pricing in Texas," *Energy Econ.*, vol. 80, pp. 1–11, Jan. 2019.

[170] *Data Miner 2*, PJM, Audubon, PA, USA. Accessed: Mar. 16, 2021. [Online] Available: http://dataminer2.pjm.com/list

[171] Q. Zhang, F. Li, W. Feng, X. Wang, L. Bai, and R. Bo, "Building marginal pattern library with unbiased training dataset for enhancing model-free load-ED mapping," *IEEE Open Access Journal of Power and Energy*, vol. 9, pp. 88-98, 2022.

[172] A. Satchwell *et al*., "A national roadmap for grid-interactive efficient buildings," LBNL, Berkeley, CA, USA, May 2021.

[173] G. Liu, Y. Tao, L. Xu, Z. Chen, J. Qiu, and S. Lai, "Coordinated management of aggregated electric vehicles and thermostatically controlled loads in hierarchical energy systems," *Int. J. Electr. Power Energy Syst*, vol. 131, pp. 107090, 2021.

[174] M. Xiong, X. Xu, K. Sun, and B. Wang, "Approximation of the frequency-amplitude curve using the homotopy analysis method," *2021 IEEE Power & Energy Society General Meeting (PESGM)*, Washington, DC, USA, 2021, pp. 1-5.

[175] H. Li, Z. Wang, T. Hong, and M. A. Piette, "Energy flexibility of residential buildings: A systematic review of characterization and quantification methods and applications," *Advances in Applied Energy*, vol.3, pp. 100054, 2021.

[176] M. Xiong, R. Yao, Y. Liu, K. Sun, and F. Qiu, "Semi-analytical electromagnetic transient simulation using differential transformation," *2022 4th International*

Conference on Smart Power & Internet Energy Systems (SPIES), Beijing, China, 2022, pp. 481-486.

[177] F. Conte *et al*., "Performance analysis of frequency regulation services provided by aggregates of domestic thermostatically controlled loads," *Int. J. Electr. Power Energy Syst*, vol. 131, pp. 107050, 2021.

[178] Z. Yi, Y. Xu, J. Zhou, W. Wu, and H. Sun, "Bi-level programming for optimal operation of an active distribution network with multiple virtual power plants," *IEEE Trans. Sustain. Energy*, vol. 11, no. 4, pp. 2855–2869, Oct. 2020.

[179] B. She *et al*., "Inverter PQ control with trajectory tracking capability for microgrids based on physics-informed reinforcement learning," *IEEE Trans. Smart Grid*, early access, 2023.

[180] H. Karimi, R. Bahmani, and S. Jadid, "Stochastic multi-objective optimization to design optimal transactive pricing for dynamic demand response programs: A bi-level fuzzy approach," *Int. J. Electr. Power Energy Syst*, vol. 125, pp. 106487, 2021.

[181] Q. Zhang, F. Li, and X. Wang, "Cyber-impact analysis for ISO revenue adequacy considering FDIA in real-time market operations," *IEEE Trans. Power Syst*., early access, 2022.

[182] K. Ma *et al*., "Hybrid control of aggregated thermostatically controlled loads: Step rule, parameter optimisation, parallel and cascade structures," *IET Gener., Transm. Distrib*., vol. 10, no. 16, pp. 4149-4157, Dec. 2016.

[183] M. Vahid-Ghavidel *et al.*, "Novel hybrid stochastic-robust optimal trading strategy for a demand response aggregator in the wholesale electricity market," *IEEE Trans. Ind. Appl*., vol. 57, no.5, pp. 5488-5498, Sept.-Oct. 2021.

[184] X. Kou and F. Li, "Interval optimization for available transfer capability evaluation considering wind power uncertainty," *IEEE Trans. Sustain. Energy*, vol. 11, no. 1, pp. 250–259, Jan. 2020.

[185] Z. Zheng, Z. Sun, J. Pan, and X. Luo, "An integrated smart home energy management model based on a pyramid taxonomy for residential houses with photovoltaic-battery systems", *Applied Energy*, vol. 298, pp. 117159, 2021.

[186] B. Stappers, N. G. Paterakis, K. Kok, and M. Gibescu, "A class-driven approach based on long short-term memory networks for electricity price scenario generation and reduction," *IEEE Trans. Power Syst*., vol. 35, no. 4, pp. 3040-3050, July 2020.

[187] Y. Chen, Y. Wang, D. Kirschen, and B. Zhang, "Model-free renewable scenario generation using generative adversarial networks," *IEEE Trans. Power Syst*., vol. 33, no. 3, pp. 3265-3275, May 2018.

[188] B. She, F. Li, H. Cui, J. Zhang, and R. Bo, "Fusion of microgrid control with model-free reinforcement learning: Review and vision," *IEEE Trans. Smart Grid*, early access, 2022.

[189] X. Wang, Z. Hu, M. Zhang, and M. Hu, "Two-stage stochastic optimization for unit commitment considering wind power based on scenario analysis," *2016 China International Conference on Electricity Distribution (CICED)*, Xi'an, China, 2016, pp. 1-5.

[190] A. Sinha, P. Malo, and K. Deb, "A review on bilevel optimization: From classical to evolutionary approaches and applications," *IEEE Trans. Evol. Comput.*, vol. 22, no. 2, pp. 276-295, April 2018.

[191] R. Palma-Behnke, C. Benavides, F. Lanas, B. Severino, L. Reyes, J. Llanos, and D. Sáez, "A microgrid energy management system based on the rolling horizon strategy," *IEEE Trans. Smart Grid*, vol. 4, no. 2, pp. 996-1006, June 2013.

[192] NREL., Solar Integration National Dataset Toolkit, [Online] Available: https://www.nrel.gov/grid/sind-toolkit.html.

[193] M. C. Bozchalui, S. A. Hashmi, H. Hassen, C. A. Canizares, and K. Bhattacharya, "Optimal operation of residential energy hubs in smart grids," *IEEE Trans. Smart Grid*, vol. 3, no. 4, pp. 1755-1766, Dec. 2012.

[194] Federal Energy Regulatory Commission (FERC), Order No. 755, "Frequency regulation compensation in the organized wholesale power markets," Oct. 20, 2011. [online]. Available: https://www.ferc.gov/sites/default/files/2020-06/OrderNo.755.pdf.

[195] Federal Energy Regulatory Commission (FERC), Order No. 841, "Electric storage participation in markets operated by regional transmission organizations and

independent system operators," Feb. 15, 2018. [Online]. Available: https://www.ferc.gov/media/order-no-841.

[196] L. Xu and D. Tretheway, "Flexible ramping products," California Independent System Operator, Folsom, CA, USA, 2012.

[197] H. Chen, S. Baker, S. Benner, A. Berner, and J. Liu, "PJM integrates energy storage: Their technologies and wholesale products," *IEEE Power Energy Mag*., vol. 15, no. 5, pp. 59-67, Sep. 2017.

[198] R. Fernández-Blanco, Y. Dvorkin, B. Xu, Y. Wang, and D. S. Kirschen, "Optimal energy storage siting and sizing: A WECC case study," *IEEE Trans. Sustain. Energy*, vol. 8, no. 2, pp. 733-743, Apr. 2017.

[199] W. Wei *et al*., "Impact of energy storage on economic dispatch of distribution systems: A multi-parametric linear programming approach and its implications," *IEEE Open Access J. Power Energy*, vol. 7, pp. 243-253, 2020.

[200] S. A. Rafiei, B. Mohammadi-ivatloo, S. Asadi, S. Goldani, and H. Falaghi, "Bi-level model for generation expansion planning with contract pricing of renewable energy in the presence of energy storage," *IET Renewable Power Gener*., Vol. 13, no. 9, pp. 1544-1553, 2019.

[201] R. E. Brown and M. Marshall, "Budget constrained planning to optimize power system reliability," *IEEE Trans. Power Syst*., vol. 15, no. 2, pp. 887-892, May 2000.

[202] K. Mongird, V. Viswanathan, J. Alam, C. Vartanian, V. Sprenkle, and R. Baxter, "2020 Grid energy storage technology cost and performance assessment," United States Dept. Energy, Pacific Northwest Nat. Lab., Richland, WA, USA, Tech. Rep. DOE/PA-0204, Dec. 2020.

[203] C. Opathella, A. Elkasrawy, A. A. Mohamed, and B. Venkatesh, "Optimal scheduling of merchant-owned energy storage systems with multiple ancillary services," *IEEE Open Access J. Power Energy*, vol. 7, pp. 31-40, 2020.

[204] H. Cui, F. Li, X. Fang, H. Chen, and H. Wang, "Bilevel arbitrage potential evaluation for grid-scale energy storage considering wind power and LMP smoothing effect," *IEEE Trans. Sustain. Energy*, vol. 9, no. 2, pp. 707-718, April 2018.

[205] Q. Shi *et al.*, "Network reconfiguration and distributed energy resource scheduling for improved distribution system resilience," *Int. J. Electr. Power Energy Syst*., vol. 124, pp. 1-10, Jan. 2021.

[206] S. Ma, L. Su, Z. Wang, F. Qiu, and G. Guo, "Resilience enhancement of distribution grids against extreme weather events," *IEEE Trans. Power Syst*., vol. 33, no. 5, pp. 4842-4853, Sep. 2018.

[207] Q. Shi *et al.*, "Resilience-oriented DG siting and sizing considering stochastic scenario reduction," *IEEE Trans. Power Syst.*, vol. 36, no. 4, pp. 3715-3727, July 2021.

[208] H. Shuai *et al*., "Post-storm repair crew dispatch for distribution grid restoration using stochastic Monte Carlo tree search and deep neural networks," *Int. J. Electr. Power Energy Syst*., vol. 144, pp. 108477, 2023.

[209] A. Dinger *et al*., "Batteries for electric cars: Challenges, opportunities, and the outlook to 2020," Boston Consulting Group, Boston, MA, 2010.

[210] M. Stecca, L. R. Elizondo, T. B. Soeiro, P. Bauer and P. Palensky, "A comprehensive review of the integration of battery energy storage systems into distribution networks," *IEEE Open Journal of the Industrial Electronics Society*, vol. 1, pp. 46-65, 2020.

[211] H. H. Abdeltawab and Y. A.-R. I. Mohamed, "Mobile energy storage scheduling and operation in active distribution systems," *IEEE Trans. Ind. Electron*., vol. 64, no. 9, pp. 6828–6840, Sep. 2017.

[212] X. Wang, F. Li, L. Bai, and X. Fang, "DLMP of competitive markets in active distribution networks: Models, solutions, applications, and visions," *Proceedings of the IEEE*, early access, 2022.

[213] B. She *et al*., "Decentralized and Coordinated V-f control for islanded microgrids considering DER inadequacy and demand control," *IEEE Trans. Energy Convers*., early access, 2023.

[214] S. Mohammadi, M. R. Hesamzadeh, and D. W. Bunn, "Distribution locational marginal pricing (DLMP) for unbalanced three-phase networks," *IEEE Trans. Power Syst.*, vol. 37, no. 5, pp. 3443-3457, Sept. 2022.

[215] X. Wang, F. Li, *et al*., "Tri-level hybrid interval-stochastic optimal scheduling for flexible residential loads under uncertainties", *Int. J. Electr. Power Energy Syst*., vol. 146, pp. 108672, 2023.

[216] S. Park, J. Lee, S. Bae, G. Hwang, and J. K. Choi, "Contribution-based energy-trading mechanism in microgrids for future smart grid: A game theoretic approach," *IEEE Trans. Ind. Electron.*, vol. 63, no. 7, pp. 4255-4265, July 2016.

[217] A. Paudel, K. Chaudhari, C. Long, and H. B. Gooi, "Peer-to-peer energy trading in a prosumer-based community microgrid: A game-theoretic model," *IEEE Transactions on Industrial Electronics*, vol. 66, no. 8, pp. 6087-6097, Aug. 2019.

[218] F. Luo, Z. Y. Dong, G. Liang, J. Murata, and Z. Xu, "A distributed electricity trading system in active distribution networks based on multi-agent coalition and blockchain," *IEEE Trans. Power Syst.*, vol. 34, no. 5, pp. 4097-4108, Sept. 2019.

[219] J. Li, C. Zhang, Z. Xu, J. Wang, J. Zhao, and Y. -J. A. Zhang, "Distributed transactive energy trading framework in distribution networks," *IEEE Trans. Power Syst*, vol. 33, no. 6, pp. 7215-7227, Nov. 2018.

[220] T. Morstyn, A. Teytelboym, and M. D. McCulloch, "Bilateral contract networks for peer-to-peer energy trading," *IEEE Trans. Smart Grid*, vol. 10, no. 2, pp. 2026-2035, March 2019.

[221] E. Sorin, L. Bobo and P. Pinson, "Consensus-based approach to peer-to-peer electricity markets with product differentiation," *IEEE Trans. Power Syst.*, vol. 34, no. 2, pp. 994-1004, March 2019.

[222] X. Xiao, F. Wang, M. Shahidehpour, Y. Zhai, and Q. Zhou, "Peer-to-peer trading in distribution system with utility's operation," *CSEE J. Power Energy Syst*., early access.

[223] J. Zhang *et al*. "A distributed consensus-based optimal energy management approach in DC microgrids." *Int. J. Elect. Power Energy Syst*., vol. 140, pp. 108015, 2022.

[224] A. Esmat, M. de Vos, Y. Ghiassi-Farrokhfal, P. Palensky, and D. Epema, "A novel decentralized platform for peer-to-peer energy trading market with blockchain technology," *Appl. Energy*, vol. 282, pp. 116123, 2021.

[225] L. Chen, N. Liu, C. Li, and J. Wang, "Peer-to-peer energy sharing with social attributes: A stochastic leader–follower game approach," *IEEE Trans. Ind. Inform*., vol. 17, no. 4, pp. 2545-2556, April 2021.

[226] L. Chen, N. Liu, C. Li, S. Zhang, and X. Yan, "Peer-to-peer energy sharing with dynamic network structures," *Appl. Energy*, vol. 291, pp. 116831, 2021.

[227] J. Guerrero, A. C. Chapman, and G. Verbič, "Decentralized P2P energy trading under network constraints in a low-voltage network," *IEEE Trans. Smart Grid*, vol. 10, no. 5, pp. 5163-5173, Sept. 2019.

[228] M. H. Ullah and J.-D. Park, "Peer-to-peer energy trading in transactive markets considering physical network constraints," *IEEE Trans. Smart Grid*, vol. 12, no. 4, pp. 3390-3403, July 2021.

[229] D. F. Botelho, L. W. de Oliveira, B. H. Dias, T. A. Soares, and C. A. Moraes, "Integrated prosumers–DSO approach applied in peer-to-peer energy and reserve tradings considering network constraints," *Appl. Energy*, vol. 317, pp. 119125, 2022.

[230] C. Feng, B. Liang, Z. Li, W. Liu, and F. Wen, "Peer-to-peer energy trading under network constraints based on generalized fast dual ascent," *IEEE Trans. Smart Grid*, vol, vol. 14, no. 2, pp. 1441-1453, March 2023.

[231] Q. Shi *et al*., "Co-optimization of repairs and dynamic network reconfiguration for improved distribution system resilience," *Appl. Energy*, vol. 318, pp. 119245, 2022.

[232] N. Liu, C. Li, L. Chen, and J. Wang, "Hybrid data-driven and model-based distribution network reconfiguration with lossless model reduction," *IEEE Trans. Ind. Inform*., vol. 18, no. 5, pp. 2943-2954, May 2022.

[233] S. Boyd, "Distributed optimization and statistical learning via the alternating direction method of multipliers," *Found. Trends® Mach. Learn.*, vol. 3, no. 1, pp. 1–122, 2010.

[234] Data Miner 2, PJM, Audubon, PA, USA. Accessed: Feb. 10, 2023. [Online] Available: http://dataminer2.pjm.com/list.

[235] A. Akrami, M. Doostizadeh, and F. Aminifar, "Optimal reconfiguration of distribution network using μPMU measurements: A data-driven stochastic robust optimization," *IEEE Trans. Smart Grid*, vol. 11, no. 1, pp. 420-428, Jan. 2020.

[236] R. Vargas, L. H. Macedo, J. M. Home-Ortiz, J. R. S. Mantovani, and R. Romero, "Optimal restoration of active distribution systems with voltage control and closed-loop operation," *IEEE Trans. Smart Grid*, vol. 12, no. 3, pp. 2295-2306, May 2021.

[237] https://drive.google.com/file/d/19iLWTASrP2XIM8w93xiwC0y1Zc_yH_IX/view?usp=share_link

Appendices

Appendix A Supplemental Materials of Chapter 3

A.1 Nomenclature

Sets

T	Set of time slots
H	Set of HVAC aggregators
E	Set of EV aggregators
G	Set of all generators
B	Set of all nodes
S	Substation

Constants

$P_{i,t}^{MT,min}/P_{i,t}^{MT,max}$	Minimum/maximum active power of MT i at time t
α_i	Power factor of DG i
$P_{i,t}^{PV,fore}$	Forecasted active power of PV i at time t
$Q_{i,t}^{SVC,min}/Q_{i,t}^{SVC,max}$	Minimum/maximum reactive power of SVC i at time t
η^C, η^D	Charge/discharge efficiency of EV
$P_{i,t}^{C,max}/P_{i,t}^{Dis,max}$	Maximum charge/discharge power of EV aggregator i at time t
$SOC_i^{E,\min}$	Minimum state of charge of EV aggregator i
$SOC_i^{E,\max}$	Maximum state of charge of EV aggregator i
E_i^R	Rated energy capacity of EV aggregator i
N_i^e	Number of EVs participating in aggregator i
N_i^{piles}	Number of charging piles in charging station i
p_j^C	Rated charging power of EV j
E_j^{rated}	Rated energy of EV j
e_j^d	Driving energy consumption of EV j per mile
d_j	Driving distance over a day
a_j, b_j, g_j	Coefficients of the thermal function of HVAC j
θ_{out}	Day-ahead forecasted outdoor temperature

$\theta^{min}/\theta^{max}$	Comfortable temperature boundary
R_j, C_j	Thermal resistance and capacitance of HVAC j
η^H	Cooling efficiency of HVAC
P^{rated}	Rated power of HVAC
$\tilde{a}_i$, $\tilde{b}_i$, $\tilde{g}_i$	Coefficients of the thermal transfer function of HVAC aggregator i
N_i^h	Number of HVACs participating in aggregator i
$syn_i^{\min}/syn_i^{\max}$	Minimum/maximum synchronicity rate of HVAC aggregator i
$\Delta u_i^{dr}/\Delta u_i^{ur}$	Ramp down/up rate of HVAC aggregator i
$SOC_i^{H,\min}$	Minimum state of charge of HVAC aggregator i
$SOC_i^{H,\max}$	Maximum state of charge of HVAC aggregator i
$\sigma_{S,t}^p/\sigma_{S,t}^q$	Active/reactive LMP at the substation at time t
$\sigma_{i,t}^p/\sigma_{i,t}^q$	Active/reactive bidding price of generator i at time t
$P_{i,t}^D/Q_{i,t}^D$	Fixed active/reactive load demand of node i at time t
V^{min}/V^{max}	Minimum/maximum voltage constraints

Variables

P_t^S/Q_t^S	Active/reactive power drawn from the wholesale market at time t
$P_{i,t}^{MT}/Q_{i,t}^{MT}$	Active/reactive power of MT i at time t
$P_{i,t}^{PV}/Q_{i,t}^{PV}$	Active/reactive power of PV i at time t
$Q_{i,t}^{SVC}$	Reactive power of SVC i at time t
$E_{i,t}$	Energy of EV aggregator i at time t
$P_{i,t}^C/P_{i,t}^{Dis}$	Charge/discharge power of EV aggregator i at time t
$\theta_{j,t}$	Indoor temperature of building j at time t
$u_{j,t}$	Binary variable stating the ON/OFF of HVAC j at time t
$\tilde{\theta}_{i,t}$	Equivalent indoor temperature of HVAC aggregator i at time t
$\tilde{u}_{i,t}$	ON-state ratio of HVACs in aggregator i at time t
$P_{i,t}^H$	Active power of HVAC aggregator i at time t
$SOC_{i,t}$	State of charge of HVAC aggregator i at time t
$\pi_{i,t}^p$	Active DLMP of node i at time t
P_t^{loss} / Q_t^{loss}	Active/reactive power loss at time t

$V_{j,t}$	Voltage of node j at time t
$\pi_{i,t}^{p}$	Active DLMP at node i at time t
λ_t^p / λ_t^q	Lagrangian multipliers associated with active/reactive power balance constraints
$\omega_{i,t}^{(.),\min}$, $\omega_{i,t}^{(.),\max}$	Lagrangian multipliers associated with the voltage constraints, and the power output limits
$\kappa_{i,t}^{-}$, $\kappa_{i,t}^{+}$	Lagrangian multipliers associated with reactive power constraints

A.2 Additional Discussion on DLMP Step Change

In Figure 3.10, the DLMP does not go to \$70/MWh which is the active power bidding price of MT. The main reason is: in the distribution system, voltage constraint involves both active power and reactive power even if in a linearized model, such as (3.28). This means reactive power can also contribute to the voltage profile. In the MT model (3.18) (3.19), MT generates both active power and reactive power. Therefore, once the MT is turned on, both active power and reactive power will support the voltage. Meanwhile, in Section IV, the reactive power price is set to 0. Thus, regarding voltage improvement by the same amount, the active power provided by MT is less than that of the MW-only provider. Therefore, under the same active power price, the marginal voltage support cost of the former should be less than that of the latter.

To make this point clearer, here is an example. The task is to improve the voltage at node 18 by ΔV.

1) Scenario 1: MT provides active power $\Delta P1>0$ and reactive power $\Delta Q1>0$. The additional cost is $\$70\cdot\Delta P1+\$0\cdot\Delta Q1=\$70\cdot\Delta P1$.
2) Scenario 2: MT provides active power $\Delta P2>0$ and reactive power $\Delta Q2=0$. The additional cost is $\$70\cdot\Delta P2$.

Then we could have $\Delta P1 < \Delta P2$ because there is no reactive power support in Scenario 2 which demands more real power to raise the voltage. Since $\Delta P1 < \Delta P2$, we have $\$70\cdot\Delta P1 < \$70\cdot\Delta P2$. If $\Delta P2 = 1$, it means the marginal cost (DLMP) of Scenario 2 is \$70/MWh, and DLMP of Scenario 1 is less than \$70/MWh. This is the reason why the DLMP at node 18 does not reach \$70/MWh.

Finally, based on Scenario 2, a new simulation is carried out: assume MT only provides active power and does not provide reactive power. Based on Case 0, the DLMP under different system load levels is shown in Figure A1. It can be observed that the DLMP at node 18 reaches $70/MWh, which validates the above reasoning. Similar patterns can also be found from Case 1 to Case 4 which are not elaborated here.

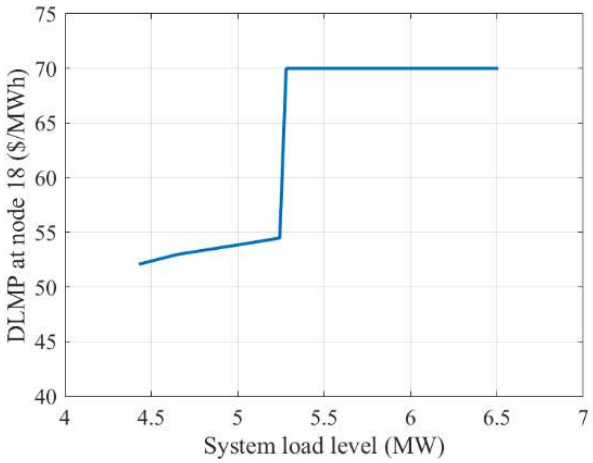


Figure A1. DLMP with step changes under different system load levels

Appendix B Supplemental Materials of Chapter 4

B.1 Modeling of EWH

A single EWH can be modeled with the following expressions [193]:

$$\theta_{t+1}^{w} = a^{w}\theta_{t}^{w} - b^{w}W_{t}^{D} + g^{w}u_{t}^{w} + c^{w} \tag{B1}$$

$$\theta^{w,\min} \le \theta_{t}^{w} \le \theta^{w,\max} \tag{B2}$$

$$a^{w} = \left(1 - \frac{3600\Delta t H_{r}}{40mc_{p}}\right) \tag{B3}$$

$$c^{w} = \frac{3600H_{r}\theta_{t}^{h}}{40mc_{p}} \tag{B4}$$

$$g^{w} = 3600 \cdot \frac{P^{w,rated}}{mc_{p}} \tag{B5}$$

$$b^{w} = \frac{\left(\theta_{t}^{w} - \theta^{w,co}\right)}{m} \tag{B6}$$

where $P^{w,rated}$ is the rated power of the heating element, m is the mass of the water inside the water tank, c_p is the specific heat of water (4.2kJ/kg℃), 3600 is to transfer time unit from hour to second, H_r represents the amount of water tank heat loss to the ambient per second, and $\theta^{w,co}$ is the temperature of inlet cold water. When obtaining b^w, it is assumed that the consumed hot water has a constant temperature of 55℃, since the used water temperature is always within the upper and lower limits.

The typical parameters of a single EWH are shown in Table B1. Note, the indoor temperature θ_t^h is assumed constant (20℃) in this model because it fluctuates within a tight range due to the HVAC in the house, and $\theta_t^{w,co}$ is also assumed constant (10 ℃).

Table B1. Parameters of a single EWH

Parameter	Typical values
P^{rated}	3 (kW)
m	184 (kg)
H_r	0.07 (kW)
θ^{co}	10 (℃)
W^D	L/h
θ^{max}	60 (℃)
θ^{min}	50 (℃)
Δt	1 hour

Appendix C Supplemental Materials of Chapter 5

C.1 Nomenclature

Sets

Ω_T	Set of time slots
Ω_G	Set of generators, $\Omega_G = \Omega_{MT} \bigcup \Omega_{SVC}$
Ω_{MT}	Set of MTs
Ω_{SVC}	Set of SVCs
Ω_N	Set of buses
Ω_{BS}	Set of candidate buses for BESS installation
Ω_V	Set of buses that voltage constraints can be maintained
S	Set of scenarios

Constants

c^{Mf} / c^{Mv}	Fixed/variable O&M cost
$N_{BS}^{\max}$	Maximal number of BESSs
k^p / k^e	Fixed power/energy cost for installing a BESS
C^{Bgt}	Budget limit
$P^{\min} / P^{\max}$	Minimum/maximum rated power of a BESS
$E^{\min} / E^{\max}$	Minimum/maximum rated energy of a BESS
$p(s)$	Probability of scenario s
η_i	Round-trip efficiency of BESS i
$SOC_i^{\min} / SOC_i^{\max}$	Minimum/maximum SOC of BESS i
$\sigma_{sub,t}^{p,s} / \sigma_{sub,t}^{q,s}$	Active/reactive LMP of the substation at time t
$\sigma_{i,t}^{p,s} / \sigma_{i,t}^{q,s}$	Active/reactive bidding price of generator i at time t
$P_{i,t}^{D,s} / Q_{i,t}^{D,s}$	Fixed active/reactive load demand of bus i at time t
$V^{\min} / V^{\max}$	Minimum/maximum voltage limits

$V_{sub,t}^{s}$	Voltage of the substation at time t
$P_i^{G,\min} / P_i^{G,\max}$	Minimum/maximum active power of generator i at time t
$Q_i^{G,\min} / Q_i^{G,\max}$	Minimum/maximum reactive power of generator i at time t
α_i	Power factor of generator i
Z^p / Z^q	Matrices of nodal voltage change concerning net active/reactive power injection

Variables

$P_i^{rated} / E_i^{rated}$	Rated power/energy of BESS i
δ_i	Binary variable indicating whether a BESS is installed at bus i
$\pi_{i,t}^{s}$	Active DLMP of node i at time t
$P_{i,t}^{c,s} / P_{i,t}^{d,s}$	Charging/discharging power of BESS i at time t
$P_{i,t}^{BESS,s}$	Power exchange of BESS i at time t with the power grid
$E_{i,t}^{s}$	Energy stored in BESS i at time t
$P_{sub,t}^{G,s} / Q_{sub,t}^{G,s}$	Active/reactive power drawn from the wholesale market at time t
$P_{i,t}^{G,s} / Q_{i,t}^{G,s}$	Active/reactive power of generator i at time t
$P_t^{L,s} / Q_t^{L,s}$	Active/reactive power loss at time t
$V_{j,t}^{s}$	Voltage of bus j at time t
$\lambda_t^{p,s} / \lambda_t^{q,s}$	Lagrangian multipliers associated with active/reactive equality power constraints
$\omega_{i,t}^{(.)\min,s} / \omega_{i,t}^{(.)\max,s}$	Lagrangian multipliers associated with inequality voltage and active/reactive power constraints
$\kappa_{i,t}^{-,s} / \kappa_{i,t}^{+,s}$	Lagrangian multipliers associated with inequality reactive power constraints

C.2 Cost of LFP Batteries

According to [202], BESS cost mainly consists of capital and operation costs. The capital cost refers to the BESS installation cost which includes power-related costs and

energy-related costs. The former consists of power equipment costs (costs of the converter, protection, breaker, communication, software, etc.), controls & communication costs (cost of the energy management system for the BESS), and grid integration costs (cost of integrating the BESS to the power system, including transformers and isolation breakers).

The energy-related costs consist of storage block costs (cost of the storage elements in a BESS), storage balance of system costs (cost of supporting components like containers, cabling, switchgears, flow battery pumps, and HVAC), system integration costs (costs of integrating subcomponents of a BESS into a functional system), and project development costs (costs of permitting, power purchase agreements, etc.). Operation costs include the fixed and variable costs for O&M. The fixed O&M cost refers to the cost necessary to keep the BESS operational, such as planned maintenance. The variable O&M cost represents the usage impacted cost necessary to operate the storage system.

BESS costs are summarized in Table C1. Specifically, in this paper, BESSs are lithium-ion iron phosphate (LFP) batteries due to their good performance in safety and life span. References [209][210] have presented a detailed analysis and comparison among different types of batteries, one can refer to these papers for more details.

C.3 Comparison Between BESS and MES

Mobile energy storage (MES) is another promising storage technology [211] in addition to BESS. BESS and MES share many similar functions such as load shifting, peak shaving, reactive power support, renewable energy integration, transmission and distribution upgrade deferral, energy arbitrage, and voltage profile improvement. The general differences between BESS and MES from the operational and economic perspectives are summarized in Table C2. It can be concluded that the main advantage of BESS is its lower cost (e.g., investment plus transportation), while the main advantage of MES is its better location-based services (e.g., voltage regulation and power losses minimization) due to its locational flexibility. In a competitive distribution system, it may be difficult to claim that BESS will always be more attractive than MES, or vice versa. Thus, the preliminary conclusion regarding the decision of investment in BESS or MES depends on the requirement and preference of the investors and the feature of the distribution system. A more rigorous study should be conducted for a given system to make the best decision.

Table C1. Cost of LFP batteries

k^p ($/kW)	156
k^e ($/kWh)	408
c^{Mf} ($/kW-yr)	4.4
c^{Mv} ($/kWh)	0.5125e-3

Table C2. Differences between BESS and MES

Features	BESS	MES
Investment cost	Expensive	Very expensive
Operation style	Stationary	Transportable
Moving time	No	Yes
Transportation cost	No	Yes
Localized services	Good	Excellent

Appendix D Supplemental Materials of Chapter 6

D.1 Nomenclature

Sets

Ω_N	Set of buses
Ω_L	Set of distribution lines
Ω_G	Set of generation resources
Ω_T	Set of time slots in a day
Ω_{CB}	Set of CBs
Ω_B	Set of buyers in a P2P market
Ω_S	Set of sellers in a P2P market
sub	Substation

Constants

$\delta(j)$	Set of child buses of bus j
$\pi(j)$	Set of parent buses of bus j
$q_{i,k}^{cap}$	Rated capacity of capacitor k at bus i
N_i^{CB}	Maximum action time of capacitor at bus i
N_{ij}^{S}	Maximum action time of switch in line i-j
$P_i^{G,\min} / P_i^{G,\max}$	Minimum/maximum active power of generator i
$S_{ij}^{\max}$	Maximum power flow limit of line i-j
$V^{\min} / V^{\max}$	Minimum/maximum voltage limits
$\sigma_{sub}^{p} / \sigma_i^{p}$	LMP and marginal price of generator i
C^{s} / C^{cb}	Line switch on/off cost and CB on/off cost per time
r_{ij} / x_{ij}	Resistance/reactance of line i-j
$p_b^{\min} / p_b^{\max}$	Minimum/maximum load demand of buyer b
$p_s^{\min} / p_s^{\max}$	Minimum/maximum active power of seller s

a_b, c_b, d_b	Coefficients of the utility function of buyer b
a_s, c_s, d_s	Coefficients of the cost function of seller s

Variables

s_{ij}	Switch status of line i-j
F_{ij}	Power flow of line i-j in the virtual network
$Q_{i,t}^{CB}$	Reactive power output of CBs at bus i
$u_{i,k,t}$	ON/OFF status of capacitor k at bus i
P_j^G / Q_j^G	Active/reactive power generation at bus j
P_j^D / Q_j^D	Active/reactive load demand at bus j
P_{ij} / Q_{ij}	Active/reactive power flow at line i-j
V_j	Voltage magnitude at bus j
p_b	Load demand of buyer b
p_s	Power production of seller s
p_{bs}, p_{be}	Power quantity that buyer b buys from seller s and grid
p_{sb}, p_{se}	Power quantity that seller s sells to buyer b and grid
c_b^E	Purchasing payment of buyer b from the grid
π^{DLMP}	Distribution locational marginal price
π^{FIT}	Feed in tariff
u_{bs}, u_{sb}, u_{be}, u_{eb}, u_{se}, u_{es}	Scaled dual variables in the ADMM

D.2 Solve the Exchange Problem via ADMM

Reference [233] presented the following exchange problem.

$$\min \quad \sum_{i=1}^{N} f_i(x_i) \tag{D1}$$

$$s.t. \quad \sum_{i=1}^{N} x_i = 0 \tag{D2}$$

where (D1) has a decomposition structure, and (D2) is the equilibrium constraint that each commodity clears.

This problem can be solved via the ADMM as follows:

$$x_i^{k+1} := \arg\min\left(f_i\left(x_i\right) + \left(\frac{\rho}{2} \left\| x_i - x_i^k + \overline{x}^k + u^k \right\|_2^2 \right) \right) \tag{D3}$$

$$u^{k+1} := u^k + \overline{x}^{k+1} \tag{D4}$$

where x_i^k is the value of x_i in the kth iteration, $\overline{x}^k$ is the average value of all x_i^k, u^k is the scaled dual variables. In the iteration, the x-update can be carried out independently and in parallel, the u-update averages x_i^{k+1} and sends u^{k+1} back to subproblems handling x_i. The market explanation of the ADMM in solving this exchange problem can be found in [233].

D.2 Parameters of Peers in P2P Markets

Detailed parameters of sellers and buyers in P2P market are presented in Table D1 and Table D2. Note that the load and generation range is at t = 14:00, and a scaler is applied to change the range at different time periods.

Table D1. Parameters of sellers

Bus	Seller	$p_s^{\min}$ (MW)	$p_s^{\max}$ (MW)	a_s ($/MWh^2)	c_s ($/MWh)	d_s
7	G1	0	0.04	0.1	10	0.1
	G2	0	0.06	0.1	30	0.2
	G3	0	0.08	0.1	19	0.2
14	G1	0	0.06	0.2	10	0.3
	G2	0	0.10	0.1	18	0.1
	G3	0	0.05	0.1	16	0.2
17	G1	0	0.03	0.1	10	0.2
	G2	0	0.04	0.2	20	0.3
	G3	0	0.02	0.3	22	0.2
29	G1	0	0.05	0.1	10	0.1
	G2	0	0.06	0.5	18.3	0.2
	G3	0	0.10	0.3	18.42	0.2
	G4	0	0.08	0.5	18.42	0.3
31	G1	0	0.03	0.1	15	0.1
	G2	0	0.06	0.2	20	0.2
	G3	0	0.04	0.3	22	0.1
	G4	0	0.03	0.4	24	0.2

Table D2. Parameters of buyers

Bus	Buyer	$p_b^{\min}$ (MW)	$p_b^{\max}$ (MW)	a_b ($/MWh^2)	c_b ($/MWh)	d_b
7	B1	0.02	0.04	-0.1	31	0.1
	B2	0.03	0.06	-0.1	32.95	0.2
	B3	0.04	0.08	-0.3	33.1	0.2
	B4	0.02	0.04	-0.3	33	0.5
14	B1	0.01	0.02	-0.1	28	0.2
	B2	0.015	0.03	-0.2	25	0.3
	B3	0.02	0.04	-0.1	30	0.5
17	B1	0.01	0.02	-0.4	31.2	0.1
	B2	0.015	0.03	-0.6	31.2	0.2
	B3	0.02	0.04	-0.8	31.15	0.5
	B4	0.01	0.02	-0.2	31.1	0.3
	B5	0.03	0.06	-0.3	31.1	0.2
29	B1	0.02	0.04	-0.1	31	0.5
	B2	0.03	0.06	-0.1	32.95	0.2
	B3	0.02	0.04	-0.3	30.1	0.3
31	B1	0.02	0.04	-0.1	25	0.2
	B2	0.03	0.06	-0.3	28	0.5

Appendix E Publications

Journal papers:

[J1] **X. Wang**, F. Li, et al., "Tri-level scheduling model considering residential demand flexibility of aggregated HVACs and EVs under distribution LMP," *IEEE Transactions on Smart Grid*, vol. 12, no. 5, pp. 1949-3053, Sep. 2021.

[J2] **X. Wang**, F. Li, et al, "Profit-oriented BESS siting and sizing in deregulated distribution systems," *IEEE Trans. Smart Grid*, vol. 14, no. 2, pp. 1528-1540, Mar. 2023.

[J3] **X. Wang**, F. Li, L. Bai, and X. Fang, "DLMP of competitive markets in active distribution networks: Models, solutions, applications and visions", *Proceedings of the IEEE*, in press.

[J4] **X. Wang**, F. Li, et al., "Tri-level hybrid interval-stochastic optimal scheduling for flexible residential loads under uncertainties", *International Journal of Electrical Power & Energy Systems*, vol. 146, pp. 108672, Mar. 2023.

[J5] **X. Wang**, F. Li, et al., "A hybrid two-layer pool-based and P2P distribution market integrating network constraints and transaction autonomy," *IEEE Transactions on Power Systems*, under review.

[J6] Q. Shi, F. Li, T. Kuruganti, M. Olama, J. Dong, **X. Wang**, C. Winstead, "Resilience-Oriented DG Siting and Sizing considering Stochastic Scenario Reduction", *IEEE Transactions on Power Systems*, vol. 36, no. 4, pp. 3715-3727, July 2021.

[J7] Q. Zhang, F. Li, W. Feng, **X. Wang**, "Building marginal pattern library with unbiased training dataset for enhancing model-free load-ED mapping", *IEEE Open Access Journal of Power and Energy*, vol. 9, pp. 88-98, 2022.

[J8] Q. Shi, F. Li, M. Olama, J. Dong, **X. Wang,** et al, "Co-optimization of repairs and network reconfiguration for improved distribution system resilience considering load uncertainty", *Applied Energy*, vol. 318, pp. 119245, July 2022.

[J9] H. Shuai, F. Li, B. She, **X. Wang,** et al, "AlphaZero based post-storm repair crew dispatch for distribution grid restoration", *International Journal of Electrical Power & Energy Systems*, vol. 144, pp. 108477, Jan. 2023.

[J10] Q. Zhang, F. Li, and **X. Wang**, "Cyber-impact analysis for ISO revenue adequacy considering FDIA in real-time market operations", *IEEE Transactions on Power Systems*, in press.

[J11] B. Liu, J. Dong, J. Lian, T. Kuruganti, **X. Wang,** and F. Li, "Enhanced deep neural networks with transfer learning for distribution LMP considering load and PV uncertainties", *International Journal of Electrical Power & Energy Systems*, vol. 147, pp. 108780, May 2023.

Conference papers:

[C1] Q. Shi, W. Feng, Q. Zhang, **X. Wang** and F. Li, "Overvoltage mitigation through Volt-VAR control of distributed PV systems," *2020 IEEE/PES Transmission and Distribution Conference and Exposition (T&D)*, 2020, pp. 1-5.

Vita

Xiaofei Wang joined Professor Fangxing Li's group at the University of Tennessee at Knoxville in August 2019 to pursue a Ph.D. degree in Electrical Engineering. He received his B.S. degree from North China Electric Power University in 2014, Baoding, China, in 2014, M.S. degree from Wuhan University, Wuhan, China, in 2017. His research interests include electricity market, demand response, and power system optimization.